DEPARTMENT OF MECHANICAL ENGINEERING AND MECHANICS
SCHOOL OF ENGINEERING
OLD DOMINION UNIVERSITY
NORFOLK, VIRGINIA

AUTOMATIC CONTROL OF A LIQUID NITROGEN COOLED, CLOSED-CIRCUIT, CRYOGENIC PRESSURE TUNNEL

By

S. Balakrishna

Principal Investigator: G. L. Goglia

Progress Report
For the period October 1979 - March 1980

Prepared for the
National Aeronautics and Space Administration
Langley Research Center
Hampton, Virginia

Under
Research Grant NSG 1503
Dr. R. A. Kilgore, Technical Monitor
Subsonic Transonic Aerodynamics Division

March 1980

DEPARTMENT OF MECHANICAL ENGINEERING AND MECHANICS
SCHOOL OF ENGINEERING
OLD DOMINION UNIVERSITY
NORFOLK, VIRGINIA

AUTOMATIC CONTROL OF A LIQUID NITROGEN COOLED, CLOSED-CIRCUIT, CRYOGENIC PRESSURE TUNNEL

By

S. Balakrishna

Principal Investigator: G. L. Goglia

Progress Report
For the period October 1979 - March 1980

Prepared for the
National Aeronautics and Space Administration
Langley Research Center
Hampton, Virginia 23665

Under
Research Grant NSG 1503
Dr. R. A. Kilgore, Technical Monitor
Subsonic Transonic Aerodynamics Division

Submitted by the
Old Dominion University Research Foundation
P. O. Box 6369
Norfolk, Virginia 23508

March 1980

PREFACE

This report details the control analysis phase of the project "Modeling and Control of Transonic Cryogenic Wind Tunnels," sponsored by NASA/Langley Research Center (LaRC) under research grant NSG-1503. This work was performed during the project period ending March 1980. The contents of this document complement the modeling phase activity which has been reported as "Synthesis of a Control Model for a Liquid Nitrogen Cooled Closed Circuit Cryogenic Nitrogen Wind Tunnel and its Validation" (ref. 4). This document reports the details of control law design, proof of its adequacy, microprocessor compatible software design, and electronic hardware realization and its successful performance on the 0.3-m Transonic Cryogenic Tunnel at NASA/LaRC.

TABLE OF CONTENTS

LIST OF FIGURES

(Continued)

LIST OF FIGURES (Continued)

LIST OF FIGURES (Concluded)

AUTOMATIC CONTROL OF A LIQUID NITROGEN COOLED, CLOSED-CIRCUIT, CRYOGENIC PRESSURE TUNNEL

By

S. Balakrishna[1]

INTRODUCTION

Need for realizing full flight Reynolds number airflow past scaled models in transonic wind tunnels has been keenly felt for some time now, particularly to aid in understanding shock-boundary layer interaction. In the 1970's, there was considerable review of various methods for obtaining high Reynolds number airflow in relatively small wind tunnels without any fan power or dynamic pressure penalties. The most promising among many possible techniques proved to be the concept of operating the test gas of a wind tunnel at cryogenic temperatures (ref. 1). This was elegantly demonstrated by the proof-of-concept operation of the 0.3-m Transonic Cryogenic Tunnel (TCT) facility at NASA/Langley Research Center (LaRC) in 1974 (ref. 2). Nitrogen was used as the test medium and was proven to behave perfectly under isentropic flow conditions (ref. 3). Further, the successful operation of the 0.3-m TCT was aided by contemporary advances in cryogenic materials and instrumentation techniques.

The initial operating experience on the 0.3-m TCT facility indicated that the cryogenic tunnel process was basically well behaved from a control point of view, but exhibited continuous creep of the tunnel variables. This was caused by unmatched mass-energy control inputs which integrated to large errors in time when controlled manually. Further, difficulties were experienced in manual control for large changes in the tunnel conditions because of considerable cross-coupling between the

---

[1] Research Assistant Professor of Mechanical Engineering and Mechanics Old Dominion University Research Foundation, P. O. Box 6369, Norfolk, Virginia 23508. (On leave from National Aeronautical Laboratory, Bangalore 560 017, India)

tunnel flow variables and the control inputs, making the tunnel runs rather uneconomical. Hence, the need for design of a fast, automatic, closed-loop controller for regulating the tunnel variables was keenly felt.

For these reasons, studies have been undertaken to formulate and solve the problem of closed-loop control of a fan-driven, liquid nitrogen cooled, closed-circuit, cryogenic pressure tunnel, with specific reference to the 0.3-m TCT facility at NASA/LaRC. This problem has been addressed in two phases: first, by the synthesis of a control compatible mathematical model of a cryogenic pressure tunnel starting from the basic physical laws and its experimental validation. The second phase was the design of a closed-loop, feedback controller to regulate the tunnel's total temperature and total pressure, the controller hardware realization, and its performance on the 0.3-m TCT facility.

The efforts of the synthesis of a control model of cryogenic tunnel process and its experimental validation have been successfully completed and reported in reference 4. This synthesis was based on the thermodynamic analysis of the tunnel resident gas and metal mass and their interaction with the various control inputs. The resultant lumped parameter, nonlinear, multivariable model was used to develop a cryogenic tunnel simulator on a hybrid analog/digital computer. The synthesized mathematical model was validated by reconciling the quasi-steady state and transient impulse response of the 0.3-m TCT facility and its real-time simulator responses under similar operating conditions.

In this report, the complementary problem of the control system design, performance analysis for its accuracy and stability, microprocessor-based controller software development, the microprocessor hardware specifications, and finally the performance of the designed controllers on the 0.3-m TCT facility have been detailed. Firstly, the control model has been used to design two single-input single-output (SISO) controllers for the automatic control of the tunnel's total temperature and total pressure by assuming small perturbation local linearity. In view of the global nonlinear behavior of the tunnel model, the SISO control analysis has resulted in nonlinearly gain scheduled proportional-integral-derivative (pID) control laws for

each of the temperature and pressure control loops. Strong cross-coupling of the fan power into the temperature loop has been countered by a fan power feed-forward feature. Further, in order to allow for directional nonlinearity, use of error magnitude dependent logic which switches the feed-forward on or off as necessary has been incorporated. Appropriate stability and accuracy tests have been performed to assure desired performance of the analytically designed control laws.

The control problem has also been addressed as a linear multivariable control problem, again by assuming small perturbation local linearity. A noninteractive controller so designed is shown to embrace the SISO control laws as a particular case.

These control laws have been tested on the real-time, hybrid, cryogenic tunnel simulator for the adequacy of their performance. The SISO laws have demonstrated their ability to hold the tunnel total temperature to ±0.25 K and total pressure to ±0.017 atm, with a typical step response settling time of about 20 sec for small amplitude step commands.

Further, the SISO control laws have been translated to a microprocessor-compatible, functional flow chart which is presented in Appendix A. The microprocessor hardware specifications have been generated by looking at the electronic system design as a direct digital controller. The operator control interface design has been detailed. Finally, the successful operation of the microprocessor-based tunnel closed-loop controller on the 0.3-m TCT facility, throughout the tunnel operational envelope, has been demonstrated. The ability of the controller to hold ±0.25 K in temperature and ±0.017 atm in pressure has been shown.

The analysis and design of the tunnel test section Mach number automatic control loop is presented in Appendix B. The existing fan speed control system has some singularities in fan speed wherein the fan cannot be operated. Though a design of a Mach loop controller has been presented, it cannot be implemented till appropriate improvements are made to the fan speed control system.

NOMEMCLATURE

a_{xx}	elements of matrix Z
A	area (m^2 or m^2/m^2)
b	tunnel circuit loss factor
b_{xx}	elements of matrix Z^{-1}
C_p, C_v	specific heats of nitrogen gas (KJ/kg-K)
G	feed-forward path model
GN_2	gaseous nitrogen
h	enthalpy (KJ/kg)
H	feedback path model
J	Joules (KJ = kilojoules)
K,k	gain constants (K also stands for Kelvin)
LN_2	liquid nitrogen
$\dot{m}$	mass flow rate (kg/sec)
M	test section Mach number
N	fan speed (rpm)
P	pressure (atm)
$\dot{Q}$	heat flow rate (KJ/sec)
S	Laplace operator
T	temperature (K)
t	time or time constant (sec)
U	internal energy (KJ)
V	volume (m^3)
W	mass (kg)
Z ,R,C	system matrices
α	cooling capacity of gaseous nitrogen (KJ/kg)
β	cooling capacity of liquid nitrogen (KJ/kg)
γ	ratio of specific heats
Δ	increment
τ	transport lag (sec)

Θ	thermal mass (KJ/K)
i	integer index
$\cdot$	dot over a quantity refers to $\frac{d}{dt}$ of that quantity
r	pressure ratio
η	fan efficiency
$\sigma + j\omega$	complex plane point; $j = \sqrt{-1}$
μ	micron

Controller

T	tunnel total temperature (K)
ST	set point, temperature loop (K)
ET	error, temperature loop (K)
pT	proportional gain, temperature loop
DT	derivative gain, temperature loop
IT	integral gain, temperature loop
KT	temperature loop gain
QDF	fan power (KJ/sec)
KL	full open liquid nitrogen flow (kg/sec)
ALQ	liquid valve area A_L
UT	temperature loop update rate
PL	liquid nitrogen pressure (atm)
P	tunnel total pressure (atm)
PS	tunnel test section static pressure (atm)
SP	set point, pressure loop (atm)
EP	error, pressure loop (atm)
pP	proportional gain, pressure loop
DP	derivative gain, pressure loop
IP	integral gain, pressure loop
KP	pressure loop gain
MAX	maximum allowed liquid nitrogen valve area (percent)

KB	bias gain
FF	feed-forward binary logic, on-1 off-0
LLT	liquid limit binary logic, on-1, off-0
AG	gas bleed valve area
UP	pressure loop update rate
UA	analog valve update rate
KL1	liquid valve gain, $KL = KL1 \sqrt{PL-P}$
KG	gaseous valve gain
KF	fan gain
TGR	temperature gradient (K/sec)
SISO	single input, single output
SM	set point, Mach loop
EM	error, Mach loop
KM	loop gain, Mach loop
IM	integral gain, Mach loop
pM	proportional gain, Mach loop
NS	set point, fan speed loop

Subscripts and Superscripts

F,f	fan
g	gas
L	liquid
m	metal or motor constant
s	static
1,2	analog bleed valves, or sensors
*	test section
(n)	nth sample where n is an integer = 0,1,...etc.
set	setpoint
past	previous valve

CRYOGENIC TUNNEL PROCESS

A closed-circuit wind tunnel is a device intended for testing scaled models in fluid flow in order to obtain their aerodynamic characterictics. The test section fluid flow over the model is associated with certain flow parameters to which the aerodynamic characteristics of the model are related. For meaningful scaling of model data to its full scale, it is necessary to maintain the flow similarity between the wind-tunnel test section flow and the full-scale flow. Among many flow parameters necessary for flow similarity, Mach number and Reynolds number are the most important flow parameters for stationary models. For the first time, full-scale flow Reynolds number can be obtained at transonic speeds in small wind tunnels because of the advent of the cryogenic flow wind tunnel concept (ref. 1).

The operation of a closed-circuit, fan-driven, transonic, cryogenic nitrogen tunnel and its ability to allow independent control of flow Mach number, Reynolds number, and flow dynamic pressure have been proven by the operation of the 0.3-m TCT facility at NASA/LaRC shown in figure 1 (refs. 1 and 2). This has been possible because of the ability of cryogenic tunnels to allow independent control of the tunnel gas temperature, the tunnel total pressure, and the test section mass flow achieved by three independent control inputs: viz liquid nitrogen flow into the tunnel, gaseous bleed out of the tunnel, and the fan speed.

A closed-circuit, cryogenic wind tunnel basically consists of a thermally autonomous pressure vessel designed as an aerodynamically contoured endless duct in which the fan operation results in a range of flow velocities at the test section. The thermal autonomy of a cryogenic tunnel is realized by thermal insulation either external to the tunnel metal walls or internal to the metal walls. The operation of the fan in the tunnel results in motion of the test gas with the accompanying compression heating and wall friction heating. In order to maintain the gas temperature in the presence of this heating, the liquified form of the test gas, liquid nitrogen (LN_2), is sprayed into the tunnel. The liquid nitrogen mass flow control allows either a cool down or regulation of the tunnel gas temperature. However, in this cooling process, the mass of the tunnel resident gas increases. In order to maintain the tunnel pressure, it is necessary to

bleed the warmer tunnel gas out of the tunnel, and this controlled gas bleed mass flow allows tunnel pressure control. This complex interaction of the fan-induced heating of the tunnel gas, the liquid nitrogen inflow induced enthalpy decrease and mass increase, and the gaseous nitrogen bleed induced mass and enthalpy decrease, constitutes the tunnel control problem.

This thermodynamic mass-energy interaction has been analyzed in great detail in reference 4, by graphical and analytical techniques. Such an analysis has resulted in a lumped multivariable model of a cryogenic tunnel. The role of the dominant energy storage term, the metal wall stored enthalpy, has been shown to be significant. The following equations, drawn from reference 4, present the basic behavior of a closed-circuit pressure tunnel.

Any closed-circuit wind tunnel with a finite pressure volume V, with nitrogen as the test gas, has a resident gas mass of

$$W_g = 338.9 \frac{PV}{T} \left[1 + 250 \frac{P}{T^2}\right] \text{ kg} \tag{1}$$

when the tunnel fan is run up to a speed of N rpm, the fan develops a temperature and pressure rise across itself by consuming a finite amount of power. Considering the fan compression to be isentropic, we have

$$\text{temperature rise } \Delta T = \frac{T}{\eta} \left[\frac{r^{\frac{\gamma - 1}{\gamma}} - 1}{r^{\frac{\gamma - 1}{\gamma}}} \right] \text{ kelvin} \tag{2}$$

where

$$r = \frac{P_{\text{fan outlet}}}{P_{\text{fan inlet}}}$$

This fan pressure ratio for a closed-circuit tunnel is a function of tunnel circuit losses and can be expressed as

$$\text{pressure ratio} \quad r = 1 + bM^2 \tag{3}$$

where for the 0.3-m TCT facility, the experimentally determined steady-state loss factor is

$$b = 0.197 \left(1 - \frac{7PM}{T}\right)$$

This fan pressure ratio term is a function of Reynolds number and has been expressed empirically in the above equation.

The fan consumes a finite power $\dot{Q}_F$ in creating the tunnel flow, which can be expressed as

$$\dot{Q}_F = \frac{K_F P \sqrt{T}\, M^3}{(1 + 0.2M^2)^3} \quad \text{KJ/sec} \tag{4}$$

where

$$K_F \approx \frac{6965}{\eta} A^* C_p b \left(\frac{\gamma - 1}{\gamma}\right)$$

A^* = test section throat area

Further, the fan speed and the test section mass flow are related by an expression

$$N = k_m \sqrt{T}\, M \tag{5}$$

where, for the 0.3-m TCT, the experimentally derived constant k_m is,

$$k_m = 597(1 - 0.3M)P^{-0.035}$$

In order to maintain the tunnel gas temperature, a liquid nitrogen source of pressure P_L is used to generate a controlled liquid nitrogen mass flow of $\dot{m}_L$ into the tunnel. This is obtained by varying the liquid nitrogen flow control valve area A_L.

$$\dot{m}_L = K_L A_L = K_{L1}\sqrt{P_L - P}\quad A_L \qquad \text{kg/sec} \tag{6}$$

This incoming liquid mass flow is associated with a specific cooling capacity β, which is the heat absorbed by unit mass of liquid nitrogen when taken from the source and evaporated to tunnel temperature at fixed tunnel pressure (ref. 5). Then for equilibrium conditions we have

$$\dot{m}_L\, \beta = \dot{Q}_F - \dot{Q}_t \tag{7}$$

where

$$\beta \simeq \left(121 + C_p T\right) \qquad \text{KJ/kg} \tag{8}$$

and

$\dot{Q}_t$ = Heat absorbed by metal wall

In order to maintain the tunnel pressure, the warmer tunnel gas is bled out at a mass flow rate of $\dot{m}_g$ by a throttle valve of controlled area A_g, out to atmosphere. This mass bleed has a finite enthalpy loss and has a cooling capacity of α. When the tunnel is in equilibrium we have

$$\dot{m}_g = \dot{m}_L = K_g A_g \frac{P}{\sqrt{T}} \tag{9}$$

where, for the 0.3-m TCT, the bleed valve has choked flow $K_g = 21.8$ for $P > 1.5$ atm, and unchoked flow

$$K_g = 21.8\left[2 - \left(\frac{1.5}{P}\right)^{1.7}\right] \text{for } 1 < P < 1.5 \text{ atm}$$

The cooling capacity of the gas bleed is

$$\left.\begin{aligned} \alpha &\simeq \left(C_p - C_v\right) T && \text{KJ/kg} \\ &\simeq 0.3\ T - 0.08\ P && \text{KJ/kg} \end{aligned}\right\} \qquad (10)$$

For the 0.3-m TCT, liquid nitrogen and gas bleed into and out of the tunnel are managed as shown in the schematic figure 2.

In view of the endless nature of the tunnel duct, the total tunnel resident gas mass W_g crosses a given section of tunnel at the rate of the tunnel test section mass flow $\dot{m}$. Thus, under a one-dimensional flow situation, a particle moves around the circuit in a finite time called circuit time under steady-state conditions.

$$t_c = \frac{W_g}{\dot{m}} = \frac{0.0486\ V}{A^*\ M\sqrt{T}} \left[1 + 250\ \frac{P}{T^2}\right] \left[1 + 0.2\ M^2\right]^3 \text{ sec} \qquad (11)$$

The estimated tunnel circuit time for the 0.3-m TCT facility is shown in figure 3, and varies as a function of the tunnel conditions. The fastest circuit time of 0.55 sec occurs at M = 1, P = 1 atm, and T = 300 K. The slowest circuit time of 3 sec occurs at M = 0.2, P = 5 atm, and T = 100 K.

The tunnel resident metal, which is exposed to the gas flow, has a finite amount of enthalpy which is released into the gas whenever the gas temperature differs from the metal temperature. This heat transfer is not uniform and occurs throughout the internal surface of the metal in the tunnel. The mode of heat transfer is the dominantly forced convection type. This heat flow mechanism has been detailed in reference 4, and can be expressed as a simple first order model:

$$\dot{Q}_t = \frac{W_t\ C_m\ TS}{(1 + t_m S)} \quad \text{KJ/sec} \qquad (12)$$

where t_m = metal time constant.

For the 0.3-m TCT facility, this metal-gas heat transfer time constant varies as a function of tunnel P, T, and M. A plot of t_m is shown in figure 4. The largest time constant of 500 sec occurs when heat transfer is slowest at M = 0.2, P = 1 atm, and T = 300 K. The smallest time constant of 20 sec occurs when the heat transfer is best at M = 1, P = 5 atm, and T = 100 K. From this metal time constant, a gas time constant can be defined as

$$t_g = \frac{W_g C_v}{W_g C_v + W_t C_m} \; t_m \quad \text{sec} \tag{13}$$

A plot of the estimated gas time constant is shown in figure 5 and corresponds to the 0.3-m TCT facility. The gas time constant is smallest at M = 1, T = 300 K, and P = 1 atm. The largest time constant occurs at M = 0.2, T = 100 K, and P = 5 atm.

The cryogenic tunnel thermodynamic model, shown in figure 6, can now be used to derive the cryogenic tunnel dynamic model.

Energy

$$\frac{dT}{dt}\left[\frac{1 + t_g S}{1 + t_m S}\right] = \dot{m}_L \left(\frac{\beta + \alpha}{\Theta}\right) e^{-\tau_L S} - \dot{m}_g \left(\frac{\alpha}{\Theta}\right) e^{-\tau_g S} + \frac{\dot{Q}_F}{\Theta} e^{-\tau_F S} \tag{14}$$

where

τ_L = liquid nitrogen particle transit time to the big end $\simeq 0.8\ t_c$ sec

τ_g = gas pulse particle transit time $\simeq 0.1\ t_c$ sec

τ_F = fan heat transit time $\simeq 0.6\ t_c$

$\Theta = W_g C_v + W_t C_m$

Mass

$$\frac{dP}{dt} = \frac{P}{T}\frac{dT}{dt} + \frac{P}{W_g}\left(\dot{m}_L - \dot{m}_g\right) + K_k\, bMP\, \frac{dM}{dt} \tag{15}$$

where $K_k bMP \frac{dM}{dt}$ corresponds to fan acceleration contribution to the pressure.

Tunnel/Fan

$$M\sqrt{T} = \frac{N\, e^{-\tau_g S}}{k_m(1 + t_p S)} \tag{16}$$

where

τ_a = acoustic time lag from fan to big end

t_p = equivalent first order plenum time constant

$k_m = 597(1 - 0.3\ m)\ P^{-0.035}$

These basic equations provide the lumped equivalent of the tunnel dynamical behavior, by expressing tunnel variables T, M, and P as functions of the tunnel control inputs A_L, N, and A_g. Obviously a considerable amount of cross-coupling exists amongst the tunnel variables and the inputs. These equations have been put together to form a multivariable matrix model of a cryogenic pressure tunnel, which is shown in figure 7.

This model has seven nonzero elements and associated gain terms. Equation (12) describing the tunnel temperature dynamics has three gain terms. The steady-state temperature gain for LN_2 input is $(\beta + \alpha)/\Theta$. A plot of this gain for the 0.3-m TCT is shown in figure 8. Typically, the steady-state sensitivity of the tunnel for LN_2 input is about -0.12 K/kg. To cool the tunnel from 300 K to 100 K, one needs about 1,666 kg of liquid nitrogen. However, under transient conditions, the tunnel temperature gain term is $(\beta + \alpha)/W_g C_v$. This transient gain for the 0.3-m TCT is shown in figure 9, and varies from -1 K/kg to -40 K/kg. The steady-state

temperature gain for gas bleed is $-\alpha/\theta$ and is shown in figure 10. Since $|\alpha| < |\beta|$, its contribution is very small.

The tunnel Mach number steady-state gain is a function of K_m and $1/\sqrt{T}$. It is not affected by liquid or gas inputs directly, but coupling does occur through $1/\sqrt{T}$.

The cryogenic tunnel pressure gains are basically derived from equation (15), and are functions of two opposing pressure gradient terms $\frac{P}{W_g} \Delta \dot{m}$ and $\frac{P}{T} \dot{T}$. Together they provide the characteristic pressure signature of a cryogenic tunnel for a liquid nitrogen input. This has been extensively detailed in reference 4. The tunnel pressure gain for gas bleed control input is a simple function of $\frac{P}{W_g}$, due to insignificant contributions from $\frac{P}{T} \dot{T}$. Further, the tunnel pressure gain for fan speed input is contributed to by $\frac{P}{T} \dot{T}$ and K_k bMp $\frac{dM}{dt}$.

CONTROL DEVICES

In order to control a cryogenic pressure tunnel, it is necessary to have control devices which allow fast and linear control of the liquid nitrogen flow into the tunnel, gaseous nitrogen bleed mass flow out of the tunnel, and an adequate degree of resolution and speed of response in the fan speed control. Further, it is necessary to sense the tunnel variables—total pressure, total temperature, and test section Mach number, to a high degree of resolution, accuracy, and speed of response. The details of the control and sensing devices used for the 0.3-m TCT facility are now presented.

Liquid Nitrogen Flow

The operating envelope of the 0.3-m TCT covers a tunnel pressure of 6 atm at 300 K and a test section Mach number of about 0.8. Under these conditions, the fan power consumption is very high and has been estimated from equation (4). To cancel this heat, a liquid nitrogen flow of

$$\dot{m}_L = \frac{\dot{Q}_F}{\beta} \text{ kg/sec}$$

is necessary. The maximum flow is about 10 kg/sec. The liquid nitrogen mass flow is estimated from the equation

$$\dot{m}_L = \frac{K_F P\sqrt{T} M^3}{(1 + 0.2M^2)^3(121 + T)}$$

This has been plotted as a function of tunnel test section Mach number and is shown in figure 11, which represents the tunnel under equilibrium conditions.

The liquid nitrogen injection system must hence be capable of delivering a mass flow of 10 kg/sec into a 6-atm pressure vessel. In the 0.3-m TCT facility, a positive displacement pump capable of 15 kg/sec flow at 10 atm has been used for the LN_2 system. This flow is derived from a 212,000-liter twin tank system, in which the tanks are double walled for vacuum insulation.

A schematic of this system is shown in figure 2. The pump pressure is maintained by a process control type relief valve driven pneumatically. The drive signal is from a pneumatic pI controller, operating on the difference between the set point and the liquid pressure. This system has been tuned to 1 Hz bandwidth at critical damping.

The liquid nitrogen flow is controlled by four digital valves. Each valve has a resolution of 1/1024 of full area. This is achieved by a set of 10 binary weighted orifices which are controlled by a set of solenoids. The flow orifice area starts at 1/1024 of full opening and progressively doubles in the subsequent 9 orifices. The liquid nitrogen mass flow, from the four digital valves which function in parallel, is

$$\dot{m}_L = K_{L1}\sqrt{P_L - P}\quad A_L \qquad \text{kg/sec}$$

where A_L varies from 0 to 1 in steps of 1/1024. Each solenoid has a response time of about 20 msec, and they function in parallel.

Gaseous Nitrogen Bleed

Removal of the warmer tunnel gas from the settling chamber can be performed either on a passive mode or on an active mode. In the case of the 0.3-m TCT, a passive bleed mode for removal of tunnel gas has been used. This is because the tunnel pressure is always in excess of one atmosphere. In order to maintain the tunnel pressure, the gas bleed valve must have the capability of removing a mass flow $\dot{m}_g$ which is generally greater than $\dot{m}_L$. Further, since the liquid valve has a resolution of 1/1024, the gas valve should possess somewhat similar resolution.

As indicated in figure 2, the 0.3-m TCT facility has 3 pneumatically controlled valves operated through process control pneumatic controllers. In series with one of these valves, a 10-element, 8-bit digital valve has been used for purposes of automatic control. This valve has a resolution of 1 in 256. The sonic nozzles representing these binary weighted orifices are controlled in an on-off mode by solenoid piloted pneumatic actuators. This has been necessary because of the large nozzle areas needed to create gas mass flow at low pressure differentials.

Figure 12 shows the valve area necessary to maintain the tunnel at equilibrium. Obviously when the tunnel is running at low pressures, or under unsteady conditions, the valve area required exceeds 100 percent. It is under these conditions that the other two valves can be operated as bias valves, thereby enhancing the equivalent resolution of the digital valves to about 1 in 800. The valve area is estimated as

$$A_g = \frac{K_F \, TM^3}{(1 + 0.2M^2)^3 \, (121 + T) \, K_g} \quad ; \quad \dot{m}_L = \dot{m}_g = K_g A_g \frac{P}{\sqrt{T}}$$

The response speed of the bigger elements of the digital valve is about 150 msec. In a cryogenic tunnel, any valve with a resolution of about 1 in 800 and a full area control response of about 0.5 sec can be considered adequate for pressure control.

Fan Speed Control

The closed-circuit wind tunnel test section Mach number is controlled by the mass flow, which in turn is controlled by the fan pressure ratio and the tunnel circuit loss characteristics. In the case of the 0.3-m TCT, the steady-state tunnel loss/fan characteristics have been experimentally derived and expressed as a fan speed-Mach relationship

$$N = k_m \sqrt{T} \, M$$

where

$$k_m = 597 \, (1 - 0.3M) \, P^{-0.035}$$

A plot of the fan speed as a function of steady-state tunnel variables, total pressure, total temperature, and the test section Mach number is shown in figure 13. The fan has been designed to operate away from the surge line throughout the tunnel envelope.

The tunnel fan speed control is achieved by controlling the electrical supply frequency to the two-pole induction motor driving the fan. In order to maintain motor magnetic flux density, the voltage/frequency ratio of this

variable frequency power generator is maintained constant. The speed is directly proportional to frequency as 120 × frequency/number of poles. The variable frequency supply is a rotating Kramer type of system.

The tunnel variables: total pressure, total temperature and the test section Mach number are sensed by appropriate transducers of adequate accuracy and response. The 0.3-m TCT facility has the following tunnel variable sensing transducers.

Tunnel Total Temperature

The total temperature of the tunnel gas is sensed by a copper constantan junction thermocouple of 800-μ wire diameter. This size is considered a compromise between speed of response and strength of the sensor to withstand high dynamic pressure flows. This thermocouple is located at the center of the settling chamber and downstream of the flow-straightening screens. The output of the thermocouple is nonlinear. Hence the output of the thermocouple is referred to a reference junction maintained at ice point and is linearized to provide 0.1 percent linearity and infinite resolution. Secondly, the response time constant of the thermocouple is a function of the flow conditions over the temperature sensing junction head. It is estimated that the response time constant varies from 0.5 to 3 sec over the tunnel operational envelope.

Total Pressure

The tunnel total pressure is sensed at the settling chamber, downstream of screens and upstream of the contraction using a total pressure probe. This probe is connected to a bonded strain gauge type pressure transducer through an instrument tubing. The transducer behaves linearly and, in the presence of the tube, has an estimated response time of 0.25 sec as a first order lag for small perturbation.

Mach Number

The cryogenic tunnel test section Mach number is estimated on line using two pressure signals corresponding to the tunnel total pressure and the tunnel test section static pressure. The tunnel test section static

pressure probe is connected to a bonded strain gauge transducer through a tube and has a response time of 0.25 sec. Utilizing these pressures, the Mach number is estimated as

$$M = \sqrt{5\left(\frac{P}{P_s}\right)^{-3.5} - 5}$$

The Mach number accuracy is estimated to be about 0.002 to 0.003, and the response about 0.25 sec or better.

Figure 1 shows the locations of the control inputs, the location of the sensors, and figure 14 shows the actuator and sensor performance.

CONTROL ANALYSIS

It is well known that classical and modern control theory provide the basis for the synthesis or analysis of controlling physical systems. In order to generate the appropriate control strategies, it is necessary to describe the physical system in the form of a control-compatible, input-output type of mathematical model. The cryogenic tunnel has been so modeled in the previous sections, and it uses the three control inputs, liquid nitrogen valve area A_L, fan speed N, and gaseous nitrogen bleed valve area A_g in order to control the cryogenic tunnel gas total temperature, the test section Mach number, and the total pressure. A study of the cryogenic tunnel mathematical model of figure 7 reveals that the system is time invariant in parameters, multivariable, and nonlinear in its characteristics. Obviously the closed-loop control analysis of such a system is not a very straightforward one.

In the present research effort, the nonlinearity in the tunnel model is ignored by considering the tunnel to behave linearly for small perturbation. The problem of closed-loop control analysis then becomes the design of a controller for a time-invariant, linear, multivariable, dynamical system.

Two analyses are presented in this section, the first being a further simplification of the model by ignoring the cross-coupling and analyzing the control problem as three separate SISO control efforts. The tunnel total temperature T is assumed to be controlled by the liquid nitrogen flow valve area A_L, the tunnel test section Mach number M to be controlled by the fan speed N, and the tunnel total pressure P to be controlled by the gaseous bleed flow valve area A_g. The second analysis is to seek a noninteractive multivariable controller.

Single Input/Single Output Analysis

If the cryogenic tunnel model of figure 7 were to be a truly diagonal matrix with the off-diagonal terms tending to zero, then each of the tunnel control variables T, M, and P could be uniquely controlled by the control inputs A_L, N, and A_g, respectively. However, since

the off-diagonal elements are not all zero, these can be considered as disturbance on SISO control loops. In the following analysis, the design of temperature and pressure control are considered on an SISO basis.

Temperature control loop. - The cryogenic tunnel, total temperature, control loop schematic is shown in figure 15. In this scheme the tunnel temperature is controlled by the liquid valve area A_L. The cross-coupling from the other two inputs, fan speed N and gas valve area A_g, are shown as external disturbances. The tunnel total temperature T is sensed by a thermocouple providing linear, first order output of time constant t_1. The process temperature and the set point are compared, and the error in the temperature is determined. This error is gain scheduled, a design objective to be determined in this analysis, and is operated on by a pID control law. The resultant signal is used to drive the liquid nitrogen valve, after conditioning the signal to account for valve sensitivity which varies as a function of liquid nitrogen source pressure P_L and tunnel pressure P at the injection point.

Consider the tunnel temperature dynamics of equation (14):

$$\frac{dT}{dt}\left(\frac{1 + t_g S}{1 + t_m S}\right) = K_L A_L \left(\frac{\beta + \alpha}{\Theta}\right) e^{-\tau_L S} - K_g A_g \frac{\alpha}{\Theta} e^{-\tau_g S} + \frac{\dot{Q}_F}{\Theta} e^{-\tau_F S}$$

The tunnel temperature is controlled by A_L, A_g, and $\dot{Q}_F$ (which is proportional to N). Since $|(\beta + \alpha)| > |\alpha|$, the contribution of A_g is ignored. However, $\dot{Q}_F/\Theta$ is dominant; hence a feed forward of this disturbance is necessary.

Let the temperature error (ET)	= T - (ST)
loop gain	= (KT)
liquid nitrogen valve gain	= (KL)
pID controller terms	= (pT), (DT), (IT)
transport delay	$= e^{-\tau_L S} \simeq (1 - \tau_L S)$
sensor dynamics	$= 1/(1 + t_1 S) = H(S)$
valve area	$= (A_L) = ALQ$
forward path transfer function	= G(S)

The open-loop gain product of the temperature loop is

$$G(S)\,H(S) = (KL)(A_L)\left(\frac{\beta + \alpha}{S\Theta}\right) \cdot \left[(pT)(ET) + (IT)\int (ET) + (DT)\,\frac{d}{dt}\,(ET)\right]$$

$$\cdot \frac{(1 + t_m S)}{(1 + t_g S)} \cdot \frac{(1 - \tau_L S)}{(1 + t_1 S)}$$

$$= -(KK)\left[\frac{\left\{(DT)\,S^2 + (pT)\,S + (IT)\right\}\left\{1 + (t_m - \tau_L)\,S - t_m\tau_L S^2\right\}}{S^2(1 + t_1 S)(1 + t_g S)}\right] \tag{17}$$

The system stability is determined by solving the polynomial G(S) H(S) + 1 = 0 and studying the root locations in the complex plane.

$$0 = 1 + G(S)\,H(S)$$

$$= S^4\left[t_1 t_g - (KK)(DT)\,t_m\tau_L\right]$$

$$+ S^3\left[t_1 + t_g - (KK)(DT)(t_m - \tau_L) - (KK)(pT)\,t_m\tau_L\right]$$

$$+ S^2\left[1 + (KK)\left\{(DT) + (pT)(t_m - \tau_L) - (IT)\,t_m\tau_L\right\}\right]$$

$$+ S\left[(KK)(pT) + (KK)(IT)(t_m - \tau_L)\right]$$

$$+ (KK)(IT) \tag{18}$$

where

$$KK = \frac{-(KL)(A_L)(\beta + \alpha)}{\Theta}$$

The roots of the polynomial of equation (18), when (KK) → 0, are called the poles of the system. The poles are also the roots of the denominator polynomial of equation (17). The roots of the polynomial of equation (18), when

(KK) $\rightarrow \infty$, are the zeros of the system and correspond to the roots of the numerator polynomial of equation (17). As the system gain (KK) is taken from zero to a large value, the roots of the system start from the poles and end at the zeros. These root movements can be represented graphically on the complex plane, and these loci are called the root loci of the system. The location of the roots at any finite gain (KK) provide an insight into the stability and accuracy of the system.

The poles of the temperature control loop of the 0.3-m TCT cryogenic tunnel are

$$S = 0;\ S = 0;\ S = -\frac{1}{t_g};\ S = -\frac{1}{t_1}$$

The zeros of the temperature control loop are

$$S = -\frac{1}{t_m};\ S = \frac{1}{\tau_L};\ S = \frac{-(pT) \pm \sqrt{(pT)^2 - 4(DT)(IT)}}{2(DT)}$$

The qualitative asymptotic root loci for the temperature control loop are shown in figure 16. The axes of the plot are the real and imaginary values of the root S. Typically, any point ($S = \sigma + j\omega$) on the plot corresponds to a time-dependent response of the type

$$e^{St} = e^{(\sigma \pm j\omega)t} \tag{19}$$

As long as σ is negative with ω at zero, the system response is over-damped convergence. A σ which is negative with finite $\pm j\omega$ corresponds to an oscillatory convergence. When $-\sigma = \pm j\omega$ the system is critically damped; when $\sigma = 0$ with a finite $j\omega$ the system is oscillatory and continues to oscillate at a steady value. When roots move to the right side with σ positive, the system diverges.

The temperature control system has four poles and four zeros (fig. 16). Hence the four root trajectories start at poles and end at zeros. The two integrator poles move from the origin to the negative real zero of metal and controller. These root values correspond to the time response of metal.

The other two roots corresponding to gas and sensor are on the negative real axis, but as the system gain is increased the two move towards each other and break away symmetrically into the complex plane. At low Mach numbers, these roots move to the right and cross over, suggesting oscillatory and unstable responses at high gains. When the tunnel flow Mach number is high, the roots move to the left, suggesting stable behavior. In both the cases, the roots move to the zeros and one of these moves around the Reimann sphere to arrive at either controller zero or transport zero.

These root movements are shown in the asymptotic root locus plot of figure 16. Further, figure 17 shows one quadrant of the gas roots for various Mach numbers at T = 200 K and P = 1, 3, and 5 atm. The system tends to be unstable at high gains at M = 0.2. At M = 0.4 and 0.9, the system is more stable. Figure 18 shows one quadrant motion of gas roots for varying temperatures. The following inferences can be drawn from figures 16, 17, and 18:

(1) The temperature control loop tends to go unstable at high gains and low Mach numbers.
(2) Tunnel pressure has relatively weaker effects on system stability and bandwidth.
(3) Tunnel temperature control bandwidth improves with Mach number.
(4) Tunnel temperature control is very stable at high Mach Numbers.

A set of root loci was generated by varying T from 100 K to 300 K, P from 1 to 5 atm, and m from 0.2 to 1, to cover the bulk of the tunnel operational envelope for the 0.3-m TCT facility. The loop gain necessary to operate the temperature control loop at critical damping was determined and a curve fit was made. The pID control gains were also scanned. Thus an acceptable nonlinear gain schedule was determined for (KK) as

$$(KK) \propto M\sqrt{\frac{P}{T}}$$

since

$$(KK) = (KL)(A_L)\left(\frac{\beta + \alpha}{\theta}\right), \quad A_L = \frac{(KT)}{(KL)} M\sqrt{\frac{P}{T}} \tag{20}$$

where

$$(KT) = \text{loop gain}\left(\frac{\theta}{\beta + \alpha}\right)$$

Hence, a relatively large loop gain can be used when $M \simeq 1$, $P \simeq 6$ atm, $\Delta T \simeq 100$ K, and there is a small gain at $M \simeq 0.2$, $P \simeq 1.5$ atm, and $T \simeq 300$ K. The range of gain change is about 1:20.

The steady-state accuracy of the temperature loop is very good because the system has two integrations as shown in the model of equation (17). The temperature loop also has a zero error for ramp command and hence possesses adequate accuracy of control.

Pressure control loop. - The cryogenic tunnel, pressure control loop schematic is shown in figure 19. The tunnel total pressure is assumed to be controlled by gas valve area A_g. This control loop is disturbed by liquid nitrogen mass flow input and by the tunnel temperature gradient. The tunnel total pressure is sensed by a transducer which has a first order response with a time constant of t_2 seconds. The tunnel pressure is compared with the desired pressure set point and the error is determined. This error is gain scheduled, the gain schedule being the design objective, and is operated on by a pID control law. The resultant signal is used to drive the gas bleed valve after conditioning it for valve flow gain sensitivity.

Consider the tunnel total pressure dynamics of equation (15):

$$\frac{dp}{dt} = \frac{P}{T}\frac{dT}{dt} + \frac{P}{W_g}\dot{m}_L - \frac{P}{W_g}\dot{m}_g + K_k\, bMP\, \frac{dM}{dt}$$

The tunnel pressure is controlled by A_g directly and is disturbed by A_L, $\frac{dT}{dt}$, and $\frac{dM}{dt}$. Hence

$$\frac{dP}{dt} = -\frac{P}{W_g} K_g A_g + [\text{Disturbances}] \tag{21}$$

The tunnel pressure control behavior can now be analyzed. Let

pressure loop error	$= (EP) = P - (SP)$
loop gain	$= (KP)$
gas bleed valve gain	$= (KG)$
pID controller terms	$= (pP), (DP), (IP)$
transport delay	$= e^{-\tau_g S} \simeq 1 - \tau_g S;\ \tau_g \simeq 0.1\ t_c$
pressure sensor	$= 1/(1 + t_2 S) = H(S)$
forward path transfer function	$= G(S)$

Then open-loop gain product is

$$G(S)\ H(S) = \frac{-(KG)(AG)p^2}{W_g \sqrt{T}\ S^2} \left[(pP)(EP) + (IP)\int (EP) + (DP)\ \frac{d}{dt}\ (EP)\right] \cdot \frac{(1 - \tau_g S)}{1 + t_2 S} \tag{22}$$

The stability of this loop in its automous condition can be analyzed by using root locus analysis.

$$\begin{aligned} 0 = 1 + G(S)\ H(S) = {} & S^3 \left[t_2 - (KK)\ (DP)\ \tau_g\right] \\ & + S^2\left[1 + (KK)\ (DP) - (DP)\ (KK)\ \tau_g\right] \\ & + S\left[(KK)\ (pP) - (IP)\ (KK)\ \tau_g\right] \\ & + (IP)\ (KK) \end{aligned} \tag{23}$$

where

$$(KK) = \frac{(KG)(AG)P^2}{W_g\sqrt{T}}$$

The poles of the pressure loop polynomial are

$$S = 0;\ S = 0;\ S = -\frac{1}{t_2}$$

The zeros of the pressure loop polynomial are

$$S = \frac{1}{\tau_g};\quad S = \frac{-(pP) \pm \sqrt{(pP)^2 - 4(DP)(IP)}}{2(DP)}$$

The asymptotic root trajectories for the pressure loop are shown in figure 20. This root set has three trajectories as (KK) is varied from zero to a large value. Obviously, the tunnel pressure loop is stable but oscillatory because of dominant disturbances from liquid flow, temperature gradient, and fan effects. The two integration poles break away from the origin to the left as a complex pole pair and join together at high gains to reach the transport zero by moving through the Reimann sphere pole. The inferences that can be drawn from this analysis are

(1) The pressure loop is basically stable, but always oscillatory with an underdamped convergent response.

(2) The tunnel flow Mach number does not affect the pressure loop directly, but does so through the temperature loop.

(3) Dual integration in the loop provides high steady-state accuracy but always has an overshoot.

A number of tunnel conditions were tried on the above analysis, and the pressure loop gains (KK) were determined at critical dumping for various tunnel conditions. A nonlinear gain schedule was determined for the pressure loop as

$$(KK) \propto \frac{1}{P\sqrt{T}}$$

since

$$(KK) = \frac{(KG)(AG)p^2}{W_g\sqrt{T}} \quad , \quad (AG) \propto \frac{W_g\sqrt{T}}{P^2(KG)}$$

or

$$(AG) = \frac{(KP)}{(KG)} \frac{1}{P\sqrt{T}} \tag{24}$$

where

(KP) is the loop gain term.

Multivariable Control Analysis

Consider a linear time-invariant, multivariable system described by a square (n × n) transfer function matrix [Z(S)] which is nonsingular and hence invertible. The basic principle of deriving a noninteractive controller for such a system is by diagonalization. A controller matrix [C(s)] is derived such that the open-loop system matrix product [C(S)] · [Z(S)] becomes a diagonal transfer function matrix [R(S)], whose diagonal elements form the characteristic equations of the n single input-single output systems (ref. 6).

Thus

$$[C(S)][Z(S)] = [R(S)]$$

or

$$[C(S)] = [Z^{-1}(S)][R(S)]$$

Most of the frequency domain multivariable controller design problems exist because of the characteristics of the inverse $[Z^{-1}(S)]$ and its properties.

For a typical system, prediction terms like pure lead or $e^{\tau S}$ occur in the $[Z^{-1}(S)]$ which are difficult to realize. These problems have led to analytical techniques like the concept of diagonal dominance (ref. 7) and analyses by inverse Nyquist array (ref. 8) in the design of multivariable controllers.

In the present research effort, it has been assumed that $[Z^{-1}(S)]$ is physically realizable by ignoring the transport delay terms.

If a matrix Z is a 3×3 matrix of type

$$Z = \begin{bmatrix} a_{11} & a_{12} & a_{13} \\ 0 & a_{22} & 0 \\ a_{31} & a_{32} & a_{33} \end{bmatrix}$$

then

$$Z^{-1} = \begin{bmatrix} b_{11} & b_{12} & b_{13} \\ 0 & b_{22} & 0 \\ b_{31} & b_{32} & b_{33} \end{bmatrix} = \frac{1}{Det} \begin{bmatrix} a_{22}a_{33} & a_{13}a_{32}-a_{12}a_{33} & -a_{22}a_{13} \\ 0 & a_{11}a_{33}-a_{13}a_{31} & 0 \\ -a_{22}a_{31} & a_{12}a_{31}-a_{11}a_{32} & a_{11}a_{22} \end{bmatrix}$$

where

$$Det = a_{22}\,[a_{11}a_{33} - a_{13}a_{31}]$$

For the 0.3-m TCT facility modeled by the equation of figure 7, we have an inverse matrix $Z^{-1}(S)$ shown in figure 21, in which contributions of the transport delay terms have been ignored. If the goal is to realize three independent loops for temperature, pressure, and Mach number described by $[R(S)]$:

$$[R(s)] = \begin{bmatrix} \frac{1}{S} & 0 & 0 \\ 0 & \frac{1}{1 + t_p S} & 0 \\ 0 & 0 & \frac{1}{S} \end{bmatrix}$$

Then the controller $[C(S)]$ is

$$[C(S)] = [Z^{-1}(S)][R(S)]$$

and the controller $[C(s)]$ is described by figure 20, in which the differentiator S is absent in columns 1 and 3 and $(1 + t_p S)$ is absent in column 2.

It may be noted that, with this noninteractive controller, the three open-loop transfer functions become

$$\frac{-K_L K_g}{k_m} \qquad \frac{(1 + t_m S)}{s^2(1 + t_p S)(1 + t_g S)} \qquad \frac{p^2 \beta}{W_g T}$$

The element b_{11} of the controller could be simplified to the SISO temperature control law of equation (20), and the element b_{33} of the controller is the SISO control law of equation (24). Thus the noninteractive controller embraces the SISO control laws as particular cases.

VALIDATION OF THE SISO CONTROL LAWS

As detailed in reference 4, the mathematical model of the 0.3-m TCT facility has been simulated on a hybrid computer. This real-time, interactive, cryogenic tunnel simulator is shown in figure 22. The hybrid scheme for simulation consists of obtaining the linear dynamical solutions on the analog computer which is updated by the nonlinear coefficients which are computed precisely on the digital processor. Figure 23 shows the basic scheme for hybrid simulation. The analog and the digital processors communicate with each other at 25 Hz. In figure 24, the temperature dynamics simulation is shown. Figure 25 shows the pressure, Mach number, and fan dynamics simulation. In figure 26 the valve control interface is shown. The SISO control laws are implemented on the hybrid tunnel simulator as shown in figure 27, and as detailed by equations (20) and (24).

This cryogenic tunnel simulator has been validated for its steady-state, quasi-steady, and transient response by good reconcilation of the 0.3-m TCT responses and the simulator responses for cool down, warm-up, and open door impulse responses for all the control inputs (ref. 4).

The tunnel temperature loop is closed as shown in figures 23 and 27, and it includes the model for a thermocouple whose response time varies as a function of tunnel conditions. The tunnel pressure loop is closed as shown in figures 24 and 27 and includes the pressure sensor dynamics. Both the tunnel temperature and pressure loop worked satisfactorily. In figure 28, the tunnel total temperature and the total pressure are on closed-loop control with the fan speed controlled on a speed-control loop maintained at a constant speed. The initial tunnel conditions are P = 2.2 atm, T = 263 K, and M = 0.69. Firstly, a temperature set point command of +16 K has been imposed. The tunnel temperature has changed from 263 K to 279 K in about 20 sec. The gas temperature responds quickly. Since the tunnel metal is still near 263 K, the gas temperature varies slowly from 278 to 279 K. During this period, the tunnel pressure loop opposes the mass variation and maintains the pressure at 2.2 atm. The pressure is disturbed in an oscillatory manner but recovers to the steady-state value in about 25 sec. The

tunnel Mach number tracks the tunnel temperature by the law $1/\sqrt{T}$. After about 90 sec, the tunnel gas temperature set point is changed from 279 K to 263 K. The control system maintains the tunnel pressure, and the temperature settles at 263 K in about 25 sec. Since the metal temperature is still near 263 K, no creep in gas temperature is evident.

Secondly, the pressure loop set point has been changed from 2.2 atm to 1.86 atm, while keeping fan speed constant and temperature set point at 263 K (fig. 28). The tunnel pressure smoothly drops to 1.86 atm and has a convergent oscillatory response as predicted. The pressure settles down in about 30 sec. The temperature loop fights the enthalpy change caused by gas valve and settles down when the pressure is steady. The tunnel Mach number is affected only by the temperature during the transition, and the change of pressure has very little effect on Mach number. Subsequently, the tunnel pressure set point has been changed back to 2.2 atm. It may be noted that the pressure response is slower in transition to a higher pressure. This is caused by the tunnel gas accumulation which occurs only at the rate of $\dot{m}_L$. The temperature loop fights the coupling and settles down when the pressure settles. Mach number is also changed back to the starting value. The pressure coupling on Mach number is through the term $P^{-0.035}$, which is very weak.

Thirdly, the tunnel fan speed has been changed such that the Mach number varies from 0.69 to 0.59 while keeping the temperature loop set point at 263 K and pressure set point at 2.2 atm. It may be noted that the control loops maintain temperature to within ±0.25 K and pressure to ±0.017 atm. The Mach number has been further changed from 0.79 to 0.59 and from 0.59 to 0.69. In the presence of these gross power changes, the pressure and the temperature have been well regulated by the controllers.

In figure 29, a similar set of set point commands for temperature, pressure, and fan speed is shown. The tunnel temperature is at 90 K, pressure at 2.2 atm, and Mach number at 0.75. Again, the temperature and pressure control systems behave adequately. When the system temperature changes from 90 K to 82 K, pressure is changed from 2.2 atm to 1.86 atm, and Mach number from 0.75 to 0.85 through 0.65.

In summary, the control laws derived in equations (20) and (24) provide satisfactory closed-loop temperature and pressure control. These SISO control laws are adequate to counter the strong cross-coupling between the tunnel process variables and the control inputs.

TUNNEL CONTROLLERS

Hitherto the detailed development of the control law for automatic control of the 0.3-m TCT facility was discussed. Further, the adequacy of these control laws to hold closed-loop control within desired specifications was proved by testing the control algorithms on the real-time cryogenic tunnel simulator. In this section, the mechanization of these control laws using electronic control hardware is discussed.

Tunnel Closed-Loop Controls

The detailed schematic diagrams for the tunnel temperature and pressure are shown in figures 30 and 31.

Temperature loop. - In figure 30, the temperature control scheme used for the 0.3-m TCT facility is detailed. The control law used is

$$(ET) = T-(ST)$$

$$(ALQ) = \frac{M\sqrt{P}(KT)}{(KL)\sqrt{T}}\left[(pT)(ET) + (IT)\int(ET) + (DT)\frac{d}{dt}(ET)\right] + (KB)(FF) \qquad (25)$$

This control law is the one derived in equation (20). Additionally, provision has been made to have fan power bias on an on-off mode. The bias is the equivalent liquid nitrogen flow to cancel fan heat. Hence,

$$(KB) = \frac{\dot{Q}_F}{\beta}$$

This has been compensated for valve gain, as

$$(KB) = \frac{(QDF)}{(121+T)(KL)} \qquad (26)$$

In a cryogenic tunnel, the fan power feed forward is necessary only while cooling down or while regulating the temperature. When the tunnel is warming up, feed forward would be a waste of liquid nitrogen. Hence the feed forward is switched on based on the following logic:

If	(ET) > 0	FF is on	
If	(ET) < -5	FF is off	(27)

This error-based switching of feed forward is shown in figure 32. This logic has a built-in 5 K hysteresis to prevent hunting in temperature.

Secondly, when the tunnel is warm at 300 K and at fairly low pressure, switching the automatic temperature loop with a 100 K set point would result in large liquid nitrogen flow on a pID law. This may lead to liquid in the tunnel and large thermal shocks. It may be noted that to cool the 0.3-m TCT nearly 1,800 kg of LN_2 is required and this cannot be done fast. Hence, a saturation term on the LN_2 flow from the controller is proposed.

$$\text{Maximum } LN_2 \text{ allowed: } \frac{\text{Fan power}}{\beta(KL)} + \begin{matrix}\text{Steady gas temperature} \\ \text{cool down at a known gradient}\end{matrix}$$

$$\text{Max} = (KB)(FF)(1-LLT) + \frac{255\ PV\ (TGR)}{T(121+T)(KL)}(1-LLT) + LLT \tag{28a}$$

Again, this saturation is used only when set point is more than 10 K away from tunnel temperature. This logic is also imposed as a hysteresis through LLT logic discussed below and illustrated in figure 32.

where	if	ET < 5 ,	LLT = 1
and	if	ET > 10 ,	LLT = 0 (28b)

Thus the temperature loop works on a gain scheduled pID law near the desired set point. When large errors are encountered, appropriate saturation and feed-forward compensation are used to prevent thermal shocks and energy wastage.

Pressure loop. - Figure 31 details the schematic diagram for the control of tunnel total pressure. The control law used is

$$(EP) = P-(SP)$$

$$(AG) = \frac{(KP)}{(KG)P\sqrt{T}}\left[(pP)(EP) + (IP)\int(EP) + (DP)\frac{d}{dt}(EP)\right] \tag{29}$$

This control law may be recognized as the control law of equation (24). The pressure loop is not affected by large errors, except that when the tunnel pressure is low and the mach number is high, valve area in excess of 100 percent of the gas bleed valve is necessary. Hence an automatic law for opening two parallel analog valves as a bias has been proposed. This logic is

$$
\begin{aligned}
&\text{SUM} = 0 \\
&\text{If} \quad A_G > 0.9 \quad , \text{SUM} = \text{SUM}_{past} + 0.125 \\
&\text{If} \quad A_G < 0.5 \quad , \text{SUM} = \text{SUM}_{past} - 0.125 \\
&\text{If} \quad \text{SUM} < 1 \quad , \text{A1} = \text{SUM} \;\; \& \;\; \text{A2} = 0 \\
&\text{If} \quad \text{SUM} > 1 \quad , \text{A1} = 1.0 \quad \text{A2} = \text{SUM}-1
\end{aligned}
\tag{30}
$$

This logic automatically opens a parallel bias valve by 12.5 percent whenever the automatic control valve reaches 90 percent on control. A maximum of 200 percent area is thus available at low pressures. The logic also automatically shuts off the bias valves. A time delay of UA is imposed in this logic to prevent hunting.

Microprocessor-Based Controller

In order to execute the complex control law on the tunnel, an electronic controller is necessary. The choice between an analog processor or a digital processor is decided by the complex nonlinear computation that needs to be performed. Analog controllers cannot perform such functions accurately. Hence, a digital microprocessor controller has been proposed. This microprocessor is required to continuously sense the various tunnel variables, compute the linear and logic components of the control law, and generate appropriate commands for driving the control input actuators. Following are the functional requirements of such a controller.

The microprocessor is required to sense the tunnel variables, total temperature to a resolution of 0.1 K or better, total pressure to a resolution of 0.006 atm, fan speed to about 0.1 percent, fan power to about 1 percent, and liquid nitrogen pressure to about 1 percent. Maximum values of these variables are 350 K, 6 atm, 7,200 rpm, 2,000 kW and 14 atm, respectively.

Hence, the microprocessor should resolve the incoming signals to about 0.025 percent resolution. This corresponds to a 12-bit AD converter having a 6-channel capability. Typically 0- to 5-V DC signals from sensors can be considered.

The bandwidth of the tunnel temperature and pressure control systems is about one rad/sec. In order to implement such a control, the microprocessor controller must function at at least 10 cycles of computation/sec.

In view of the complex nonlinear computations, the microprocessor arithmetic unit must have a floating point capability. This can be achieved only by floating point hardware, considering the quantity of computation to be performed in each cycle and the accuracy desired.

The various I/O devices on the microprocessor controller are the AD converters for signal inputs, the data entry switches for the tunnel set point variables and the loop constants, and either direct digital or DA-converted analog outputs for the actuators and displays.

For the 0.3-m TCT facility, the following I/O devices have been proposed. The tunnel variables, total pressure, static pressure, total temperature, fan speed, fan power, and liquid nitrogen pressure are digitized through a six-channel multiplexer and AD converter. The tunnel operator controls consist of dedicated decimal thumbwheel inputs for the pressure and temperature set points with their read buttons, and a set of data entry thumbwheels to put in about 60 loop constants through a key switch. The operator display consists of the tunnel set points, the tunnel variables, and the actuator commands, each for the pressure and the temperature loop. Provision for auto-hold-manual switching of each loop is provided. A view of the controller front panel is shown in figure 33. The microprocessor controller output consists of 2 10-bit pure binary digital valve drives for the liquid and gaseous nitrogen control valves, two analog outputs for liquid and gaseous nitrogen control valves (optionally), and two analog outputs for the bias analog valves.

Control Flow Chart

The detailed functional flow chart for automatic control of the 0.3-m TCT is provided in Appendix A. This flow chart is a numerical mechanization of the control laws of equations (25) to (30), shown in figures 30 and 31.

Firstly, the tunnel variables T, P, P_s, N, P_L, and the fan power are AD converted and scaled into appropriate engineering units. Then the temperature control laws of equations (25) to (28) are mechanized including the liquid valve gain adaptation. The pID control law is invoked when in "auto" mode. In the "manual" mode, the liquid valve is directly driven by the command. In the "hold" mode, the valve position is locked. The actuator for the liquid flow valve can be updated at a rate of UT cycles.

The pressure control law of equations (29) and (30) is then mechanized with provision for automatic bias valve control. The pID control law is invoked only in the auto mode. The manual and hold modes function similarly to the temperature loop.

The various statements of the flow chart in the Appendix are self-explanatory. These allow for necessary sensing, control laws—linear and logic, actuator drive, and display of 10 quantities. Further, provision has been made for fast emergency function of the pressure and the temperature control valves. The liquid valve fully closes on emergency, and the gas bleed valves open fully to avoid overpressurizing the wind tunnel.

CLOSED-LOOP CONTROL RESPONSES FOR THE 0.3-m TCT

The control laws have been realized on a Motorola 6800 microprocessor, which is an 8-bit, 24 K memory processor. The control flow chart has been translated to an assembler language program which has been burned into the Read Only Memory of the processor. The high-speed arithmetic capability has been obtained on floating point hardware mathematical chips. With this unit, the microprocessor controller is capable of performing all the control functions in about 70 msec. The program is designed to run at a rate of 100 msec per cycle using an internal clock.

This microprocessor controller has been successfully commissioned to realize pressure control to ±0.017 atm and ±0.25 K. In figure 34, a typical tunnel run of the 0.3-m TCT facility is shown, while under automatic control. Initially a temperature set point of 100 K and a pressure set point of 2.1 atm were sought, and microprocessor control was switched on auto mode. Because of large temperature error, the LN_2 flow was limited with feed forward on. The tunnel pressure built up in about 30 sec. The tunnel temperature moved slowly to 100 K in about 30 min at a typical rate of 7 K/min for the metal. Once the temperature stabilized, the pressure was built up to 5.5 atm. Initially a +2 K step was tried on temperature which was rapidly achieved. Then a number of mach number changes from 0.3 to 0.8 were tried with a high blockage model put through many angle programs. The wiggles in temperature and pressure of figure 34 are attributable to onset of these disturbances. In every case the temperature settled to within $\pm$ 0.25 K, and pressure within ±0.017 atm of set point. During the tunnel run, the pressure set points were changed from 5.5 atm to 3.4 atm and temperature from 100 to 120 K. Throughout the run of figure 34, both pressure and temperature loops worked well against various disturbances.

In figure 35, a temperature set point change and its coupling to the pressure loop are shown. The pressure has taken about 30 sec to stabilize and temperature stabilizes in about 15 sec. Since the presently used controller has a 10-bit ADC, a small limit cycle of about 0.25 K is occasionally evident in the temperature. Similarly, the pressure loop also has a small amplitude limit cycle caused by 10-bit ADC. Presently, conversion to

12-bit ADC is being planned and should reduce the occasional limit cycling to less than 0.1 K and 0.005 atm.

In figure 36, both the pressure and temperature loops have been controlled in closed loops to achieve stepped movement of P and T towards liquid gas phase transition. This diagram shows the quality of control since no Mach or model attitude disturbances are present. A pressure control instability was encountered at very low Mach number and low power conditions at high temperatures. The pressure control loop functions on the basis of mass balance between incoming liquid nitrogen $\dot{m}_L$ and gas bleed mass flow $\dot{m}_g$. Under low-power conditions, the $\dot{m}_L$ required to cancel fan heat is very low. The temperature sensitivity to $\dot{m}_L$ is high at temperatures and hence the temperature loop does not work fully in the proportional band but on the threshold of the on-off mode. The pressure control loop tracks $\dot{m}_L$ and hence has a tendency for instability due to discontinuous $\dot{m}_L$. The problem was found to alleviate itself as the power level was increased to M = 0.25.

CONCLUDING REMARKS

In this report the design of a closed-loop automatic controller for a closed-circuit cryogenic pressure tunnel has been detailed, and has been successfully used to control the 0.3-m TCT facility. The following observations sum up the achievements of this effort:

(1) The mathematical control model of a cryogenic tunnel, synthesized and validated as detailed in reference 4, has been successfully used in the control studies.

(2) Two single-input/single-output type control laws have been developed for automatic closed-loop control of the tunnel's total temperature and total pressure.

(3) The control laws devised are nonlinearly gain scheduled, pID control laws. These have provided satisfactory closed-loop control of the tunnel, firstly on the real-time cryogenic tunnel simulator and subsequently on the 0.3-m TCT facility.

(4) Presently, regulation accuracies of ±0.25 K in temperature and ±0.017 atm in pressure have been achieved on the 0.3-m TCT. Improvements to ±0.1 K and ±0.005 atm accuracy in regulation are being planned by conversion of 10-bit ADC to 16-bit ADC in the controller.

(5) The control flow chart developed is a general one and can be used on any cryogenic pressure tunnel.

(6) The nonlinear control logic has been found to provide a safe method for gross tunnel condition changes under closed-loop control.

(7) Some pressure control problems were encountered at very low Mach number and high-temperature conditions attributable to nonlinear coupling from the temperature loop into the pressure loop. The problem corrects itself at about M = 0.25 and above.

(8) It has been shown that the cryogenic tunnel process is basically well behaved and the control problem can be solved.

ACKNOWLEDGMENTS

The author wishes to acknowledge and thank the following persons from NASA/LaRC for their contributions to this project:

- Dr. R.A. Kilgore for his overall direction of the control efforts, and
- J.J. Thibodeaux for his contributions and participation in the effort.

Further, the author wishes to acknowledge the participation of Dr. G.L. Goglia, Eminent Professor and Chairperson, Department of Mechanical Engineering and Mechanics, Old Dominion University, in the project effort and thank him for his administrative guidance.

APPENDIX A

FLOW CHART FOR CLOSED-LOOP CONTROL OF A FAN-DRIVEN CRYOGENIC WIND TUNNEL

LIST OF CONTROLS AND DISPLAYS

CONTROLS

1. Four digit dedicated decimal thumbwheel controls for SP
2. Four digit dedicated decimal thumbwheel controls for ST
3. Six digit floating/fixed point with polarity decimal thumbwheel controls for all other DATA
4. Two digit dedicated decimal thumbwheel for DATA ID
5. Push buttons (12)

   Temperature Loop: Read, Emergency, Auto, Hold, Manual
   Pressure Loop: Read, Emergency, Auto, Hold, Manual
   Other: Feed Forward, LN_2 Limit

DISPLAYS

1. Four 4 digit decimal displays for SP, P, ST, T
2. Two 3 digit decimal displays for AG, ALQ
3. One 6 digit floating/fixed point display for all DATA
4. One 2 digit display for DATA entry ID
5. Four 4 digit decimal displays for GFLOW, FLOW, MAX, WG
6. LED on-off lamps for

   Two operate
   Two auto
   Two hold
   Two manual
   Two emergency
   Seven, FF on/FF off/LLT on/LLT off/MEM fault/full open/low pressure

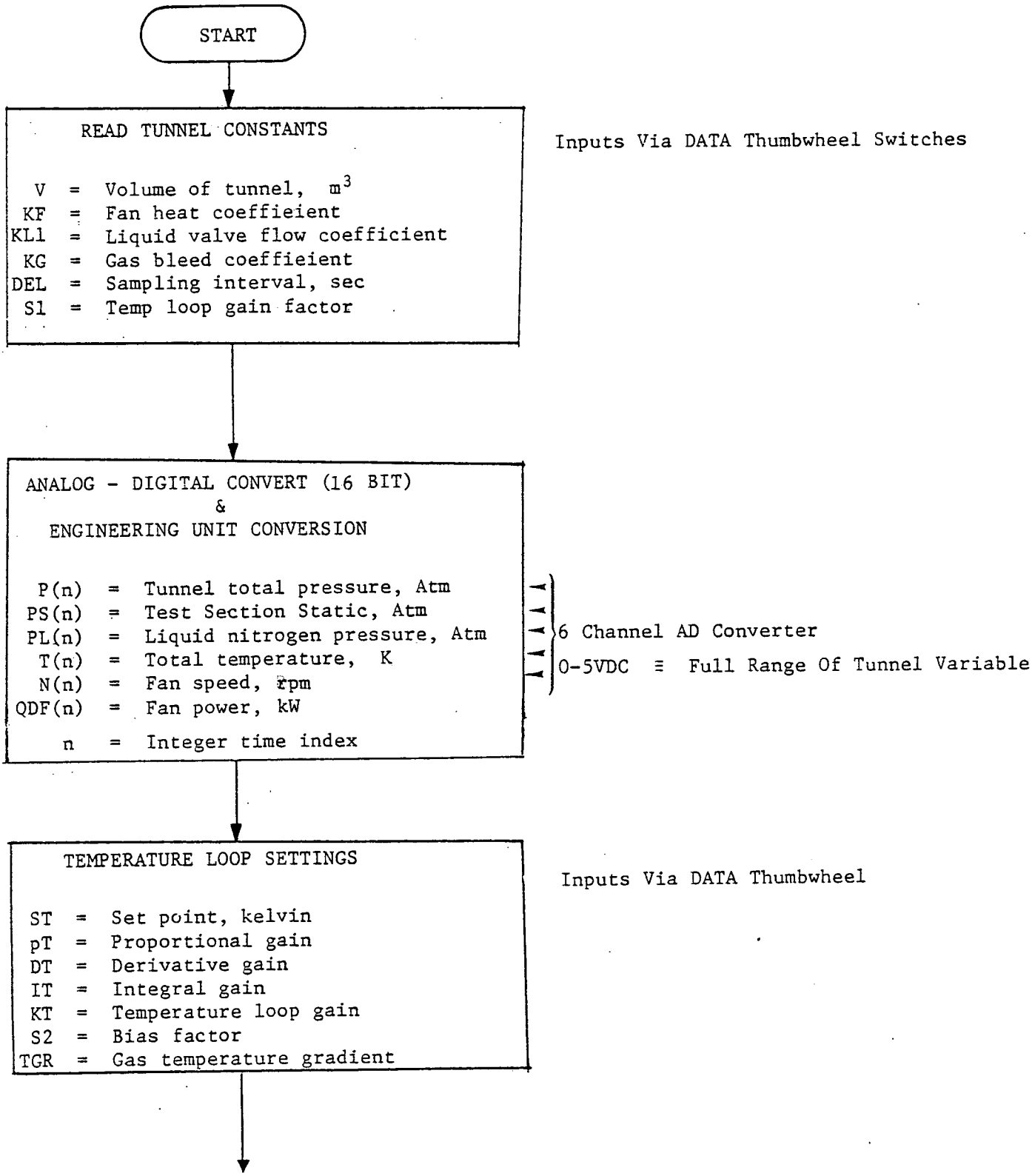
START
READ TUNNEL CONSTANTS
V = Volume of tunnel, m3
KF = Fan heat coeffieient
KL1 = Liquid valve flow coefficient
KG = Gas bleed coeffieient
DEL = Sampling interval, sec
S1 = Temp loop gain factor
Inputs Via DATA Thumbwheel Switches
ANALOG - DIGITAL CONVERT (16 BIT)
&
ENGINEERING UNIT CONVERSION
P(n) = Tunnel total pressure, Atm
PS(n) = Test Section Static, Atm
PL(n) = Liquid nitrogen pressure, Atm
T(n) = Total temperature, K
N(n) = Fan speed, rpm
QDF(n) = Fan power, kW
n = Integer time index
6 Channel AD Converter
0-5VDC ≡ Full Range Of Tunnel Variable
TEMPERATURE LOOP SETTINGS
ST = Set point, kelvin
pT = Proportional gain
DT = Derivative gain
IT = Integral gain
KT = Temperature loop gain
S2 = Bias factor
TGR = Gas temperature gradient
Inputs Via DATA Thumbwheel

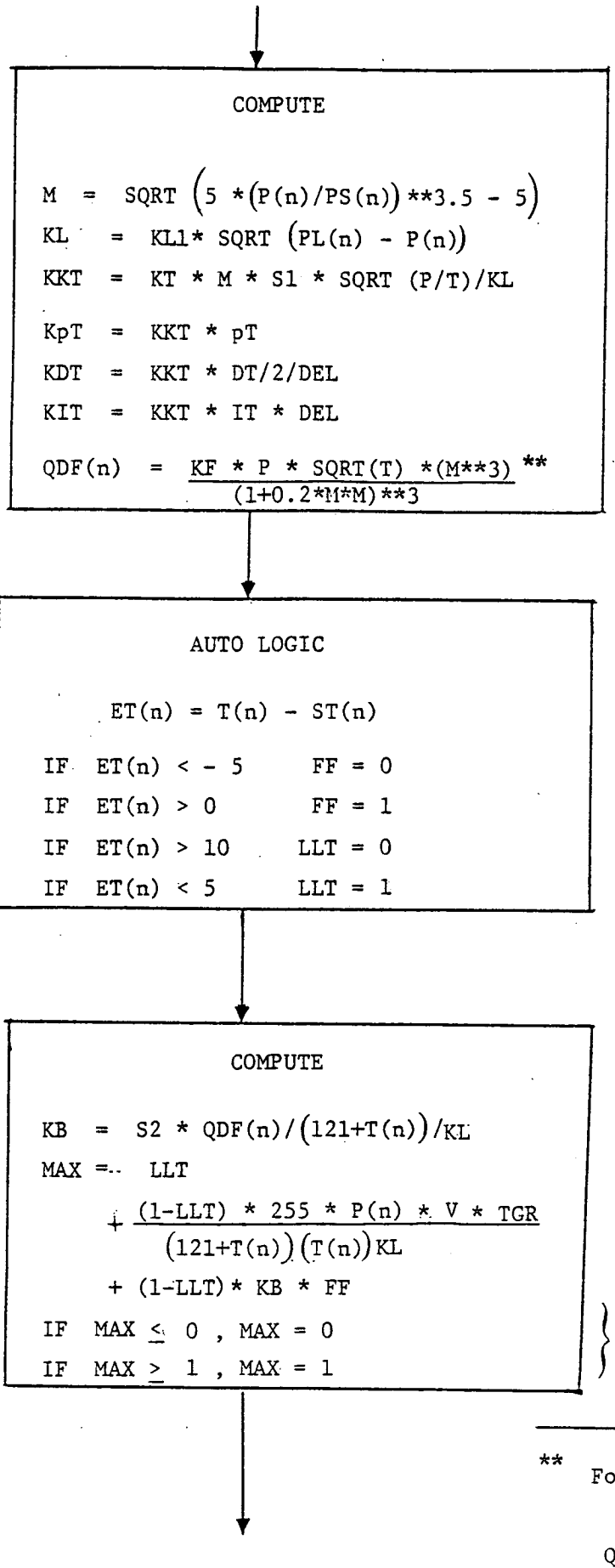

** For the 0.3-m TCT

$$QDF(n) = 100 \frac{P(n)}{\sqrt{T(n)}} \left[\frac{N}{1000}\right]^{2.4} kW$$

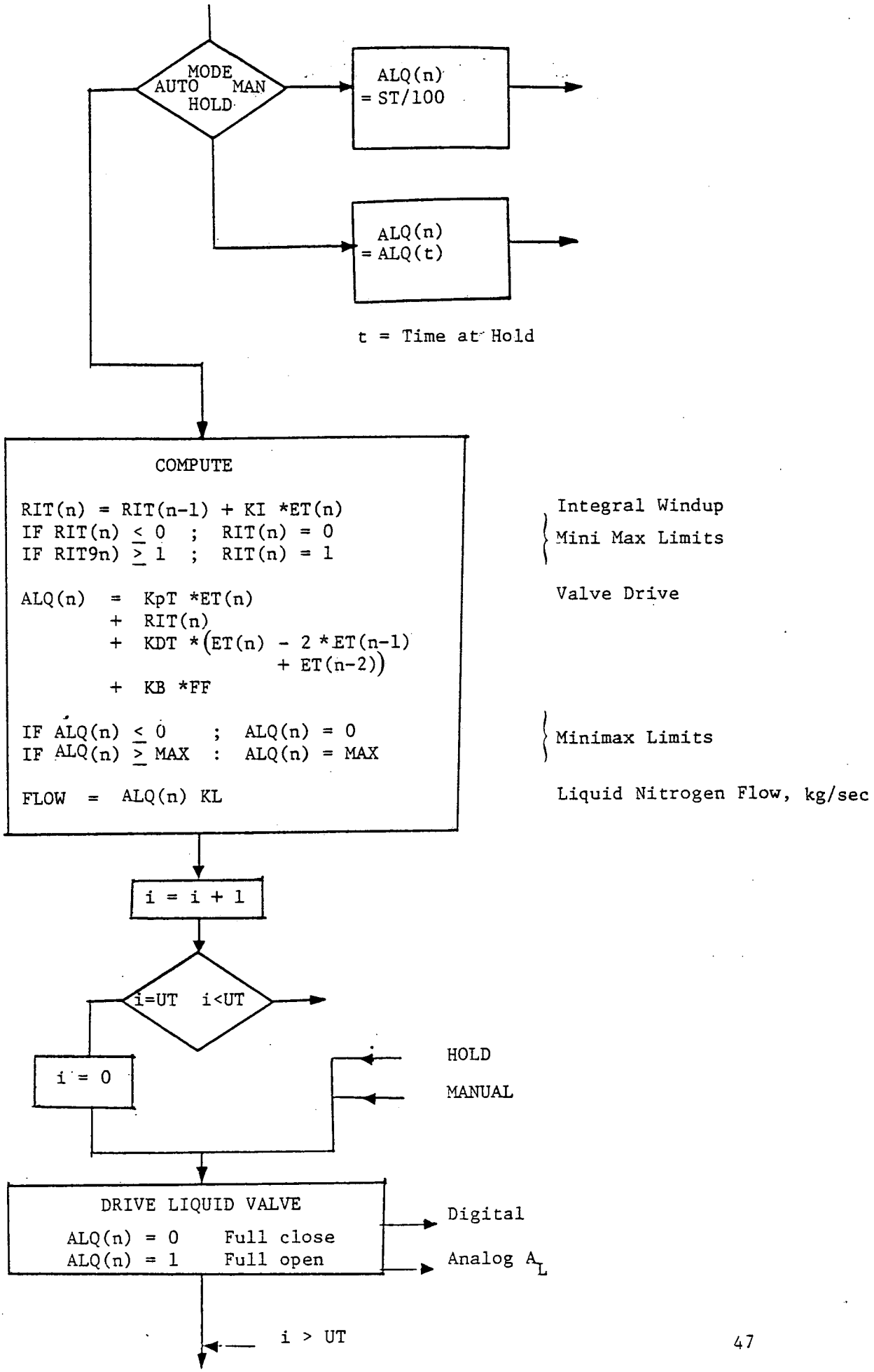
MODE
AUTO MAN
HOLD
ALQ(n)
= ST/100
ALQ(n)
= ALQ(t)
t = Time at Hold
COMPUTE
RIT(n) = RIT(n-1) + KI *ET(n)
IF RIT(n) ≤ 0 ; RIT(n) = 0
IF RIT9n) ≥ 1 ; RIT(n) = 1
Integral Windup
Mini Max Limits
ALQ(n) = KpT *ET(n)
+ RIT(n)
+ KDT *(ET(n) - 2 *ET(n-1)
+ ET(n-2))
+ KB *FF
Valve Drive
IF ALQ(n) ≤ 0 ; ALQ(n) = 0
IF ALQ(n) ≥ MAX : ALQ(n) = MAX
Minimax Limits
FLOW = ALQ(n) KL
Liquid Nitrogen Flow, kg/sec
i = i + 1
i=UT i<UT
i = 0
HOLD
MANUAL
DRIVE LIQUID VALVE
ALQ(n) = 0 Full close
ALQ(n) = 1 Full open
Digital
Analog A_L
i > UT

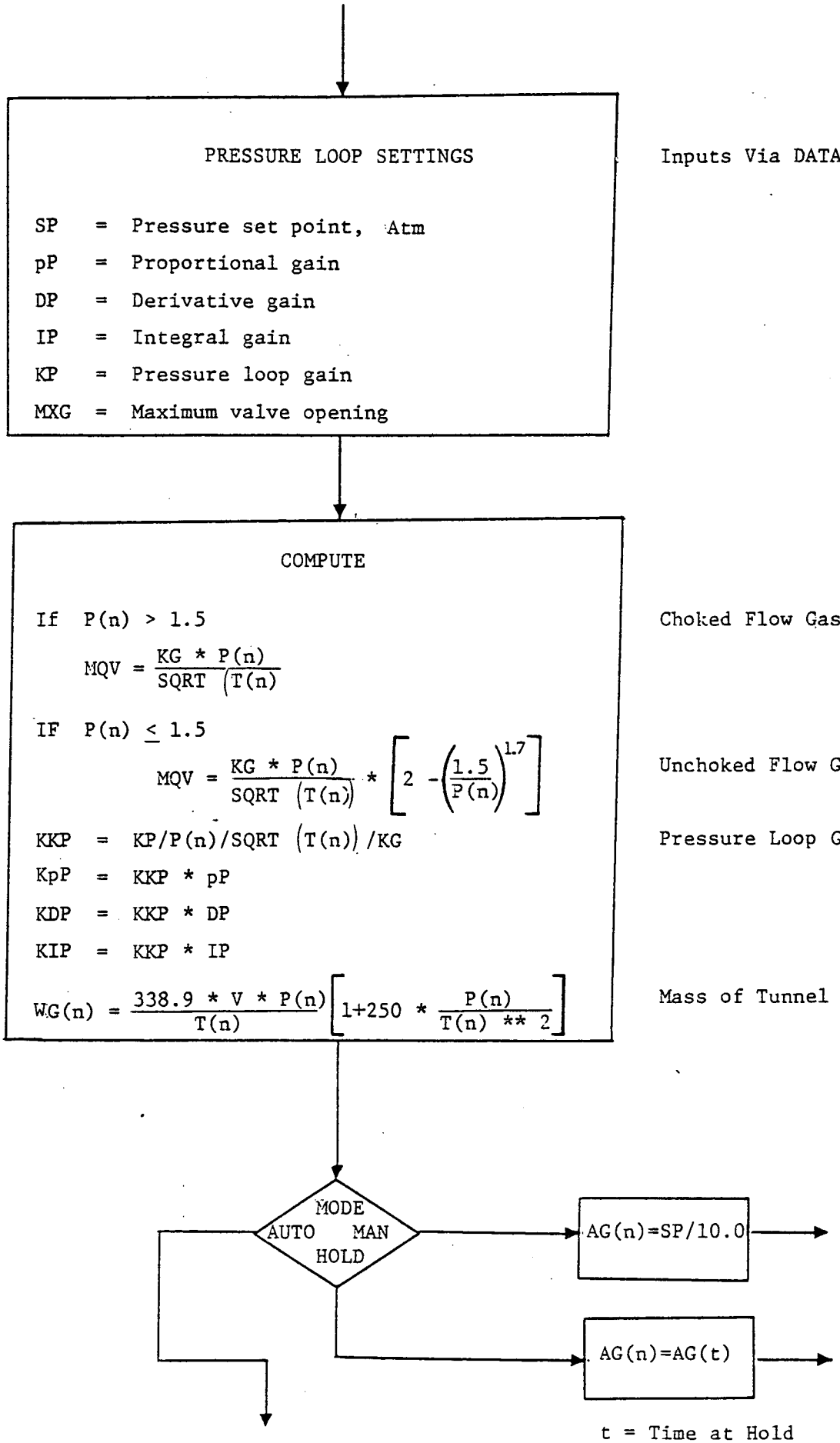
PRESSURE LOOP SETTINGS
Inputs Via DATA Thumbwheels
SP = Pressure set point, Atm
pP = Proportional gain
DP = Derivative gain
IP = Integral gain
KP = Pressure loop gain
MXG = Maximum valve opening
COMPUTE
If P(n) > 1.5
Choked Flow Gas Bleed, kg/sec
MQV = KG * P(n) / SQRT (T(n))
IF P(n) ≤ 1.5
MQV = KG * P(n) / SQRT (T(n)) * [2 - (1.5/P(n))^1.7]
Unchoked Flow Gas Bleed, kg/s
KKP = KP/P(n)/SQRT (T(n))/KG
Pressure Loop Gain Schedule
KpP = KKP * pP
KDP = KKP * DP
KIP = KKP * IP
WG(n) = 338.9 * V * P(n) / T(n) [1+250 * P(n) / T(n) ** 2]
Mass of Tunnel Resident Gas,
MODE
AUTO MAN
HOLD
AG(n)=SP/10.0
AG(n)=AG(t)
t = Time at Hold

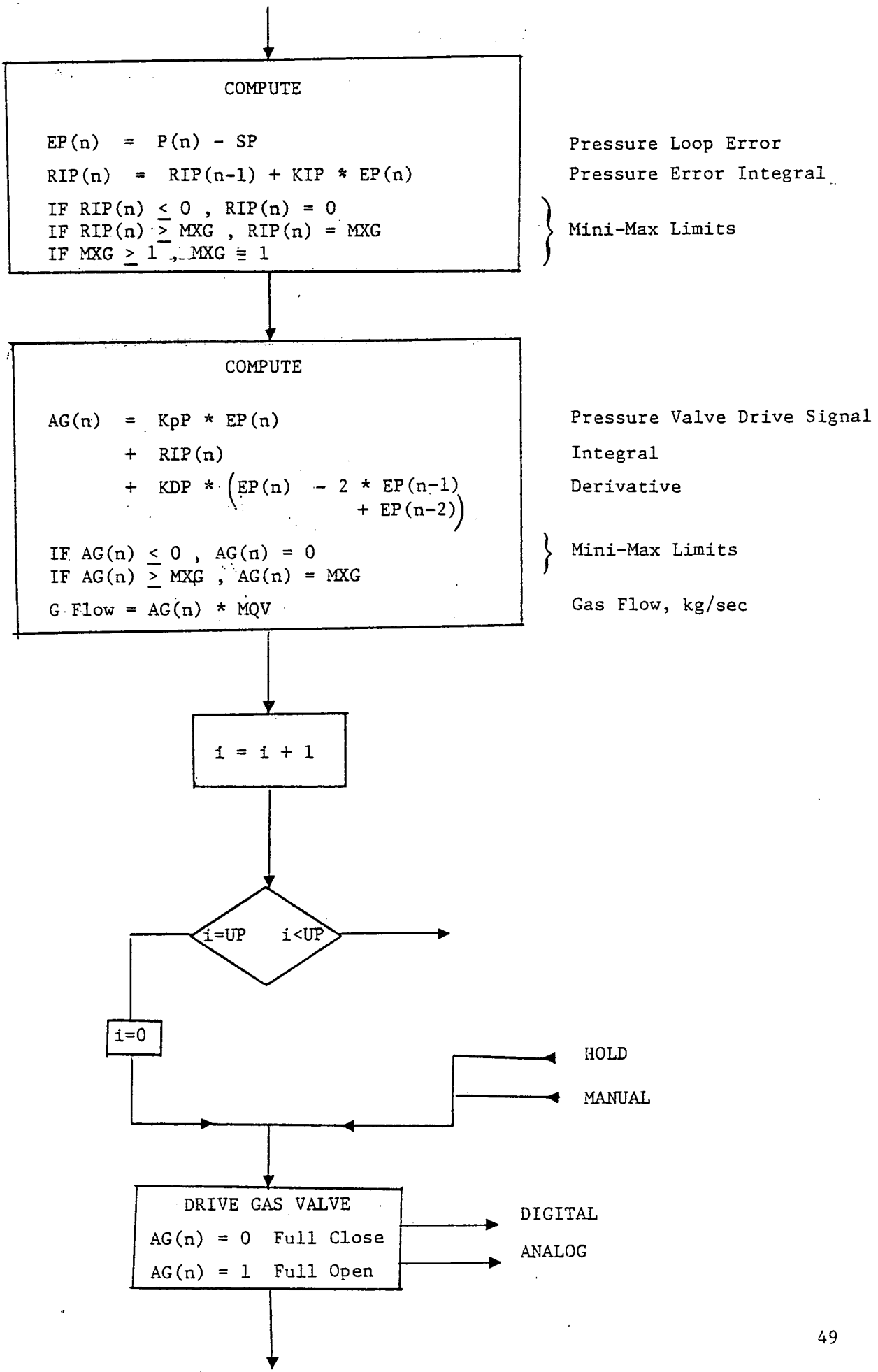
COMPUTE
EP(n) = P(n) - SP
Pressure Loop Error
RIP(n) = RIP(n-1) + KIP * EP(n)
Pressure Error Integral
IF RIP(n) ≤ 0 , RIP(n) = 0
IF RIP(n) ≥ MXG , RIP(n) = MXG
IF MXG ≥ 1 , MXG ≡ 1
Mini-Max Limits
COMPUTE
AG(n) = KpP * EP(n)
Pressure Valve Drive Signal
+ RIP(n)
Integral
+ KDP * (EP(n) - 2 * EP(n-1) + EP(n-2))
Derivative
IF AG(n) ≤ 0 , AG(n) = 0
IF AG(n) ≥ MXG , AG(n) = MXG
Mini-Max Limits
G Flow = AG(n) * MQV
Gas Flow, kg/sec
i = i + 1
i=UP
i<UP
i=0
HOLD
MANUAL
DRIVE GAS VALVE
AG(n) = 0 Full Close
AG(n) = 1 Full Open
DIGITAL
ANALOG

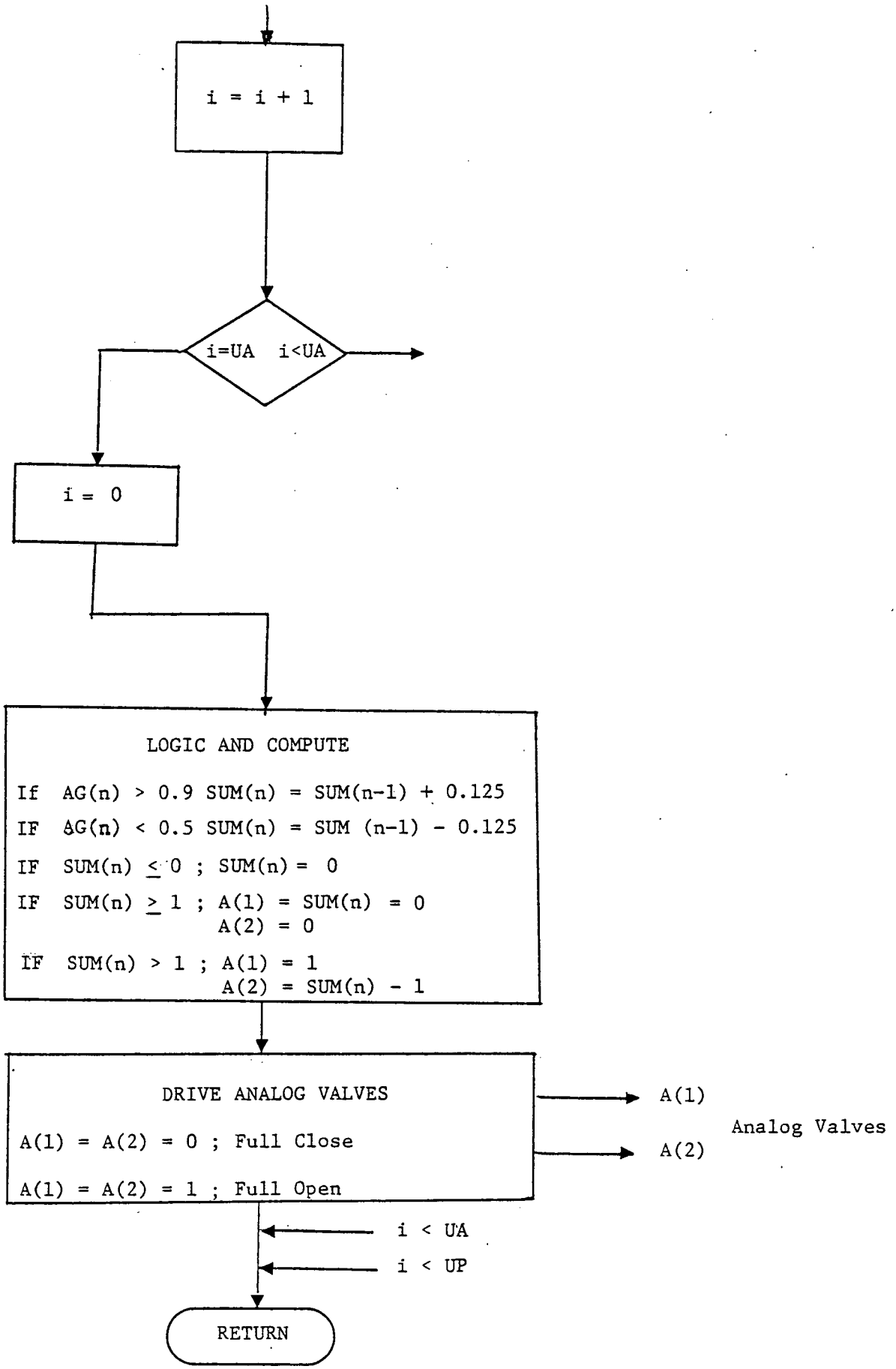
i = i + 1
i=UA i<UA
i = 0
LOGIC AND COMPUTE
If AG(n) > 0.9 SUM(n) = SUM(n-1) + 0.125
IF AG(n) < 0.5 SUM(n) = SUM (n-1) - 0.125
IF SUM(n) ≤ 0 ; SUM(n) = 0
IF SUM(n) ≥ 1 ; A(1) = SUM(n) = 0
A(2) = 0
IF SUM(n) > 1 ; A(1) = 1
A(2) = SUM(n) - 1
DRIVE ANALOG VALVES
A(1) = A(2) = 0 ; Full Close
A(1) = A(2) = 1 ; Full Open
A(1)
A(2)
Analog Valves
i < UA
i < UP
RETURN

APPENDIX B

MACH NUMBER CONTROL LOOP

The 0.3-m transonic cryogenic tunnel test section Mach number is dominantly controlled by fan speed and the tunnel gas temperature, as described by equation (5) of the main text:

$$N = k_m M\sqrt{T}\ (1 - 0.3\ M)\ P^{-0.035} \tag{5}$$

The dynamics of the tunnel test section Mach number as a function of the fan speed are represented by

$$M\sqrt{T} = \frac{N\ e^{-\tau_a S}}{k_m\left(1 + t_p S\right)}$$

where

τ_a = acoustic time delay from fan to test section, sec

t_p = plenum time constant, sec

$k_m = 597\ (1 - 0.3\ M)\ P^{-0.035}$

The fan of the 0.3-m TCT is driven by a water-cooled, 2-pole, 3-phase squirrel cage motor. The motor power is derived from a variable frequency power source which maintains a voltage-to-frequency ratio of 35 V/Hz and delivers up to 2000 MW of electrical power. The fan speed is the synchronous speed of the motor at the given frequency less a load-dependent slip which is about 0.4 percent at maximum power, and normally much less. The 0.3-m TCT fan speed–Mach number relationship in the subsonic range is shown in figure 13. The steady-state Mach number sensitivity to fan speed can be determined from equation (5) or figure 13. The sensitivity corresponds to about ±2.5 rpm for a 0.002-Mach band at 100 K and ±4.5 rpm at 300 K. The existing rotating speed/frequency control system is able to maintain a

typical speed stability of ±4 rpm, under closed-loop control. The dynamics of the speed control system have been determined by invoking identification procedures to arrive at the following description of the fan speed control system.

$$\frac{N}{N_{set}} = \frac{1}{1 + 0.56\ S + 0.2\ S^2}$$

This represents an average response of the fan speed control system for the 0.3-m TCT fan load.

Mach Number Control Loop

The automatic Mach number control scheme for the 0.3-m TCT is shown in figure 37. The schematic shows the 2-pole, 35 V/Hz motor driven by a variable frequency generator. The fan rotation sets the cryogenic tunnel gas in motion to provide varying Mach numbers at the test section. The test section Mach number is estimated from the tunnel total pressure P and the test section static pressure P_s. The transducers used to sense these pressures have a time constant of t_2 sec. The Mach number is estimated as

$$M = \sqrt{5\left[\frac{P}{P_s}\right]^{-3.5} - 5}$$

The Mach number M is compared with the set point Mach number SM. The error EM is gain scheduled, a design goal, and is operated on by a pI controller to generate the fan speed set point N_{set} in the automatic Mach control mode.

The schematic block diagram for Mach number control analysis is shown in figure 38. From this diagram, the open-loop gain product $G(s)\ H(s)$ is

$$G(s)\,H(s) = \frac{KM\,[(pM)\cdot S + (IM)]}{S} \quad \frac{}{1 + 0.56\,S + 0.2\,S^2}$$

$$\cdot \frac{e^{-\tau_a S}}{k_m \sqrt{T}\,(1 + t_p S)\,(1 + t_2 S)}$$

$$= KK \quad \frac{[(pM)\cdot S + (IM)]}{S\,(1 + 0.56\,S + 0.2\,S^2)(1 + t_p S)\,(1 + t_2 S)}$$

where $e^{-\tau_a S}$ has been ignored because of the low τ_a, which is small compared to t_p, t_2 and other constants. The system stability is determined by seeking the roots of polynomial $1 + C(s)\,H(s) = 0$ and studying their properties.

$$\begin{aligned} 1 + G(S)\,H(S) = 0 \;=\; & 0.2\,t_2\,t_p\,S^5 \\ & + \left[0.2\,(t_2 + t_p) + 0.56\,t_2\,t_p\right] S^4 \\ & + \left[0.2 + t_2\,t_p + 0.56\,t_2\,t_p\right] S^3 \\ & + \left[0.56 + t_2 + t_p\right] S^2 \\ & + \left[1 + (KK)(pM)\right] S \\ & + (IM)(KK) \end{aligned}$$

The poles of the Mach number control loop are

$$S = 0; \quad S = -\frac{1}{t_2}\;; \quad S = -\frac{1}{t_p}; \quad S = -1.4 \pm 1.2\,j$$

The zero of the Mach number control loop is generated by the controller as

$$S = -\frac{(IM)}{(pM)}$$

The Mach number control system has five poles and a zero resulting in four poles in excess of zero and hence four asymptotic trajectories. These asymptotes move in the direction of $\frac{n\pi}{2} + 45^{\circ}$ in the $S = \sigma + j\omega$ plane. A sketch of the asymptotic root locus is shown in figure 38. As the system gain is moved from zero to a large value, two of the five poles move into the right half plane, indicating possible instability. By choosing proper gain (KK), the Mach loop poles can be located at critical damping. Since (KK) turns out to be a constant,

$$KK = \frac{KM}{k_m \sqrt{T}} = \text{constant}$$

$$KM \propto k_m \sqrt{T}$$

The tunnel steady-state Mach number accuracy is determined by the open-loop integration and hence has a zero steady-state error. The pI controller contributes this integration. To prevent instability associated with this lag, a lead-time constant of $\frac{(pM)}{(IM)}$ is used and is a very large number (typically 10 to 20 sec).

Since the Mach loop is obviously very sensitive to large errors, the following saturation terms are proposed for the control law

$$N_{set} = \frac{KM\left((pM) \cdot S + (IM)\right)}{S}(EM)$$

Mini/max limits:

$$\text{If ABS } (EM) > 0.05 \quad ; \text{ ABS } (EM) = 0.05$$

$$\text{If ABS } \left(N_{set} - N\right) > 300 \text{ rpm}; \text{ ABS } \left(N_{set} - N\right) = 300$$

Since the average $\frac{\Delta N}{\Delta M} = \frac{6.0 \text{ rpm}}{0.002}$, 0.05 corresponds to 150 rpm. Hence, the Mach loop controller limits the proportional band authority of the pI controller to ±300 rpm incremental authority.

Mach Loop Closure Implementation

The existing speed control system for the 0.3-m TCT facility has a number of bands of speed singularities wherein the system cannot be operated for more than a short period. These singularities are caused by the rotating frequency converter and occur at 1000 rpm, 3500-3700 rpm, 4800-5200 rpm and 5700 rpm.

A simple Mach loop closure based on the pI control law and simple error-dependent linear/logic control laws are not intelligent enough to avoid these bands for a certain set of specific Mach numbers. Hence, it is considered inappropriate to close the Mach loop unless corrections are made for the speed singularities.

Presently used manual speed set point control of the tunnel provides adequate manual control.

Concluding Remarks

In this appendix, the design of a pI controller for the Mach number control loop has been discussed. The gain scheduling and pI settings necessary for stable Mach number control have been discussed. The bandwidth of the Mach loop is about 1.2 rad/sec and has a small perturbation settling time of 15 sec.

MACH LOOP CONTROL FLOW CHART

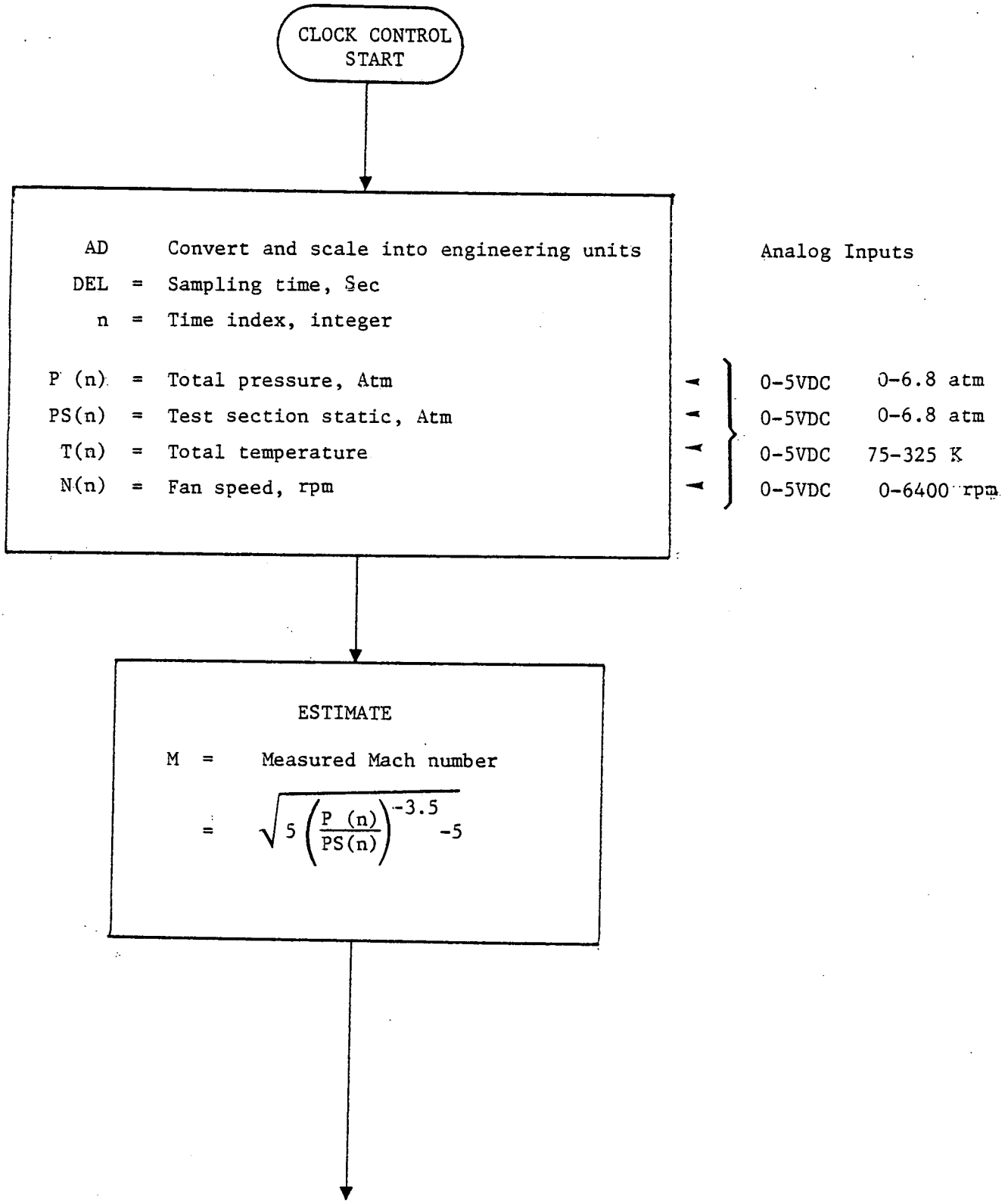

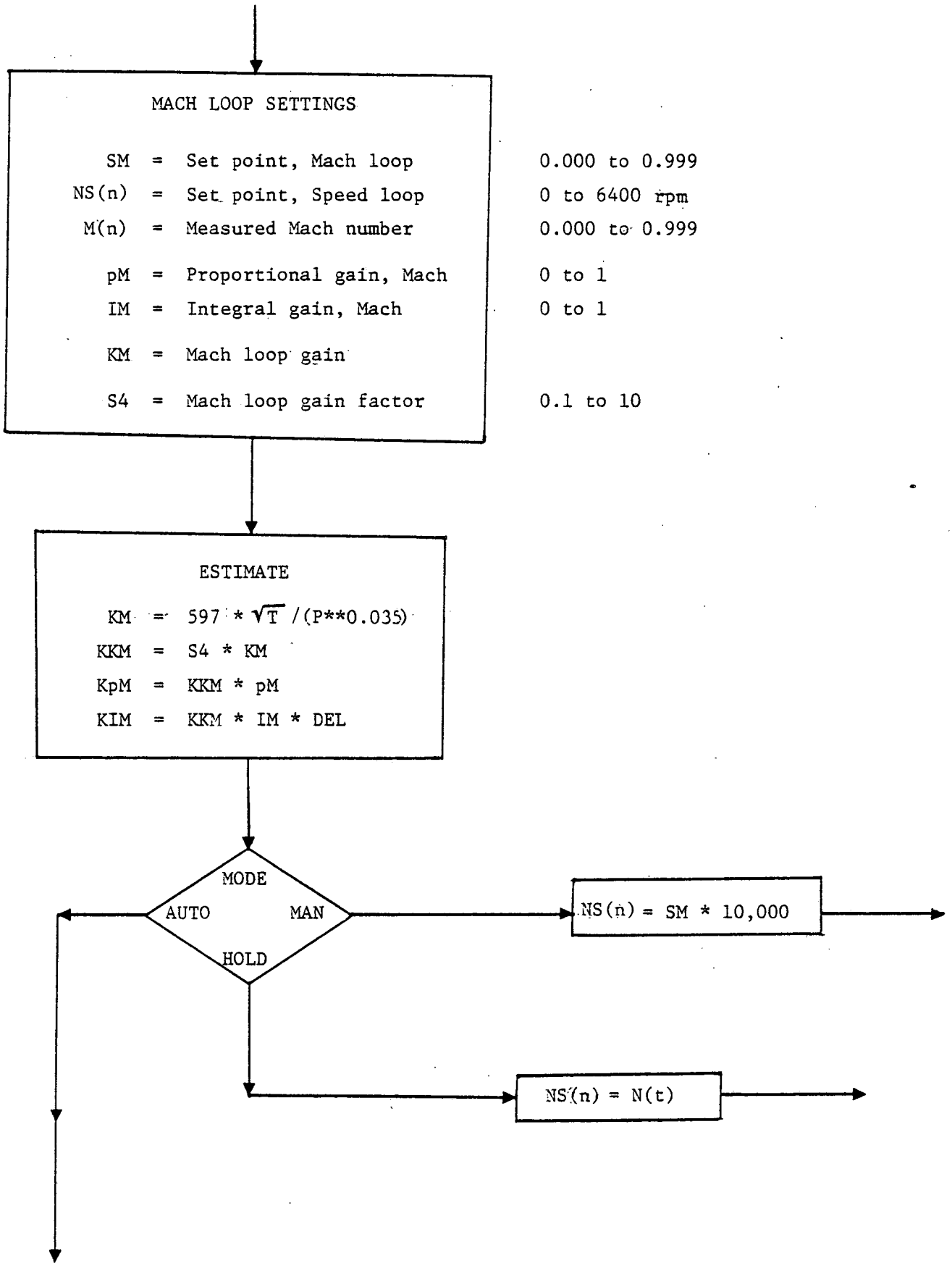
MACH LOOP SETTINGS
SM = Set point, Mach loop
0.000 to 0.999
NS(n) = Set point, Speed loop
0 to 6400 rpm
M(n) = Measured Mach number
0.000 to 0.999
pM = Proportional gain, Mach
0 to 1
IM = Integral gain, Mach
0 to 1
KM = Mach loop gain
S4 = Mach loop gain factor
0.1 to 10
ESTIMATE
KM = 597 * √T /(P**0.035)
KKM = S4 * KM
KpM = KKM * pM
KIM = KKM * IM * DEL
MODE
AUTO
MAN
HOLD
NS(n) = SM * 10,000
NS(n) = N(t)

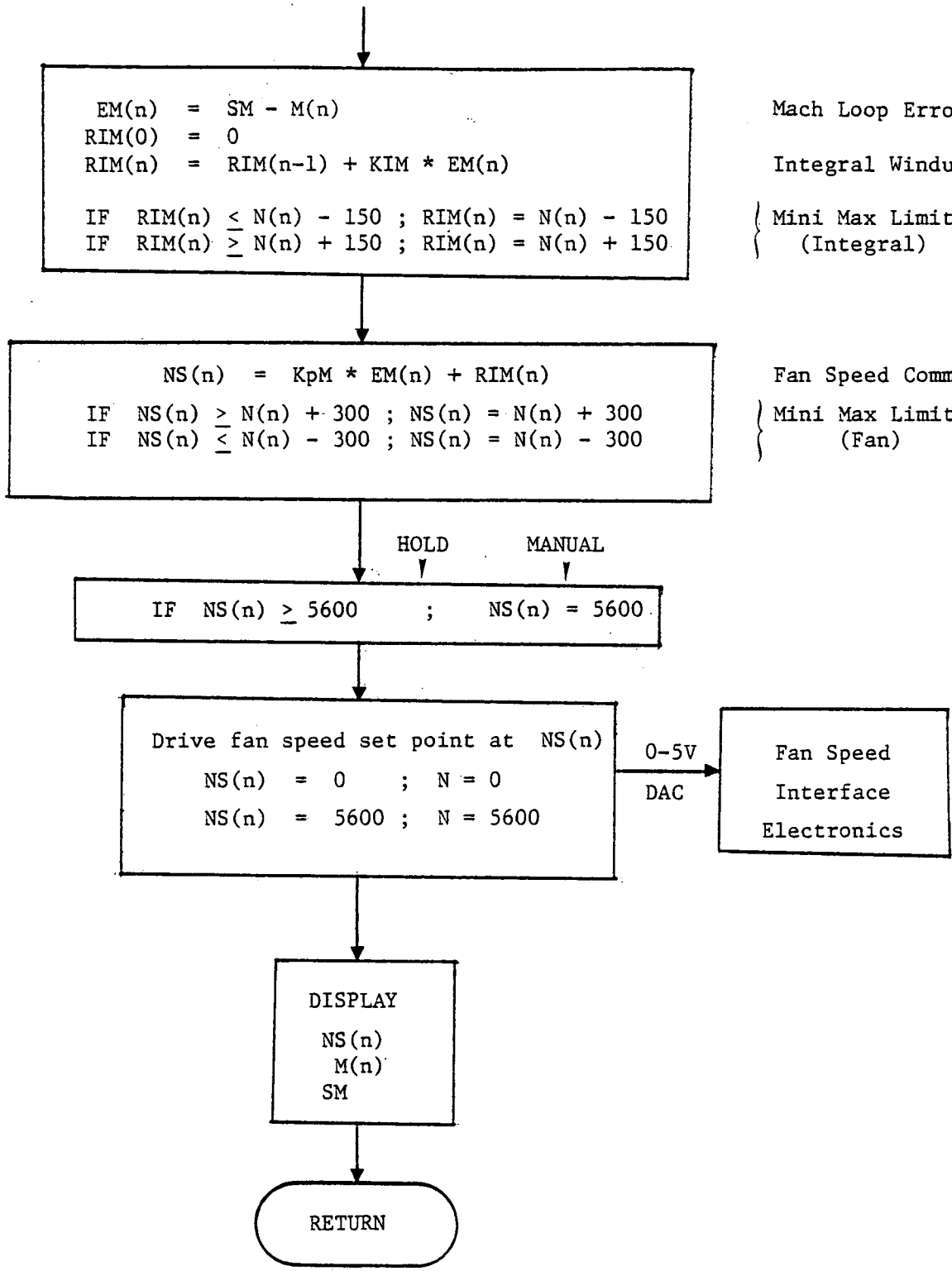

Panel Controls:

4 digit displays each for M(n), NS(n), SM

Push buttons for Auto, Hold, Manual, Emergency, Read

Thumbwheel switches 4 decimal digit for Set Point

REFERENCES

1. Kilgore, R.A.; Goodyer, M.J.; Adcock, J.B.; and Davenport, E.E.: The Cryogenic Wind Tunnel Concept for High Reynolds Number Testing. NASA TN-D-7762, Nov. 1974.

2. Kilgore, R.A.: Design Features and Operational Characteristics of the 0.3-Meter Transonic Cryogenic Tunnel. NASA-TN-D-8304, Dec. 1976.

3. Adcock, J.B.: Real Gas Effects Associated with One Dimensional Transonic Flow of Cryogenic Nitrogen. NASA TN-D-8274, Dec. 1976.

4. Balakrishna, S.: Synthesis of a Control Model for a Liquid Nitrogen Cooled, Closed Circuit, Cryogenic Nitrogen Wind Tunnel and Its Validation. NASA CR-162508, Feb. 1980.

5. Kilgore, R.A.; and Adcock, J.B.: Specific Cooling Capacity of Liquid Nitrogen. NASA-TM-X-74015, Feb. 1977.

6. Fossard, A.J.: Multivariable System Control. North Folland Publications, 1972.

7. Rosenbrock, H.H.: On Design of Linear Multivariable Control Systems. Proceedings of 3rd IFAC Congress (London), 1966.

8. Rosenbrock, H.H.: State Space and Multivariable Theory. Nelson Publications, 1970.

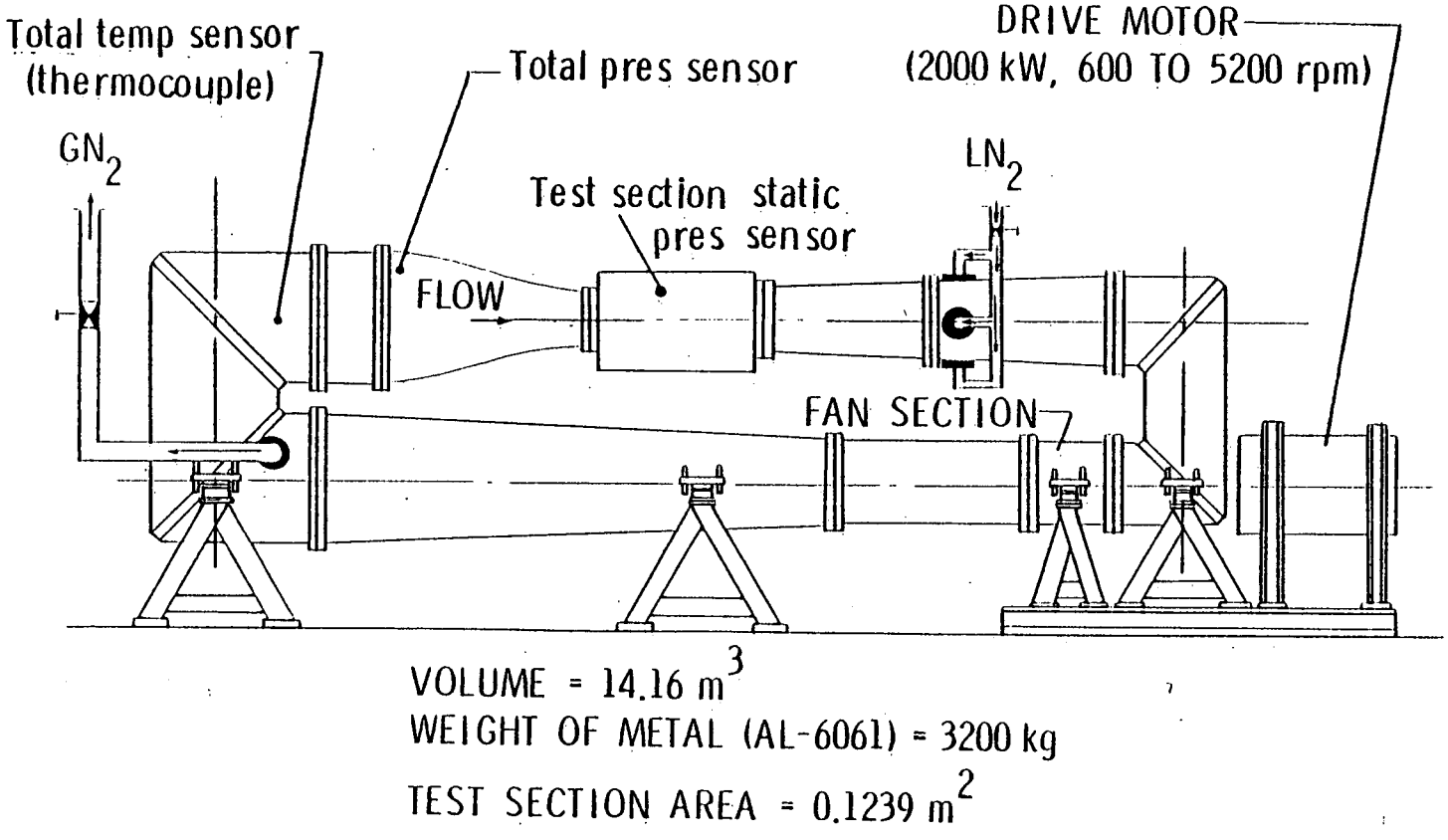

Figure 1. 0.3-m TCT control configuration.

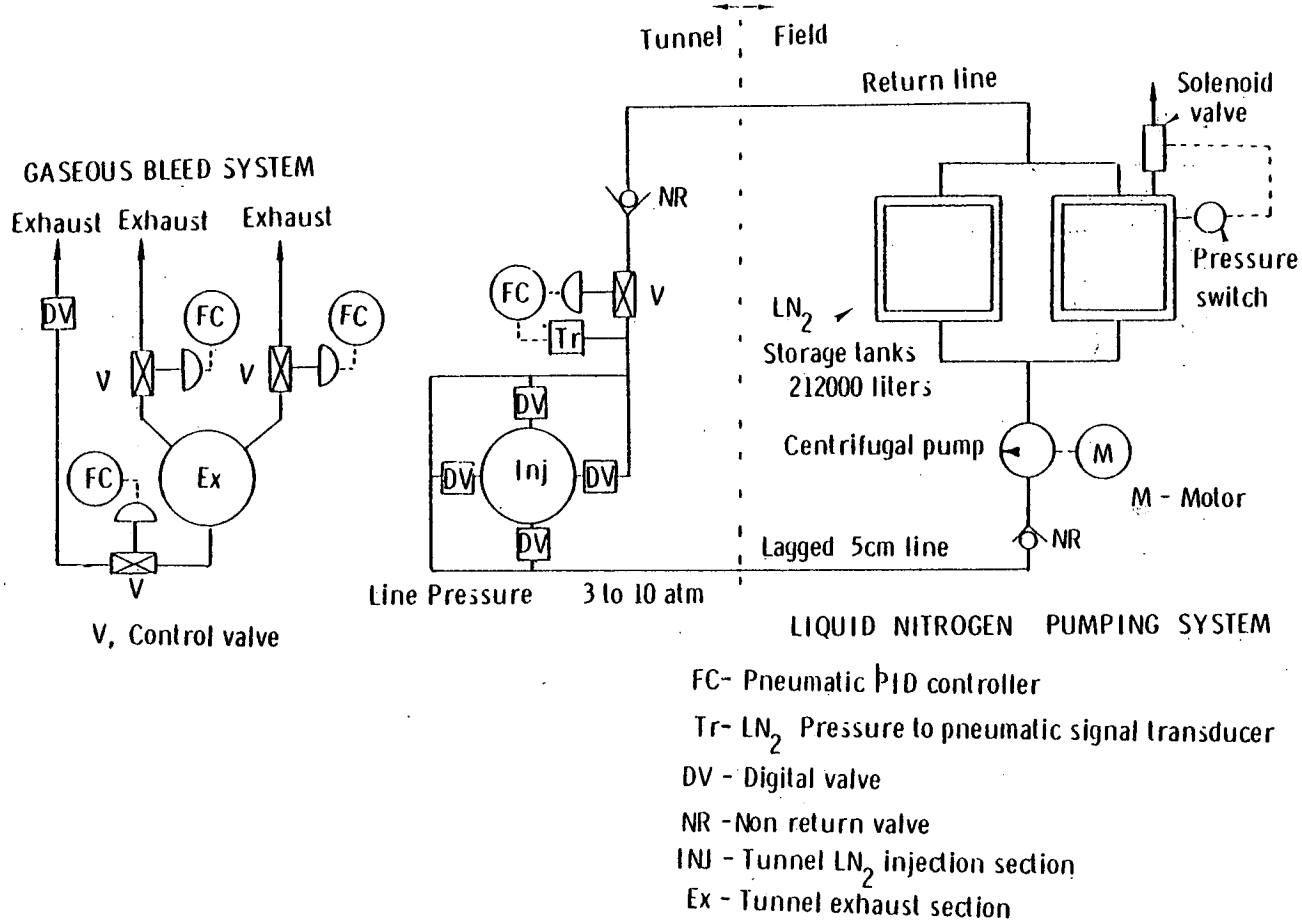

Figure 2. Liquid nitrogen charge and gaseous nitrogen bleed schematic.

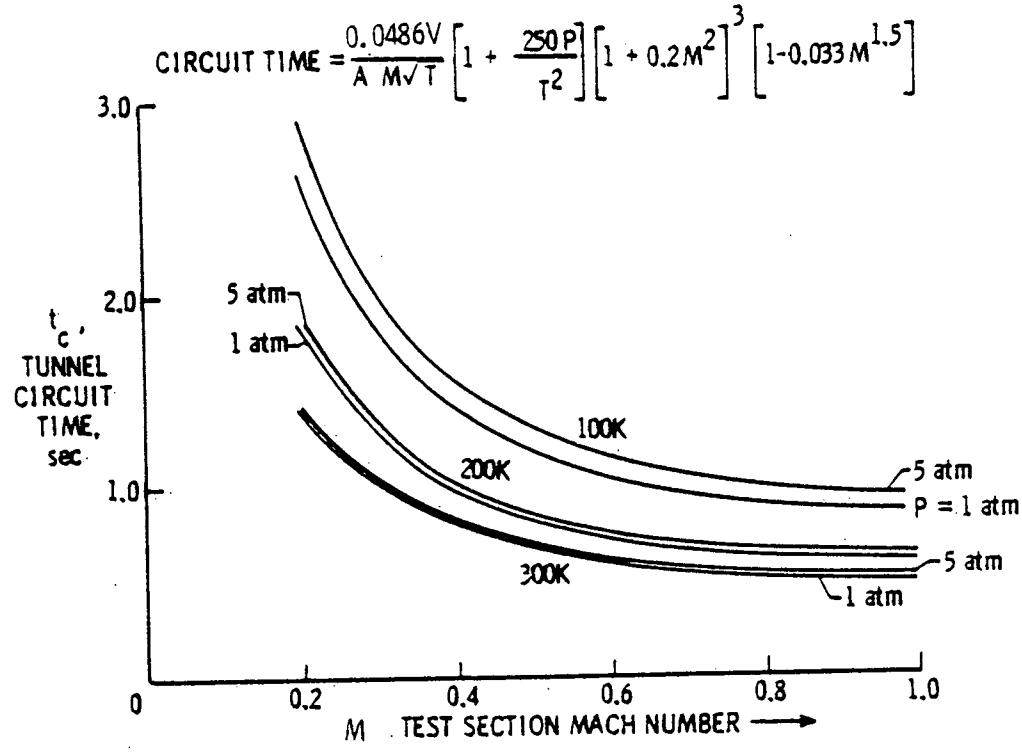

Figure 3. Tunnel circuit time.

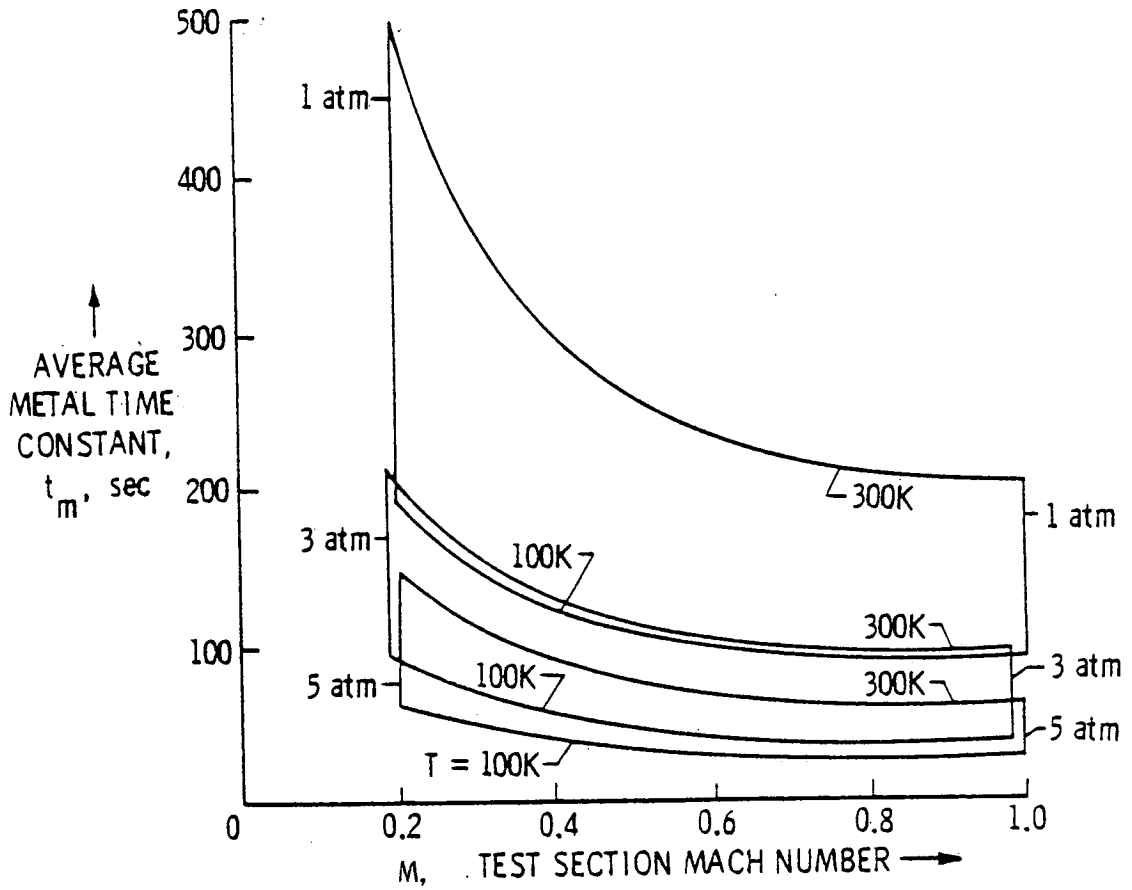

Figure 4. Tunnel average metal time constant.

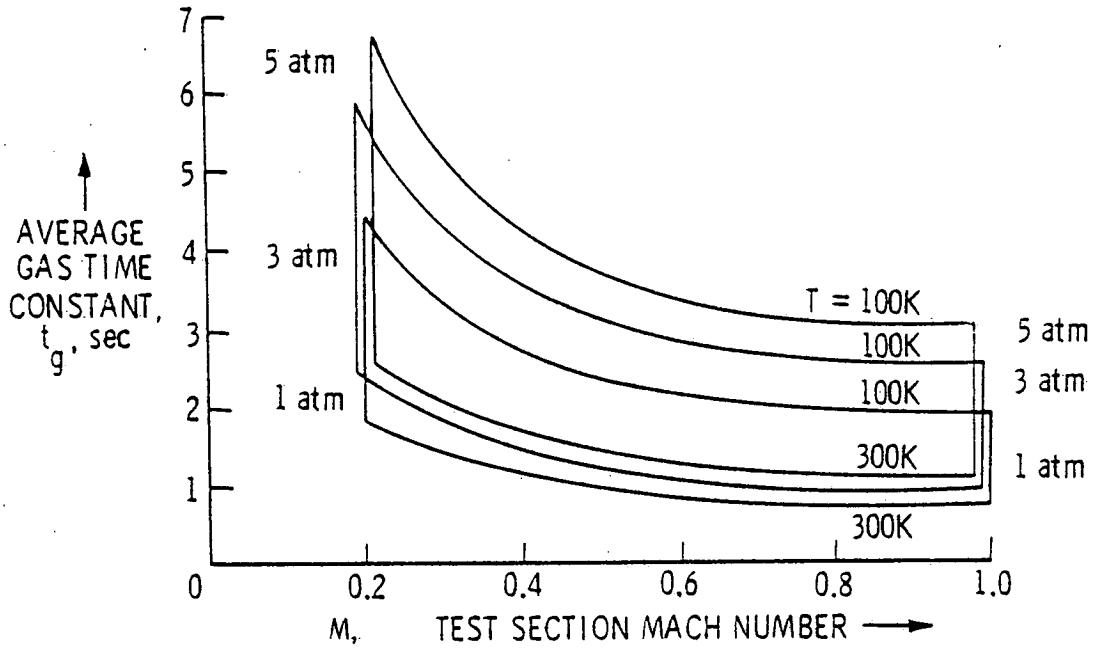

Figure 5. Tunnel average gas time constant.

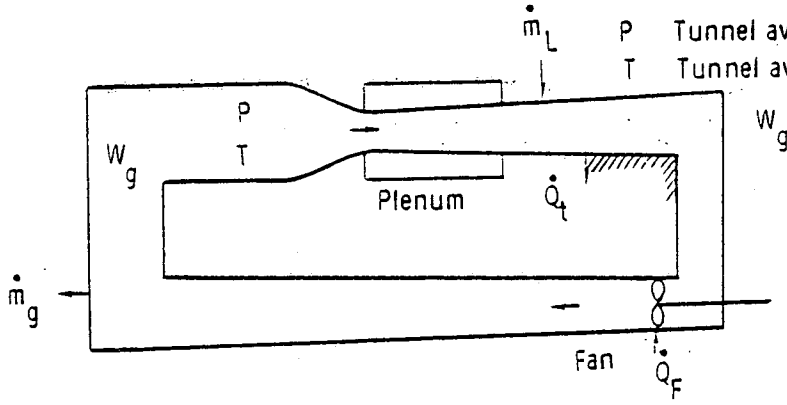

P Tunnel average pressure, atm

T Tunnel average temperature, K

W_g Weight of tunnel gas, kg

Assumptions

Perfect gas behavior
Uniform tunnel temperature
Work, potential & kinetic energy ignored

first law of thermodynamics $$-\dot{Q}_t + \dot{Q}_F + \dot{m}_L h_L - \dot{m}_g h_g = W_g C_v \frac{dT}{dt} + u(\dot{m}_L - \dot{m}_g)$$

Where

h_L Liquid nitrogen enthalpy J/kg

u Specific internal energy

h_g Gas enthalpy J/kg

$\dot{Q}_t$ Heat flow from tunnel metal wall J/sec

$\dot{Q}_F$ Heat flow from Fan operation J/sec

$\dot{m}_g$ Gaseous nitrogen bleed kg/sec

$\dot{m}_L$ Liquid nitrogen mass flow kg/sec

Figure 6. Thermodynamic model of a cryogenic tunnel.

TUNNEL PROCESS MODEL

$$\begin{bmatrix} o \\ T \\ \\ M \\ \\ o \\ P \end{bmatrix} = \begin{bmatrix} k_L \cdot \frac{\beta + a}{\theta} \cdot \frac{1 + t_m s}{1 + t_g s} e^{-\tau_L s} & \frac{k_f}{k_m} \cdot \frac{PM^2}{\theta(1+0.2M^2)^3} \cdot \frac{1 + t_m s}{1 + t_g s} e^{-\tau_f s} & -k_g \frac{Pa}{\sqrt{T\theta}} \frac{1 + t_m s}{1 + t_g s} \\ 0 & \frac{e^{-\tau_a s}}{k_m \sqrt{T}(1 + t_p s)} & 0 \\ k_L \left[\frac{P}{W_g} + \frac{P(\beta + a)}{T\theta} \frac{1 + t_m s}{1 + t_g s} \right] & \left| \frac{k_f}{k_m} \cdot \frac{P^2 M^2}{T\theta(1+0.2M^2)^3} \cdot \frac{1 + t_m s}{1 + t_g s} + \frac{bMPs}{k_m \sqrt{T}} \right| & -\frac{k_g P}{\sqrt{T}} \left[\frac{P}{W_g} + \frac{Pa}{T\theta} \cdot \frac{1 + t_m s}{1 + t_g s} \right] \end{bmatrix} \times \begin{bmatrix} A_L \\ N \\ A_g \end{bmatrix}$$

Figure 7. Multivariable model of a cryogenic tunnel.

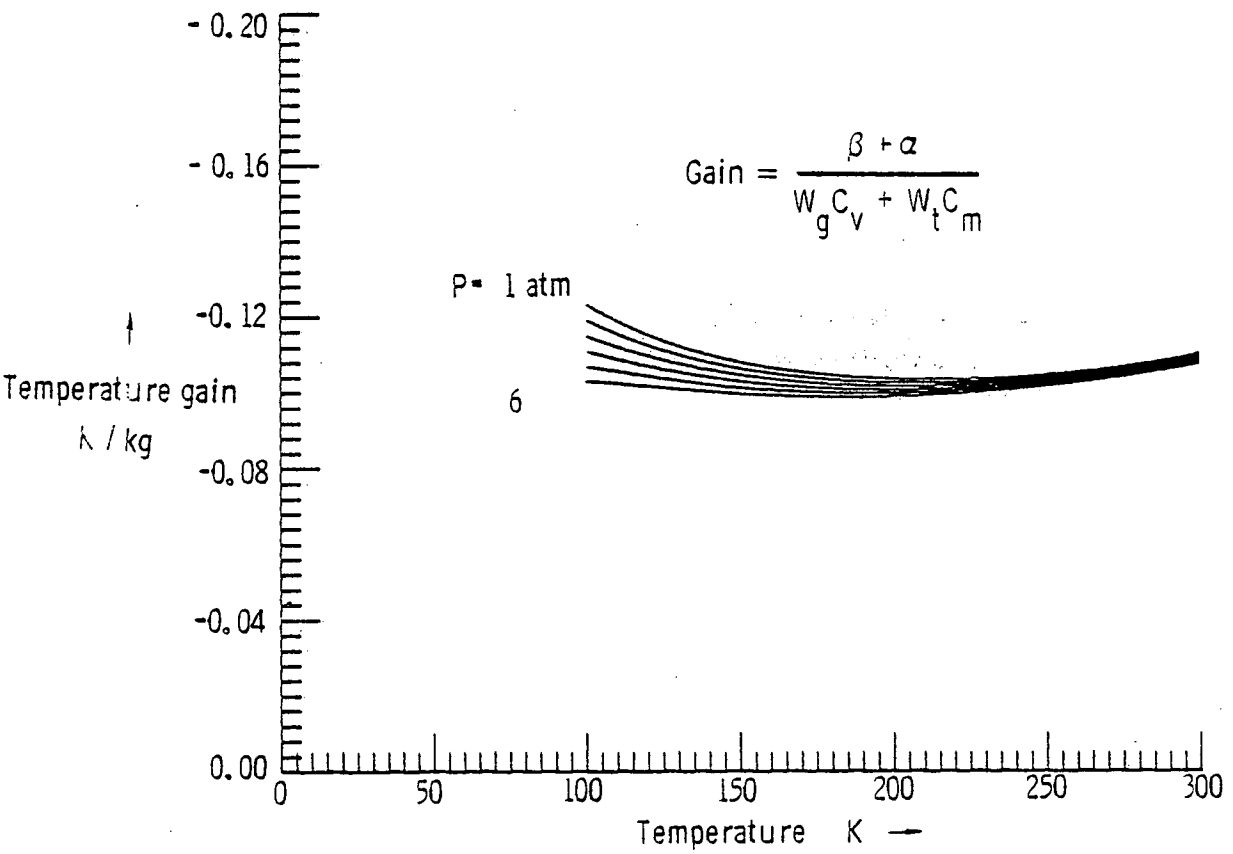

Figure 8. Steady-state temperature gain for LN_2 input.

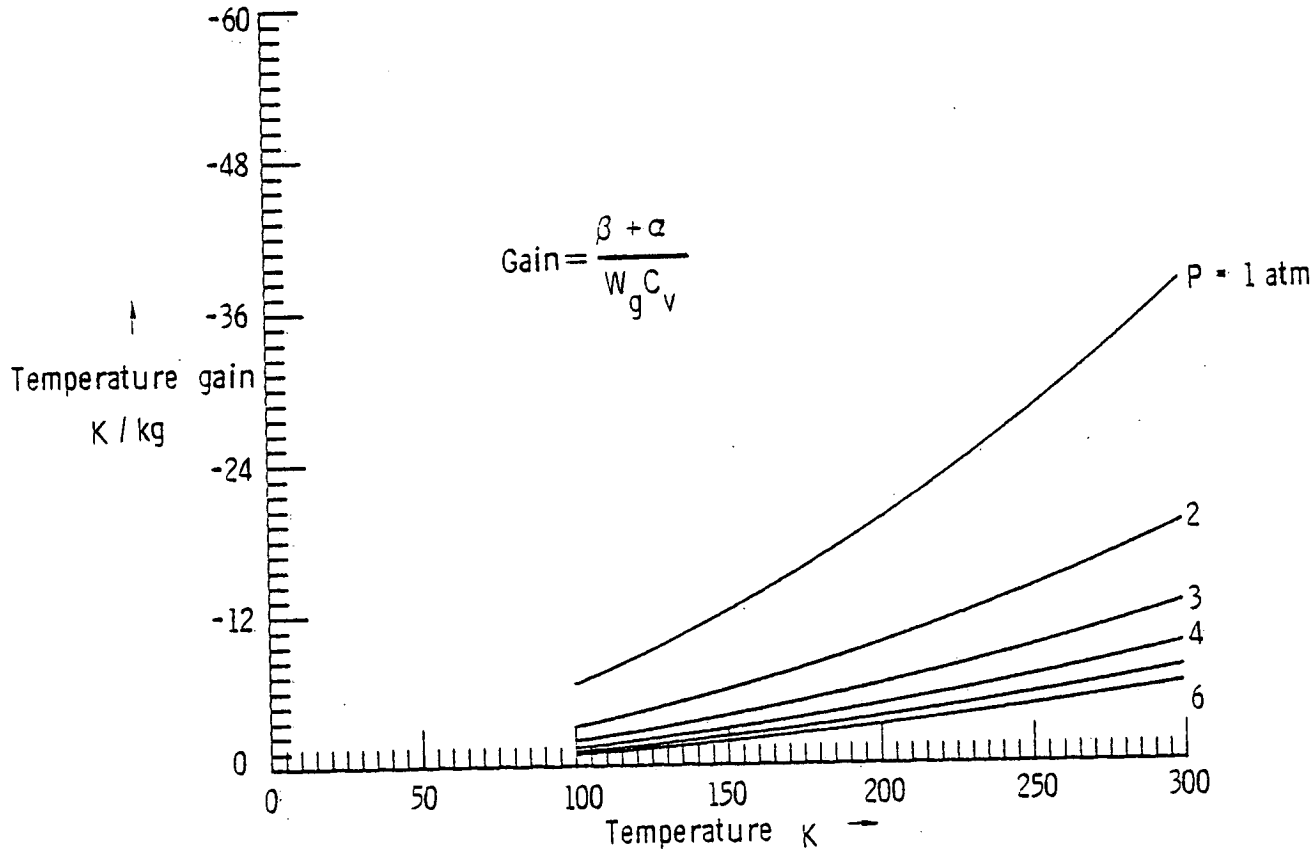

Figure 9. Transient temperature gain for LN_2 input.

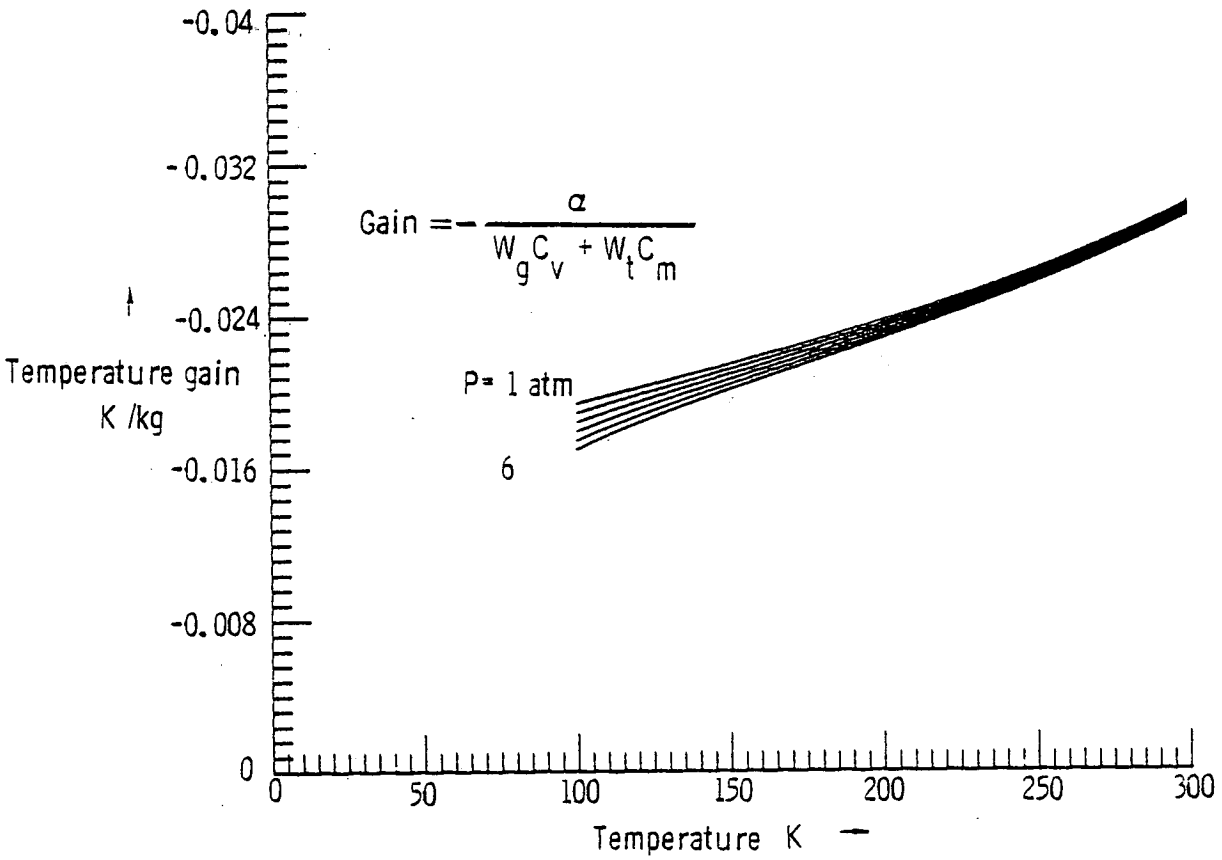

Figure 10. Steady-state temperature gain for GN_2 bleed.

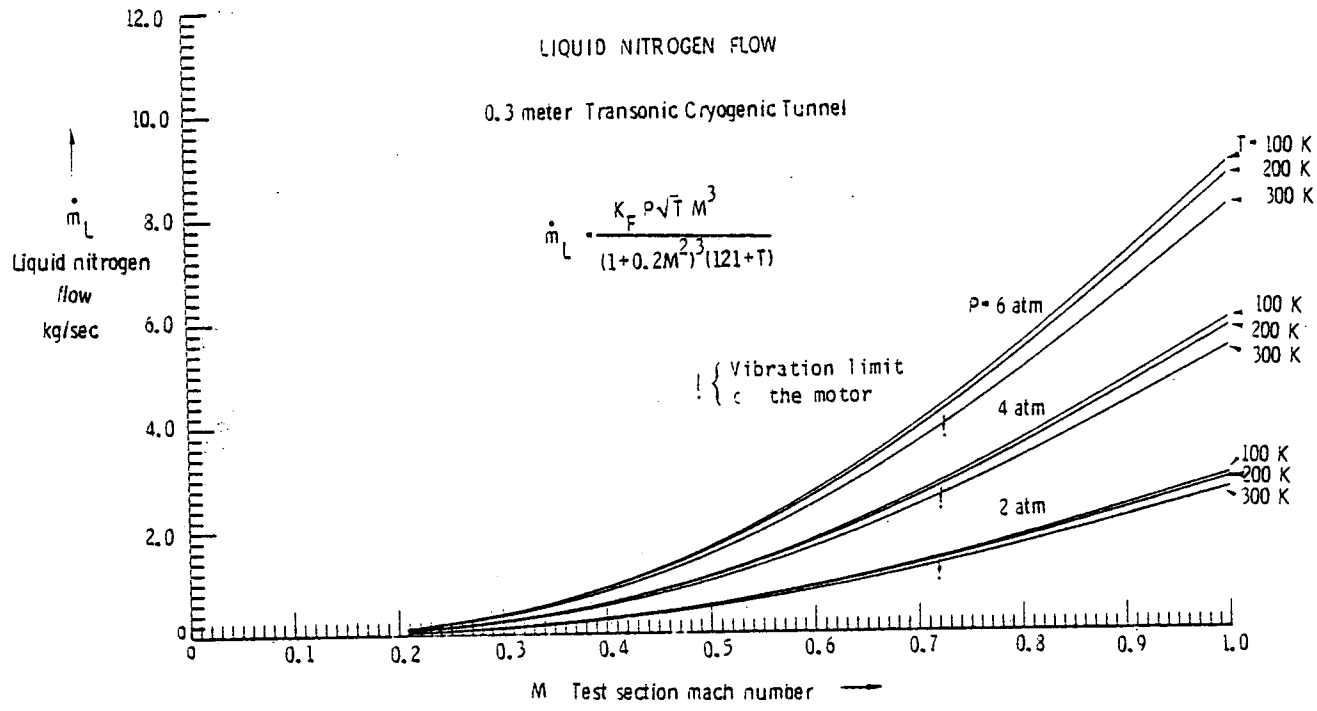

Figure 11. Liquid nitrogen flow requirement for 0.3-m TCT at steady state.

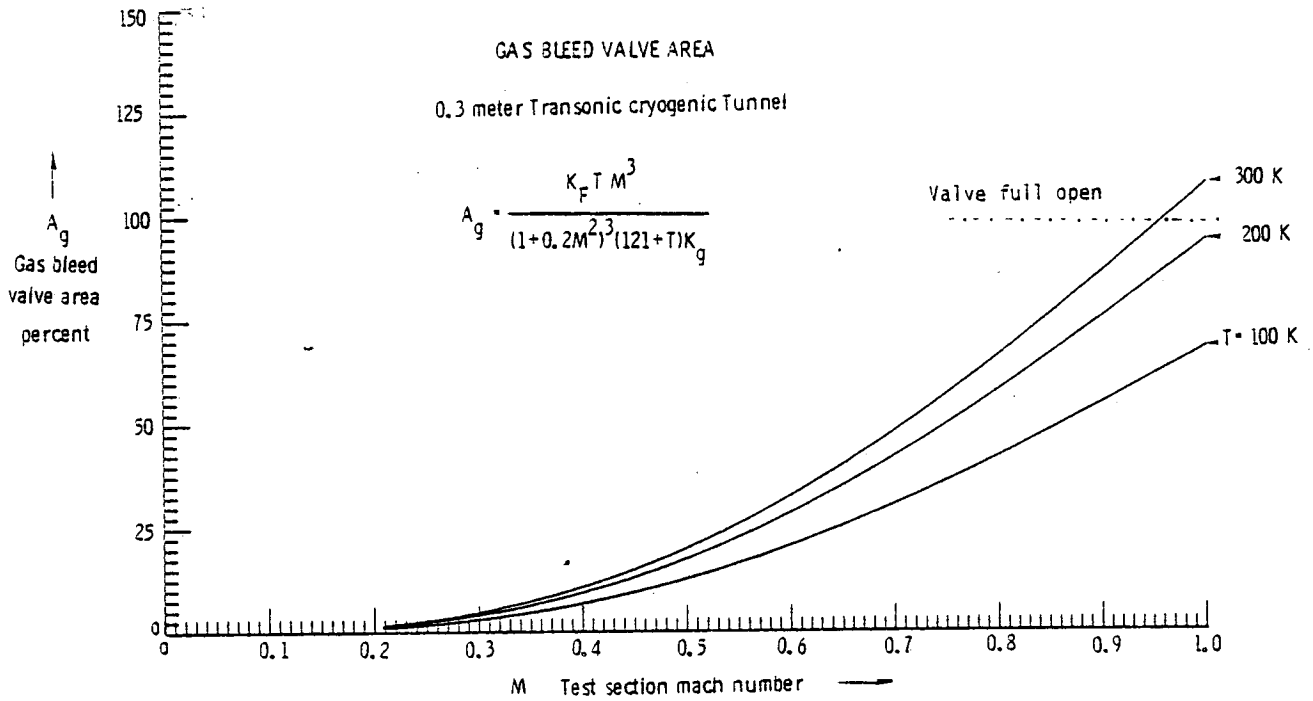

Figure 12. Gas bleed valve area requirement for 0.3-m TCT at steady state.

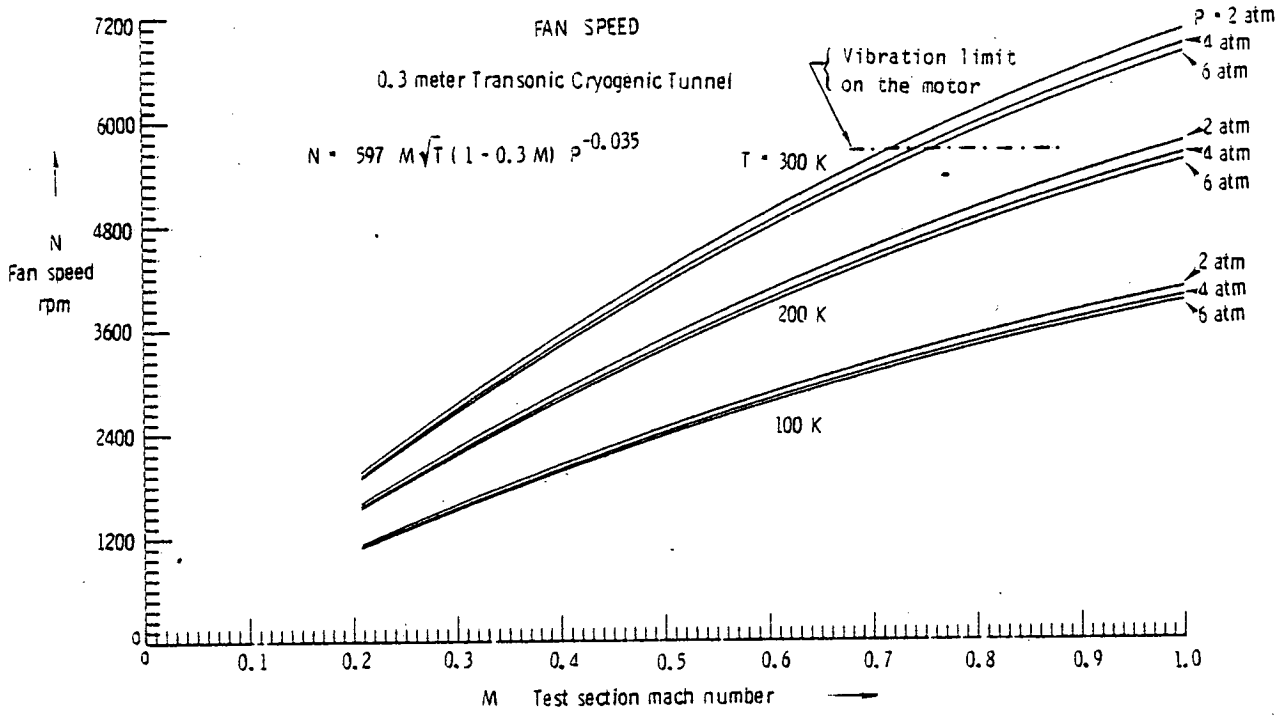

Figure 13. Fan speed requirement for 0.3-TCT at steady state.

ACTUATORS AND SENSOR MODELS

LN_2 VALVE - $\dot{m}_L = k_L A_L = 3.47 \sqrt{P_L - P}\ A_L$ $\quad 0 \le A_L \le 1$ (IN 1024 STEPS)

GN_2 VALVE - $\dot{m}_g = k_g \frac{P}{\sqrt{T}} A_g = 21.8 \frac{P}{\sqrt{T}} A_g \quad P > 1.5$

$= 21.8 \frac{P}{\sqrt{T}} \left(2 - \left[\frac{1.5}{P}\right]^{1.7} \right) A_g \quad 1 \le P \le 1.5$ $\quad 0 \le A_g \le 1$ (IN 256 STEPS)

TEMPERATURE SENSOR $\quad \frac{1}{1 + t_1 s}$ $\quad$ WHERE $t_1 = \frac{1}{2}$ TO 3 secs

PRESSURE SENSOR $\quad \frac{1}{1 + t_2 s}$ $\quad$ WHERE $t_2 = \frac{1}{4}$ secs

FAN DYNAMICS $\quad \frac{N}{N_{SET}} = \frac{5}{s^2 + 2.8 s + 5}$

Figure 14. Actuator and sensor dynamic models for 0.3-m TCT.

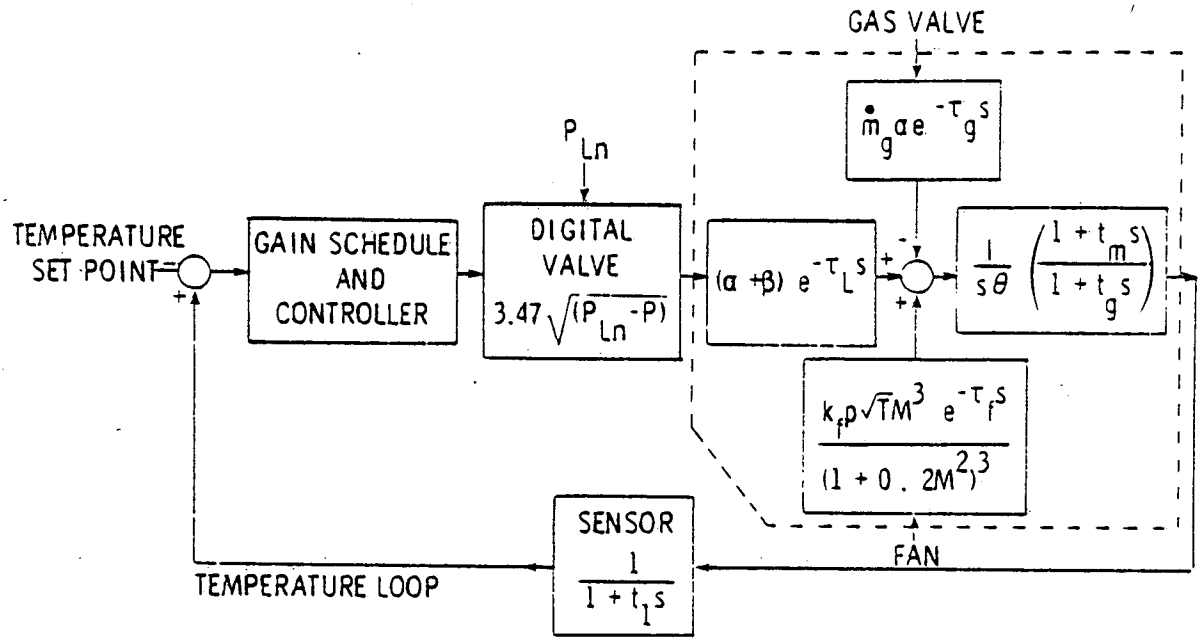

Figure 15. Cryogenic tunnel temperature control schematic.

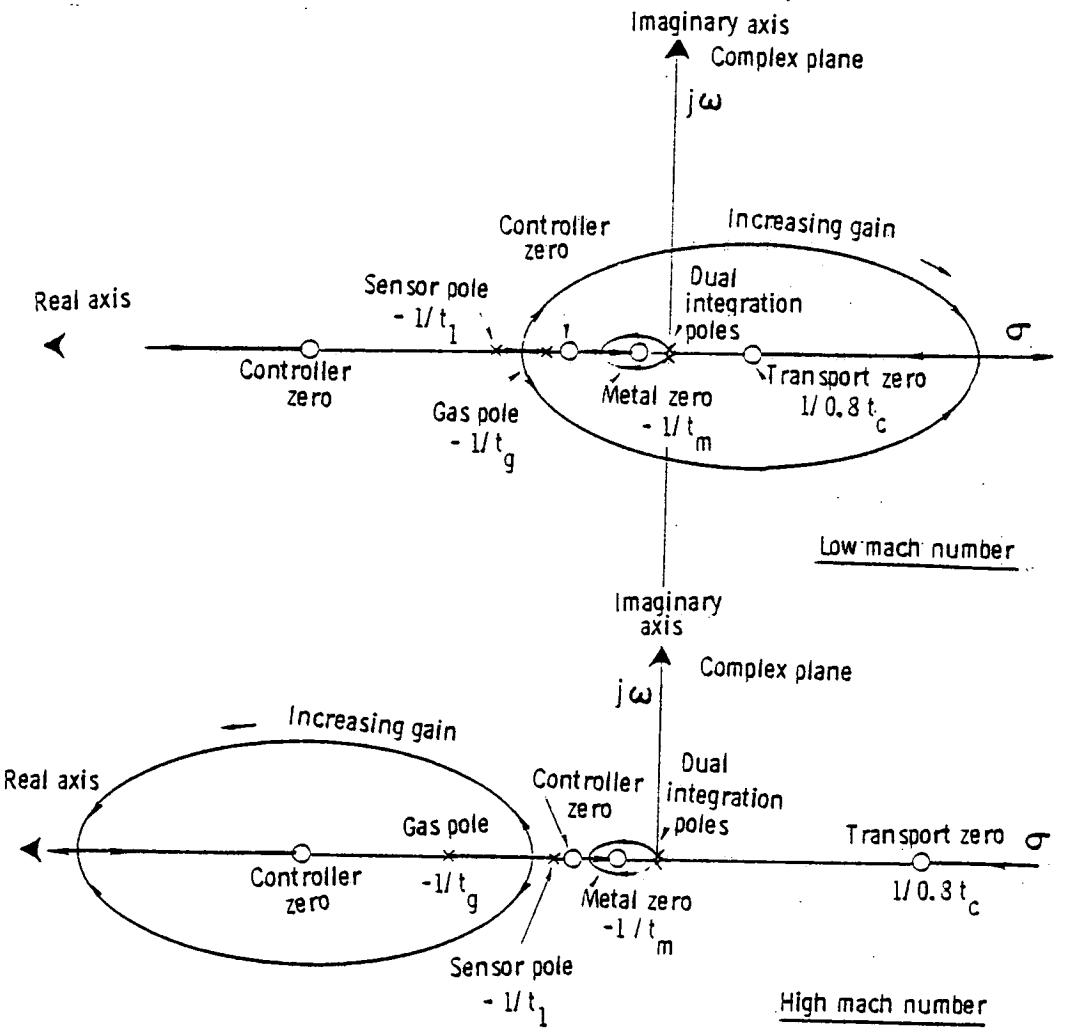

$$1 + G(s)H(s) = -(KK)\frac{\left[(DT)s^2 + (pT)s + (IT)\right]\left[1 - (t_m - \tau_L)s - \tau_L t_m s^2\right]}{s^2(1 + t_1 s)(1 + t_g s)} + 1 = 0$$

Figure 16. Asymptotic root loci for temperature loop.

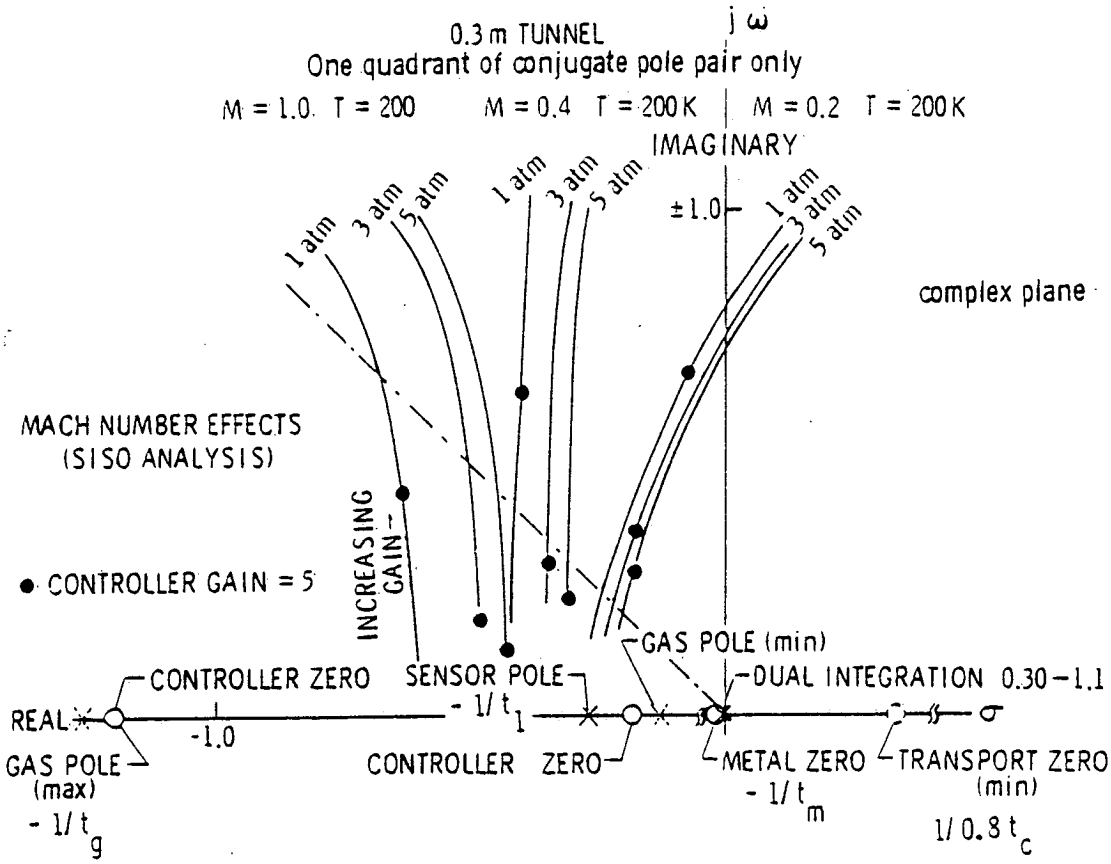

Figure 17. Root loci for temperature loop—Mach number effects.

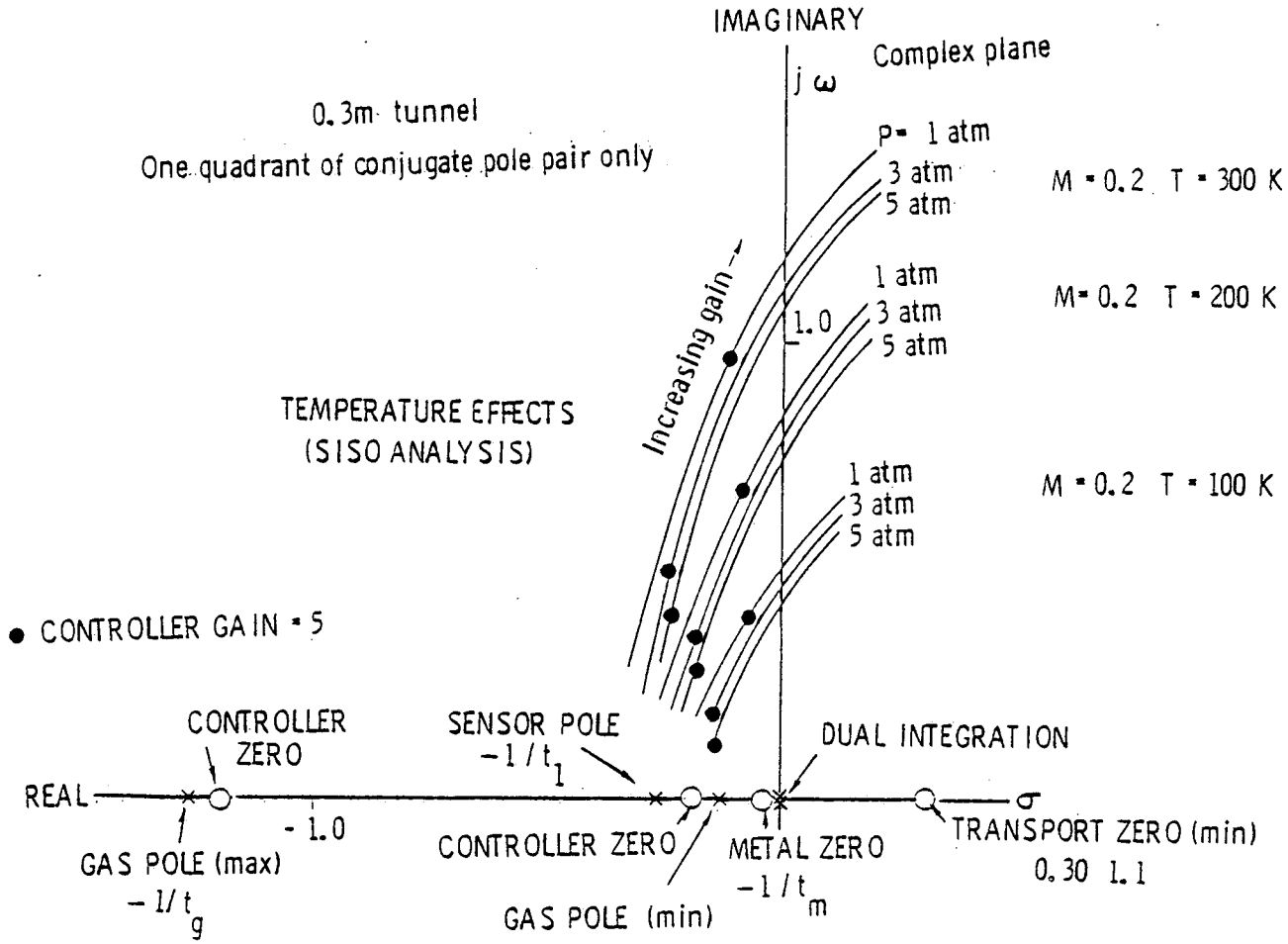

Figure 18. Root loci for temperature loop—temperature effects.

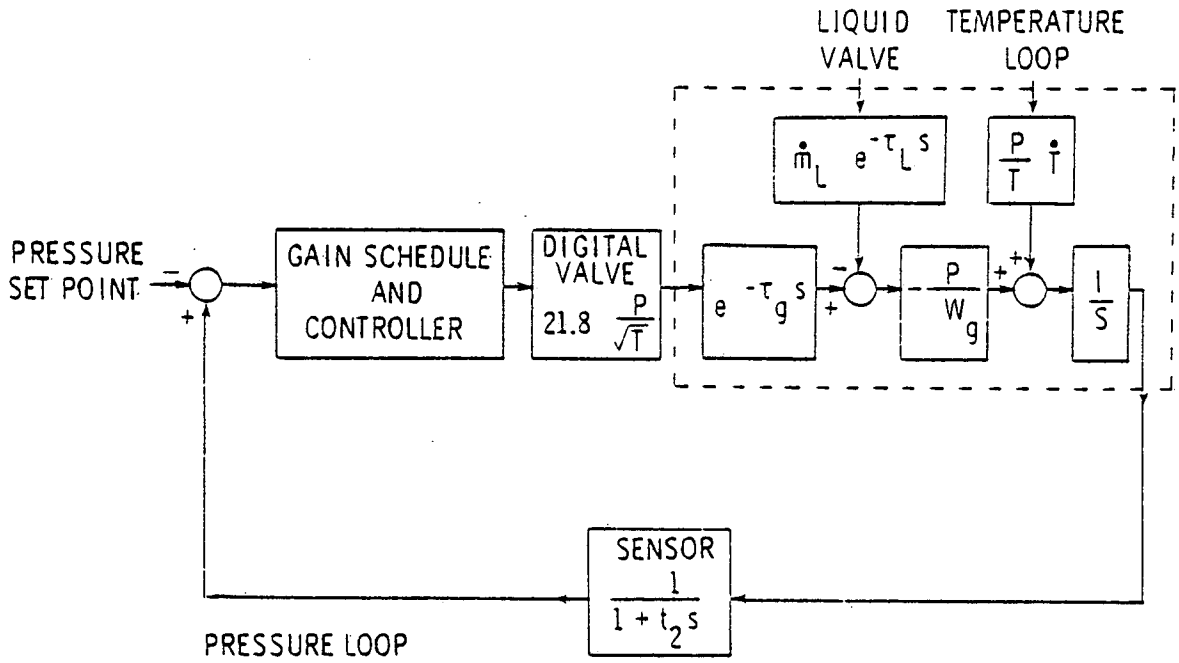

Figure 19. Cryogenic tunnel pressure control schematic.

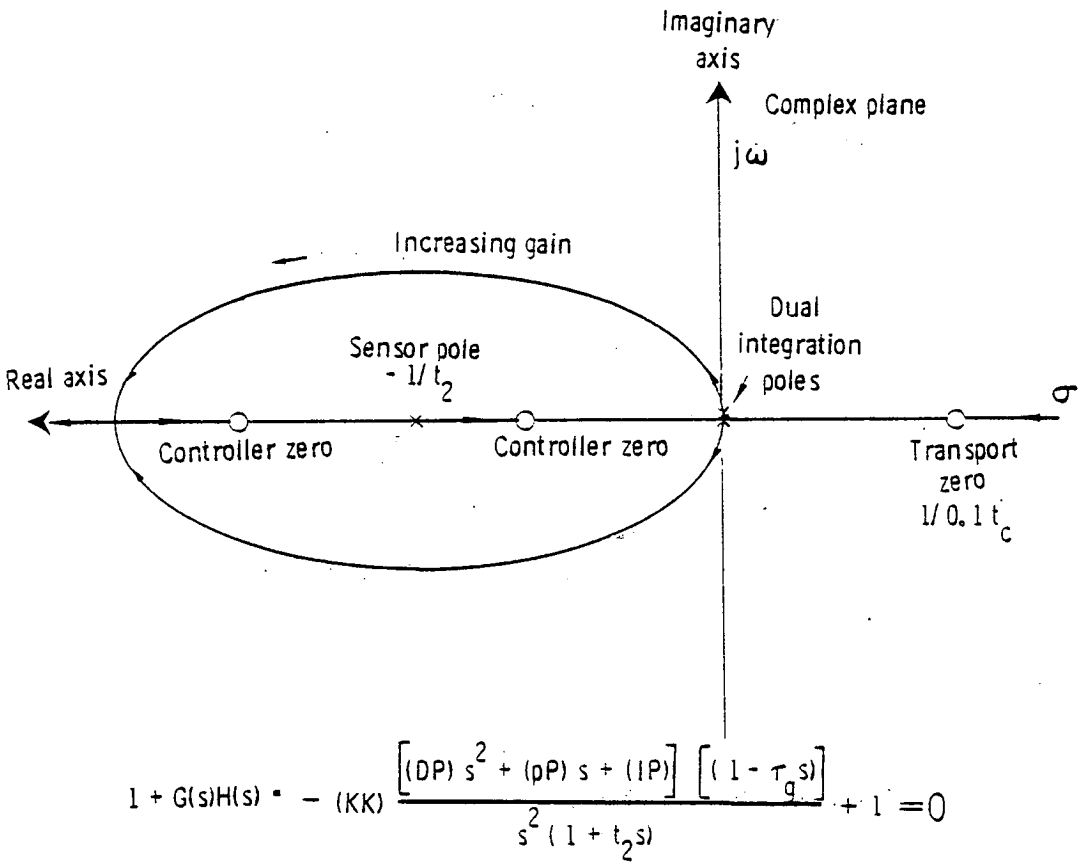

$$1 + G(s)H(s) = -(KK)\frac{\left[(DP)\,s^2 + (pP)\,s + (IP)\right]\left[(1 - \tau_q s)\right]}{s^2(1 + t_2 s)} + 1 = 0$$

Figure 20. Asymptotic root locus for pressure loop.

$$Z^{-1}(s) = \begin{bmatrix} \left[\frac{W_g \alpha}{T\beta} + \frac{\theta}{\beta}\,\frac{1+t_g s}{1+t_m s}\right]\frac{s}{k_L} & -\frac{k_f P M^2 \sqrt{T}\ (1+t_p s)}{k_L\ (1+0.2M^2)^3 \beta} & \frac{W_g \alpha\, s}{k_L P\ \beta} \\ 0 & k_m \sqrt{T}\,(1+t_p s) & 0 \\ \left[\frac{W_g(\alpha+\beta)}{T\ \beta} + \frac{\theta\ (1+t_g s)}{\beta\ (1+t_m s)}\right]\frac{s\sqrt{T}}{P\ k_g} & -\frac{k_f\ T\ M^2\ (1+t_p s)}{k_g \beta (1+0.2M^2)^3} & -\frac{W_g \sqrt{T} s\ (\alpha+\beta)}{k_g P^2 \beta} \end{bmatrix}$$

Figure 21. Noninteractive multivariable controller.

NASA
L-79-4844

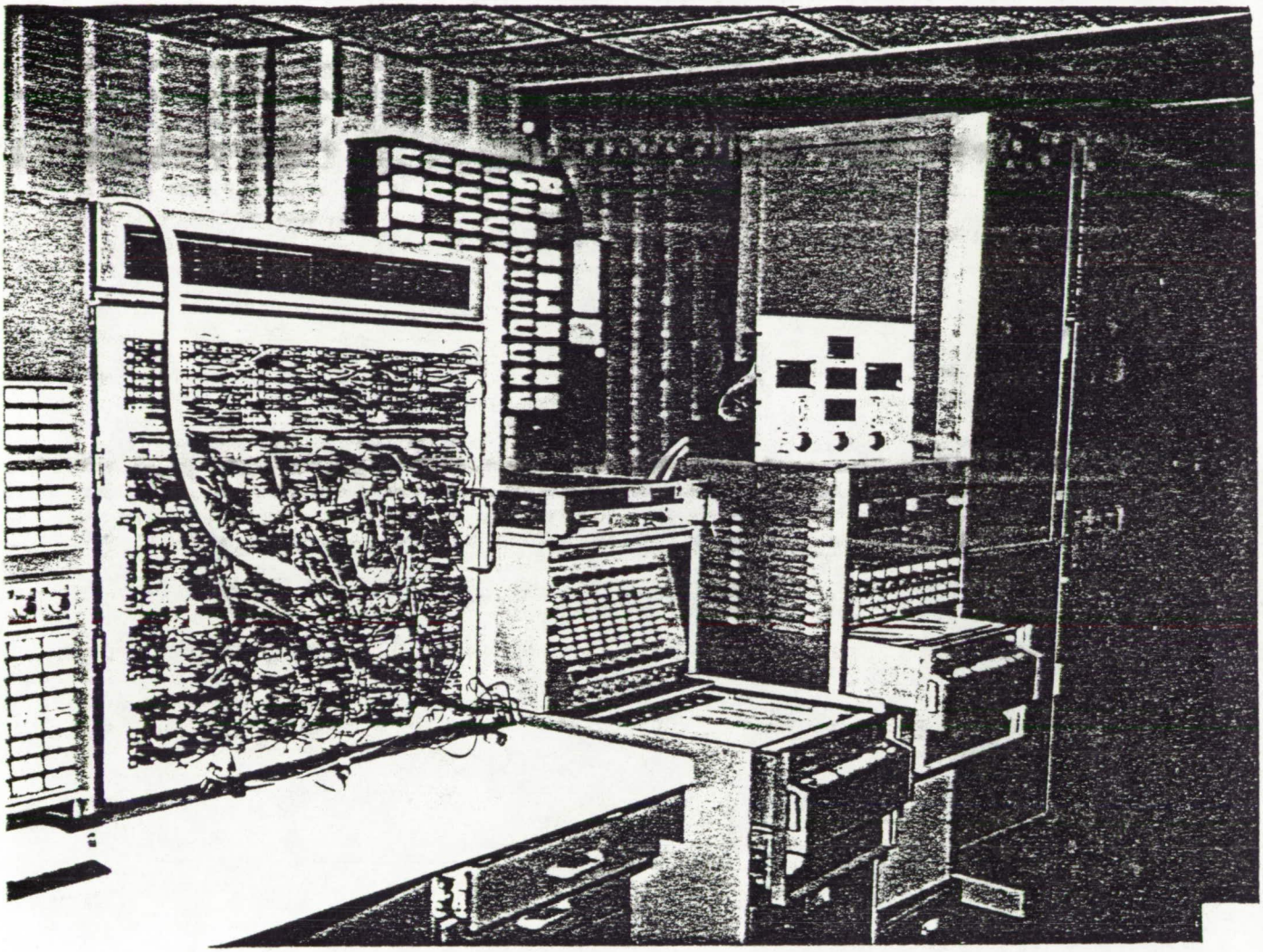

Figure 22. View of the hybrid computer-based cryogenic tunnel simulator.

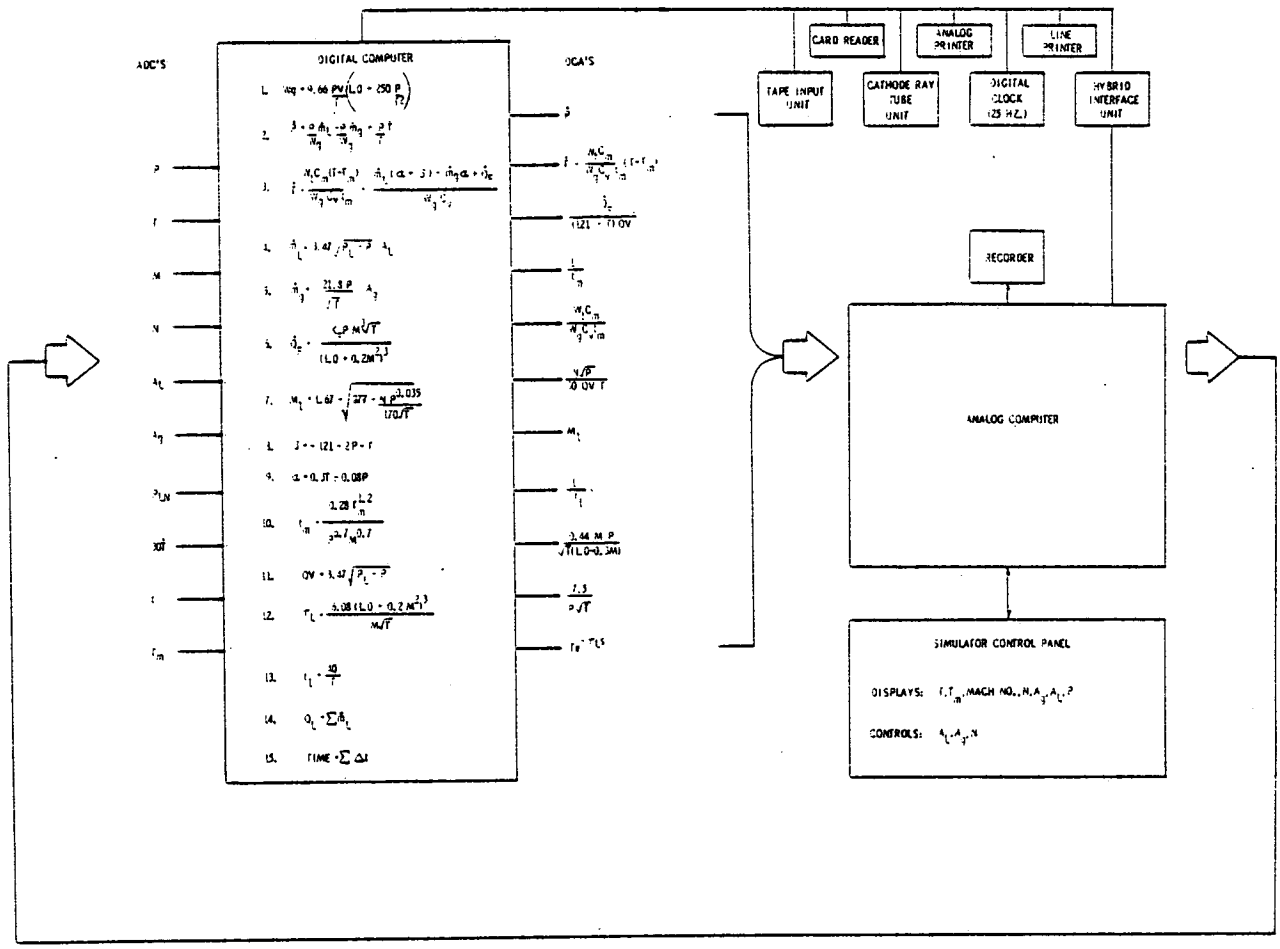

Figure 23. Cryogenic tunnel hybrid simulation scheme.

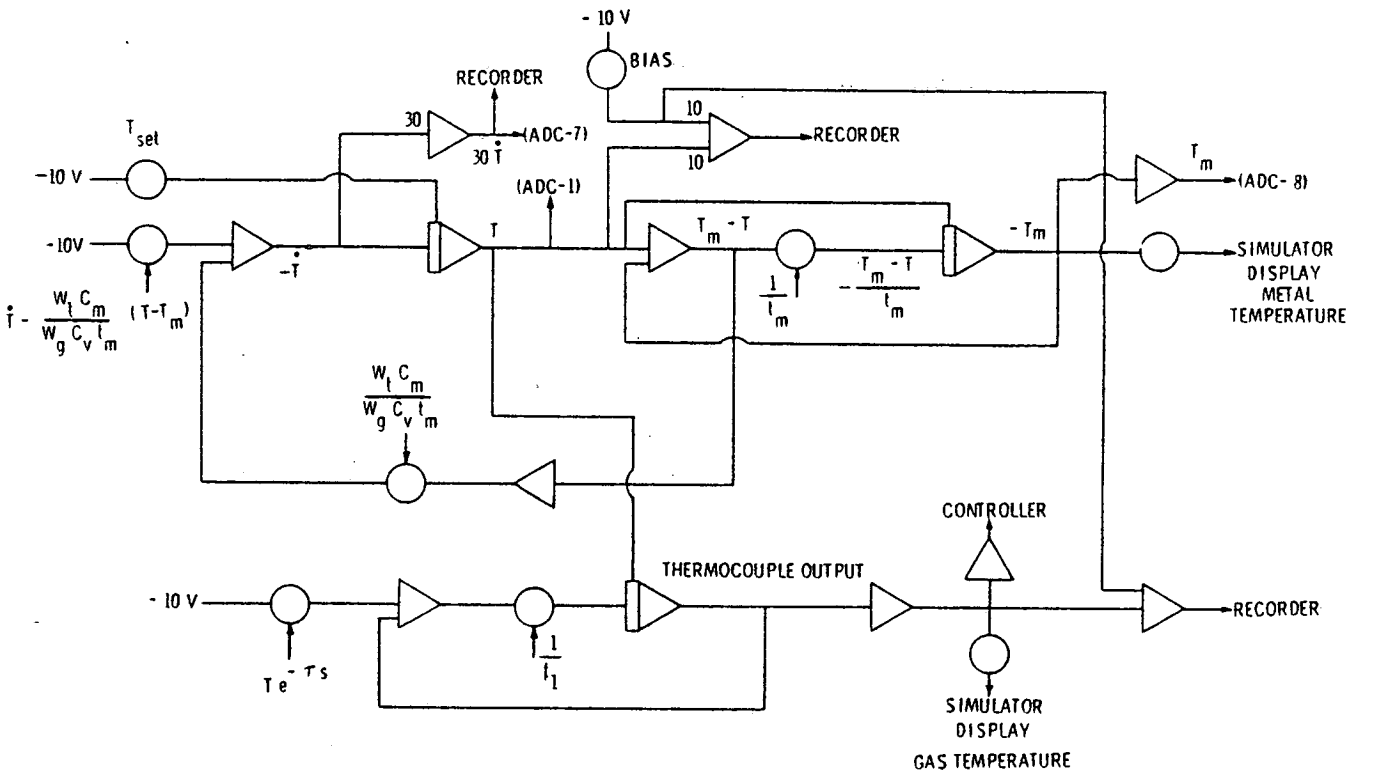

Figure 24. Tunnel temperature dynamics—analog.

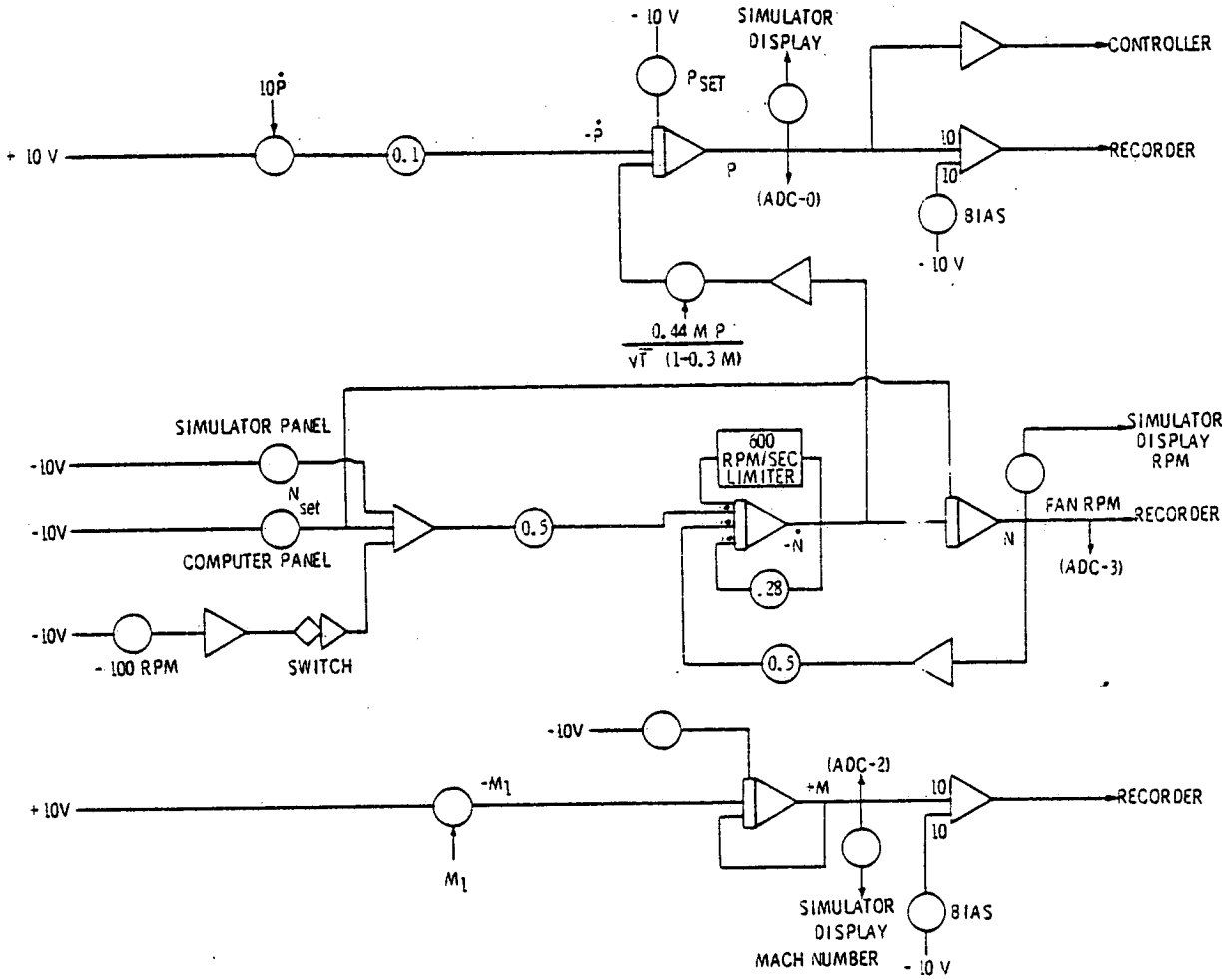

Figure 25. Tunnel pressure, fan, and Mach dynamics—analog.

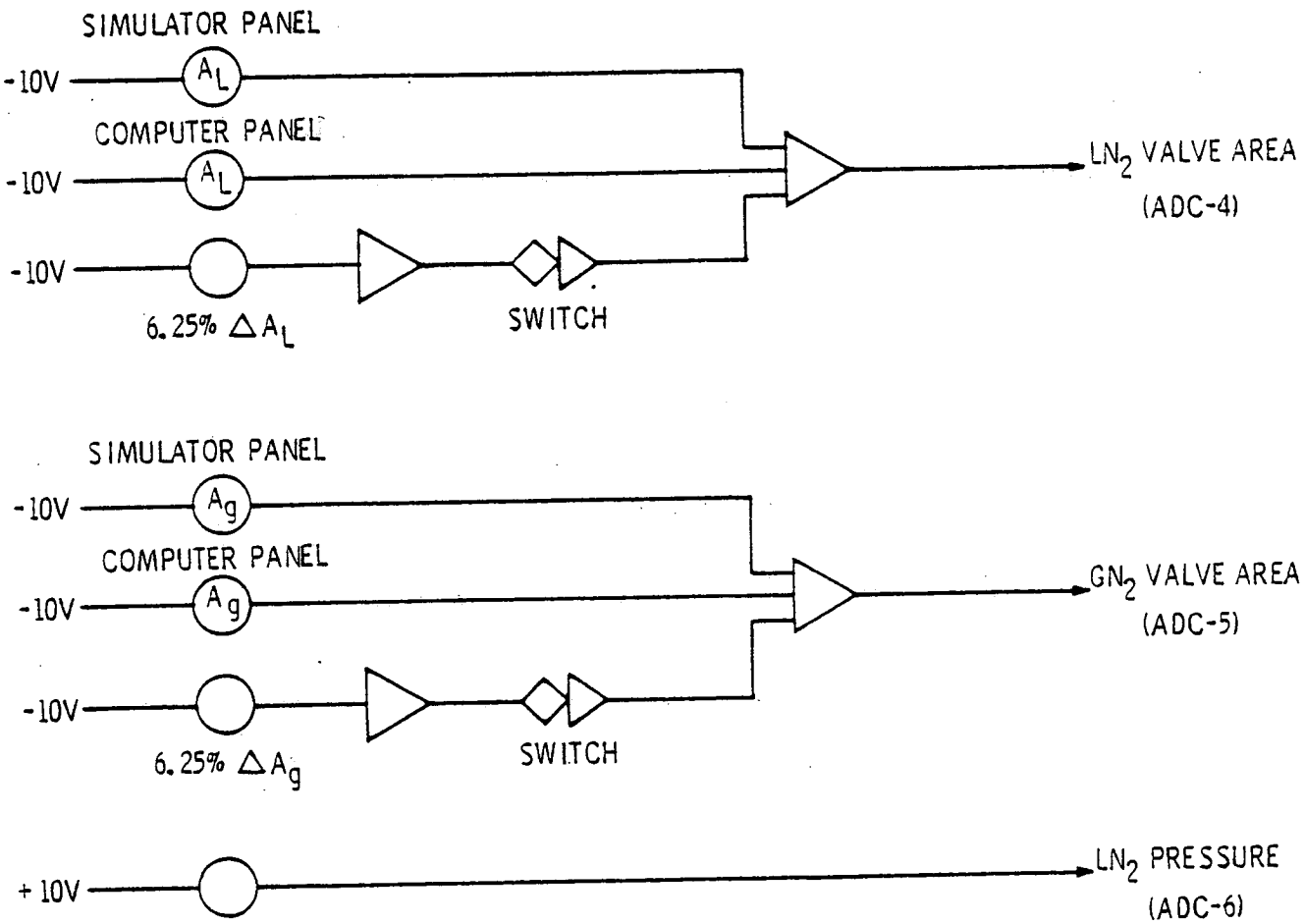

Figure 26. Tunnel valve control scheme—analog.

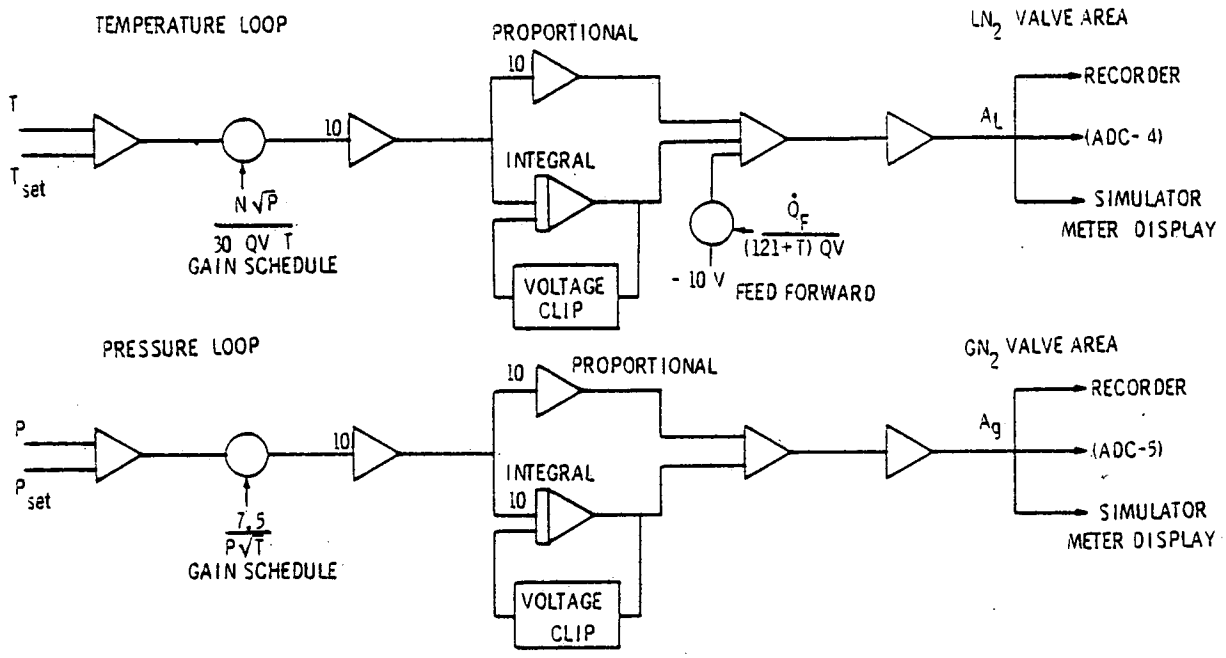

Figure 27. Tunnel pI controllers—analog.

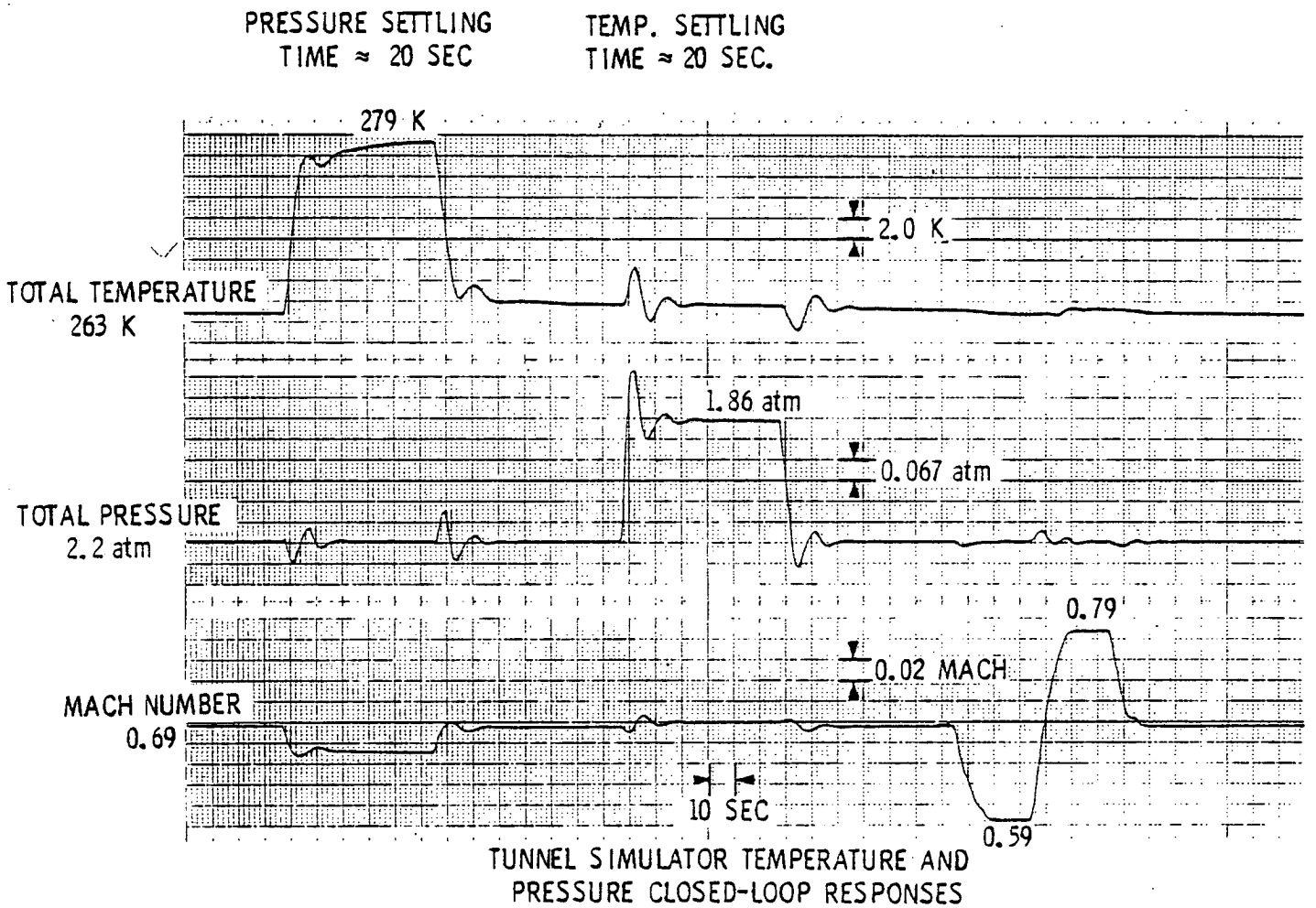

Figure 28. Simulator closed-loop control responses (270 K).

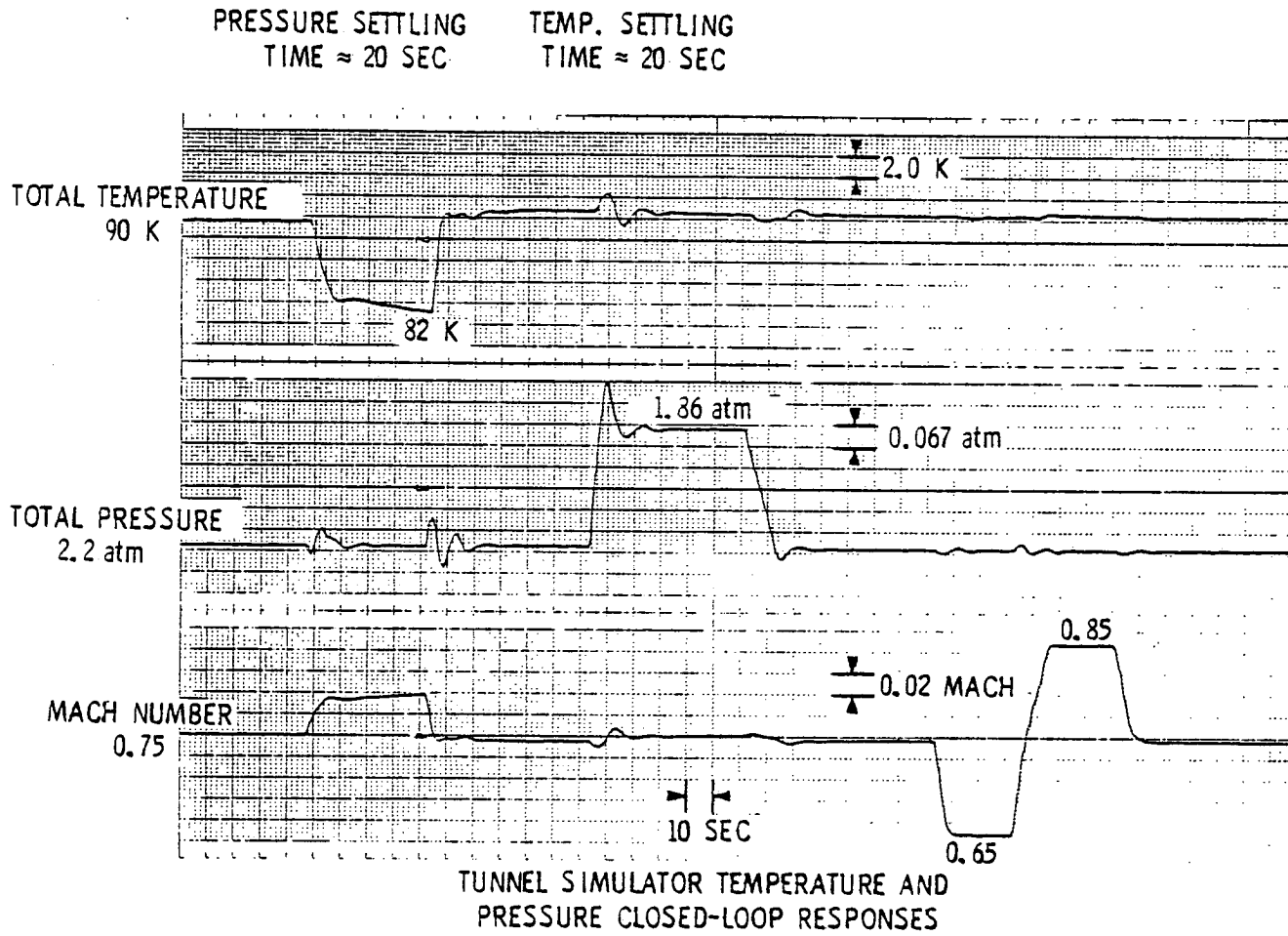

Figure 29. Simulator closed-loop control responses (90 K).

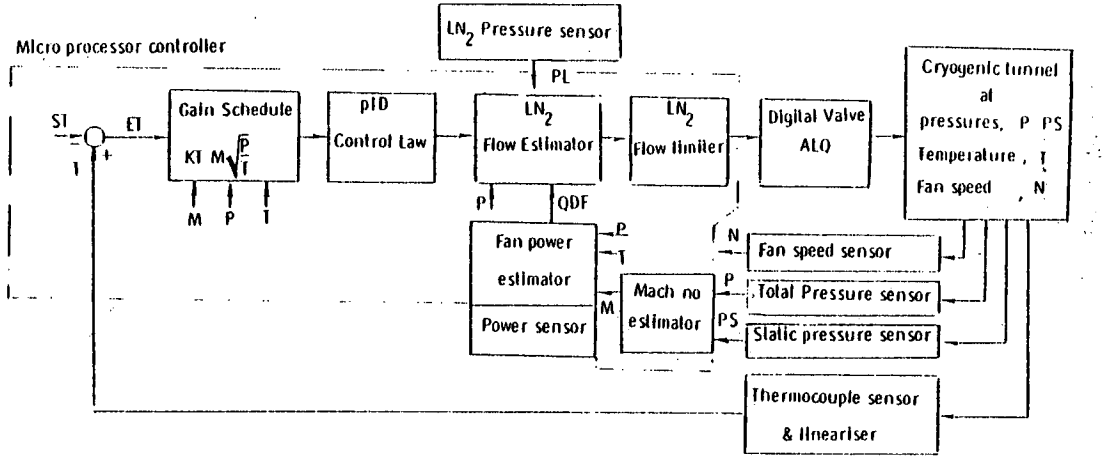

Control law

$$ET = T - ST$$

$$ALQ = \left\{ \frac{M \cdot \sqrt{P} \cdot KT}{KL \cdot \sqrt{T}} \left(pT \cdot ET + IT \cdot \int ET + DT \cdot \frac{d}{dt} ET \right) + KB \cdot FF \right\}$$

IF $ALQ \geq MAX$; $ALQ = MAX$ IF $ALQ < MAX$; $ALQ = ALQ$

$$KB = \frac{QDF}{(121+T) \cdot KL} \qquad QDF = \frac{KF \cdot P \cdot \sqrt{T} \cdot M^3}{(1 + 0.2 \cdot M^2)^3}$$

$$MAX = \left(KB \cdot FF + \frac{255 \cdot P \cdot V \cdot TGR}{T \cdot (121+T) \cdot KL} \right) \cdot (1-LLT) + LLT$$

Logic

IF $ET > 0$; $FF = 1$ IF $ET < -5$; $FF = 0$

IF $ET < 5$; $LLT = 1$ IF $ET > 10$; $LLT = 0$

Figure 30. Automatic temperature control scheme for a cryogenic tunnel.

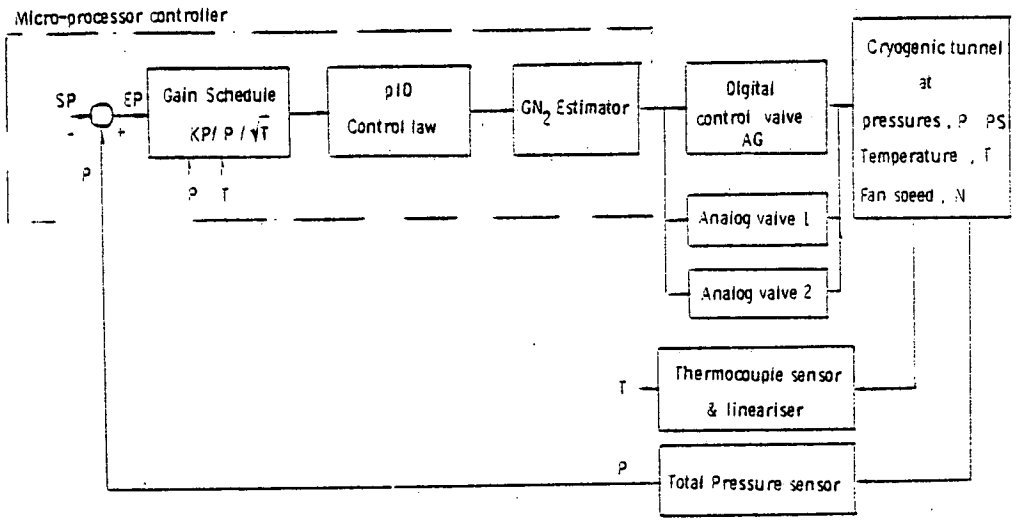

Control law

$$EP = P - SP$$

$$AG = \frac{KP}{KG\, P\sqrt{T}} \left[PP \cdot EP + IP \int EP + DP \cdot \frac{d}{dt} EP \right]$$

Logic

$SUM = 0$ $\quad SUM_{past} =$ SUM, UA seconds ago

IF $AG > 0.9$; $SUM = SUM_{past} + 0.125$

IF $AG < 0.5$; $SUM = SUM_{past} - 0.125$

IF $SUM < 1$; $A1 = SUM \quad A2 = 0$

IF $SUM > 1$; $A1 = 1.0 \quad A2 = SUM - 1$

Figure 31. Automatic pressure control scheme for a cryogenic tunnel.

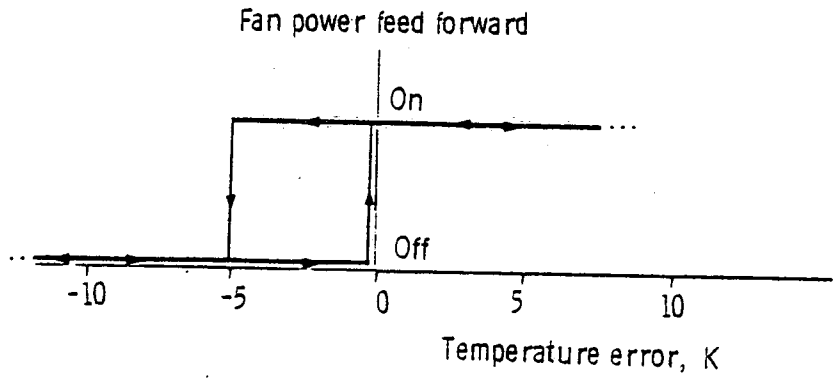

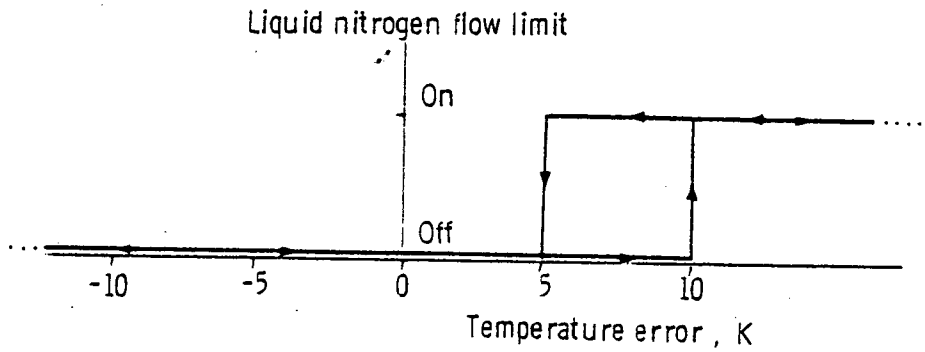

Figure 32. Cryogenic tunnel temperature control loop logic functions.

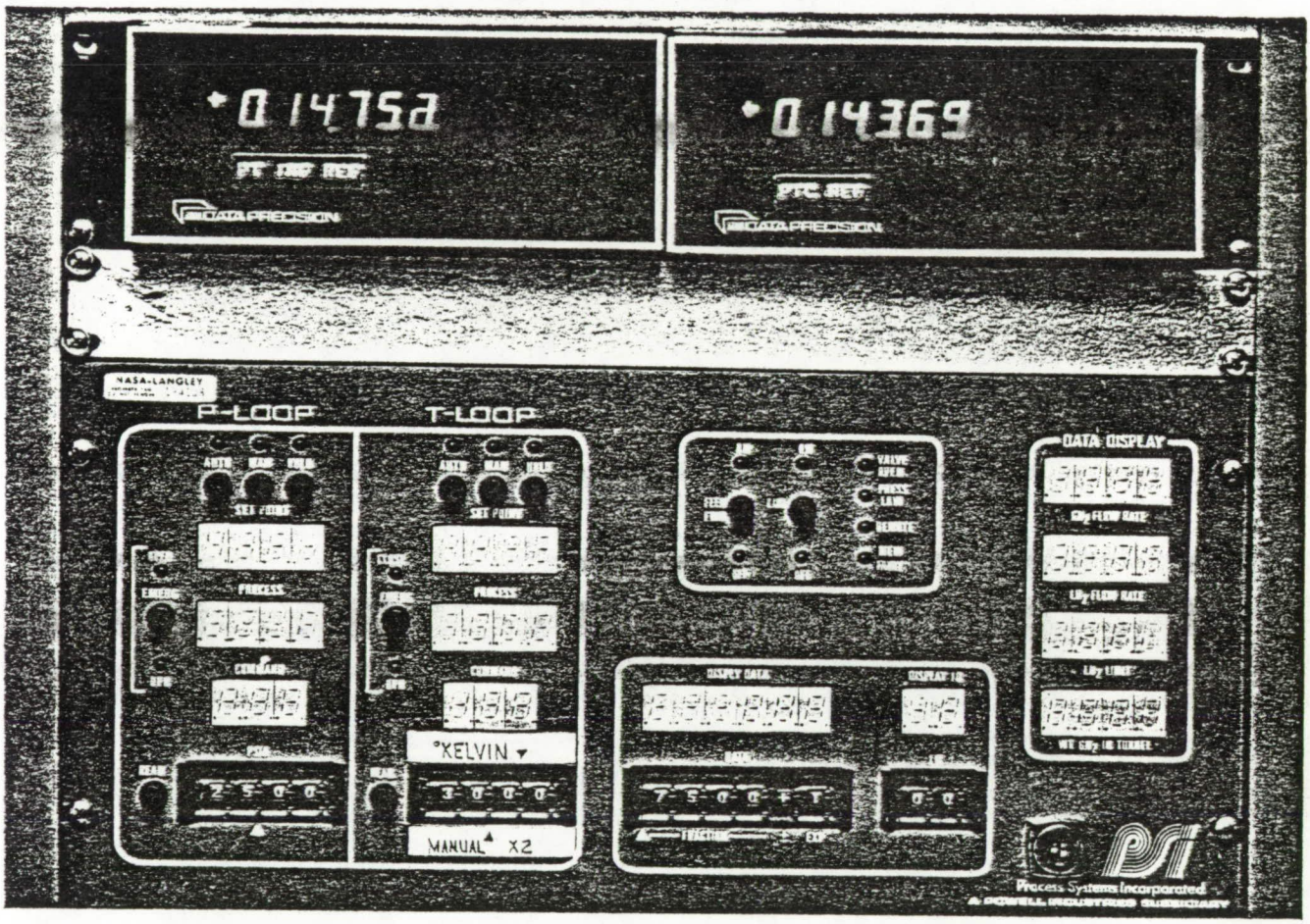

NASA
L-80-470

Figure 33. View of the microprocessor-based controller for 0.3-m TCT.

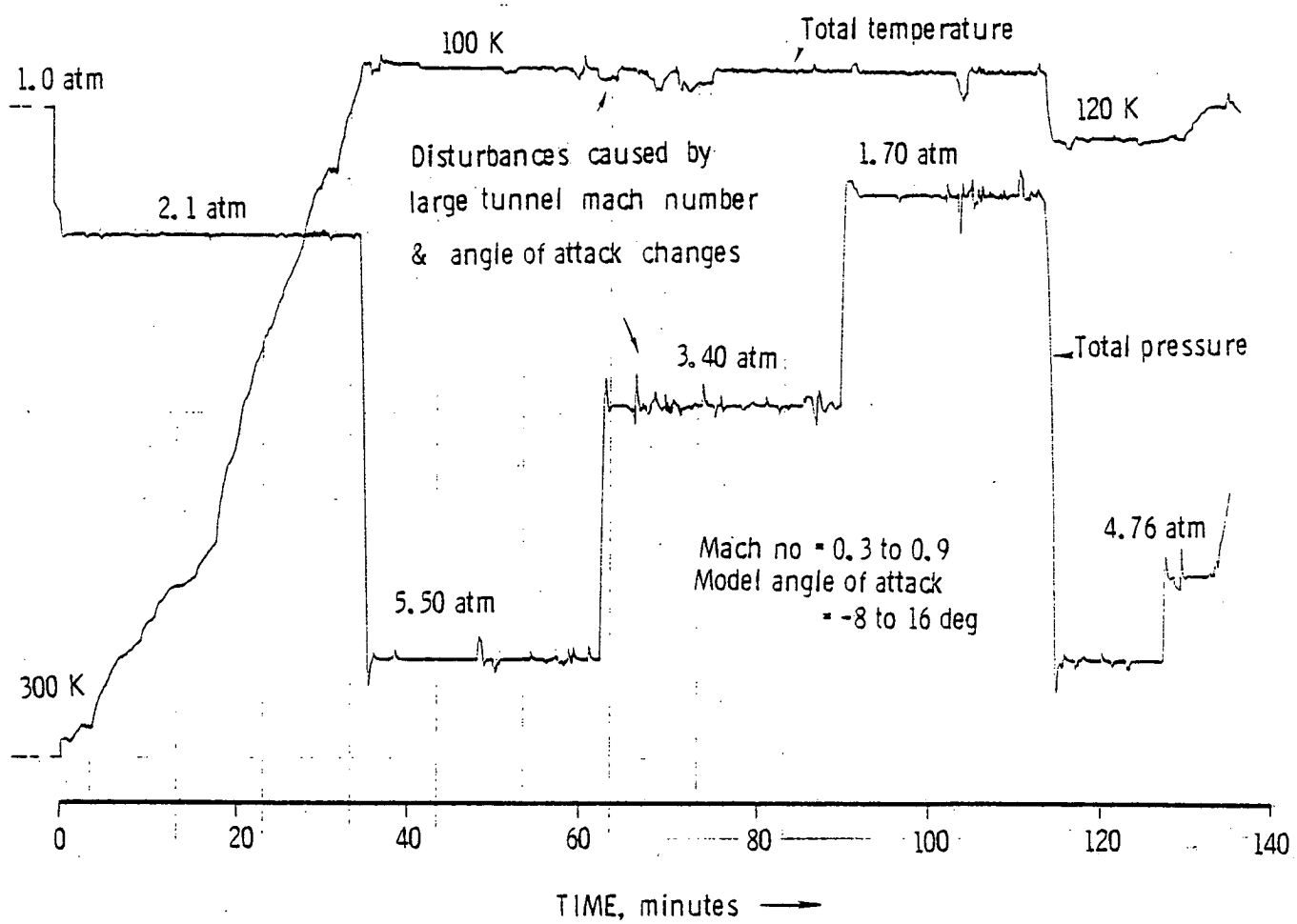

Figure 34. Typical 0.3-m TCT test with temperature and pressure automatic control.

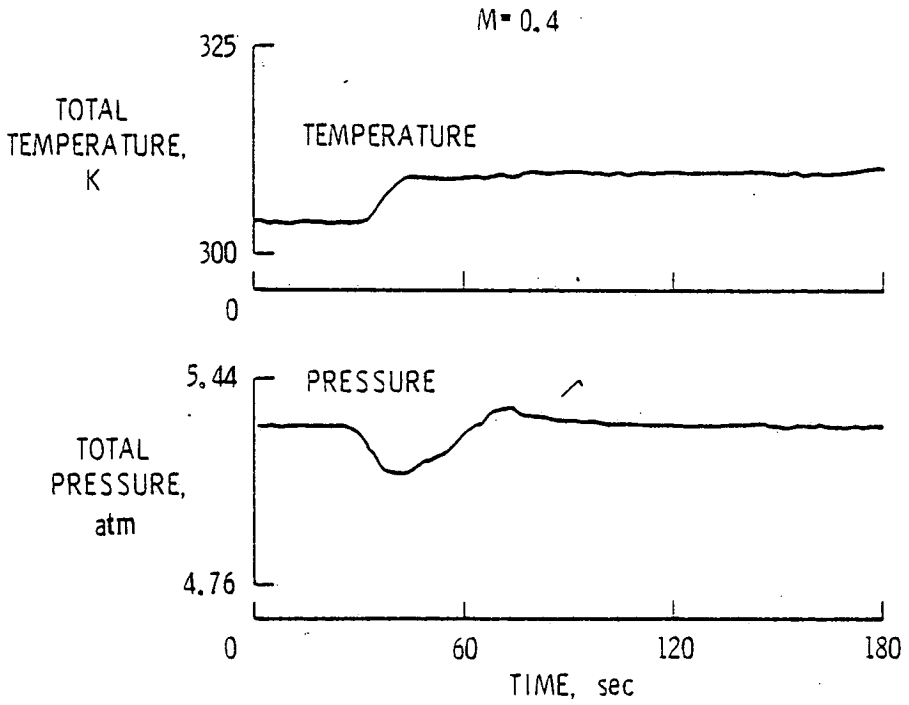

Figure 35. Typical temperature response and pressure coupling under closed-loop control.

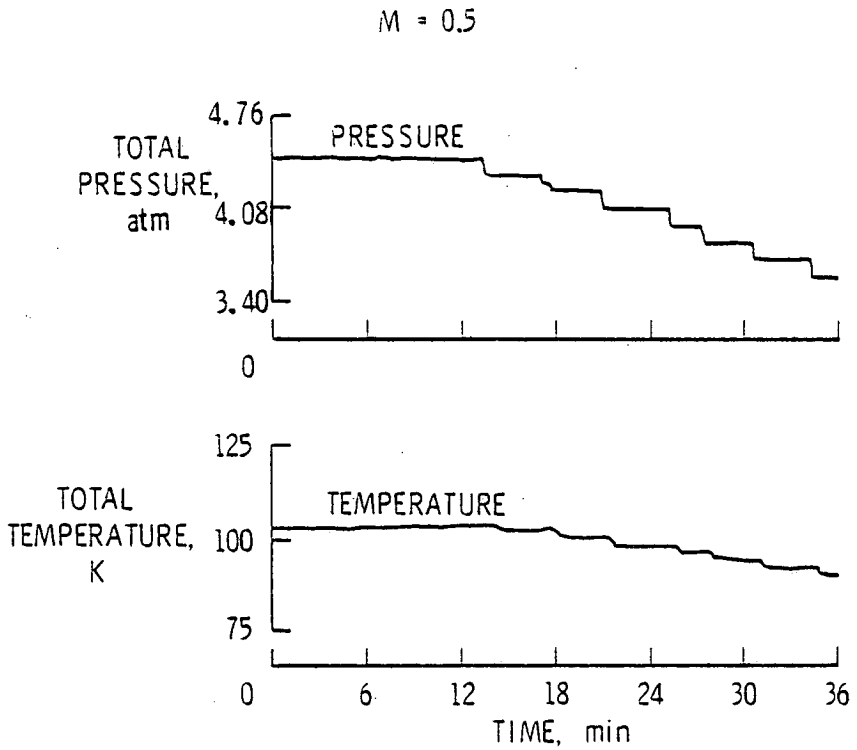

Figure 36. Typical 0.3-m TCT test with temperature and pressure automatic control.

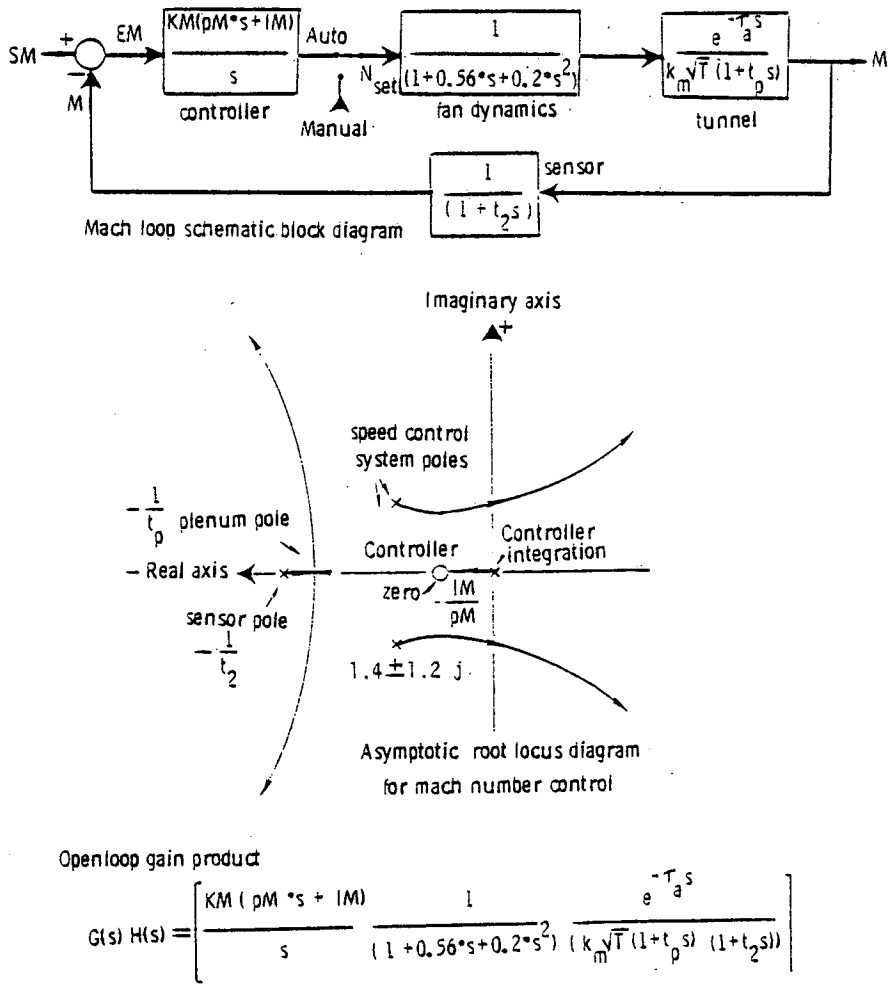

Figure 37. Automatic Mach number control scheme for a cryogenic wind tunnel.

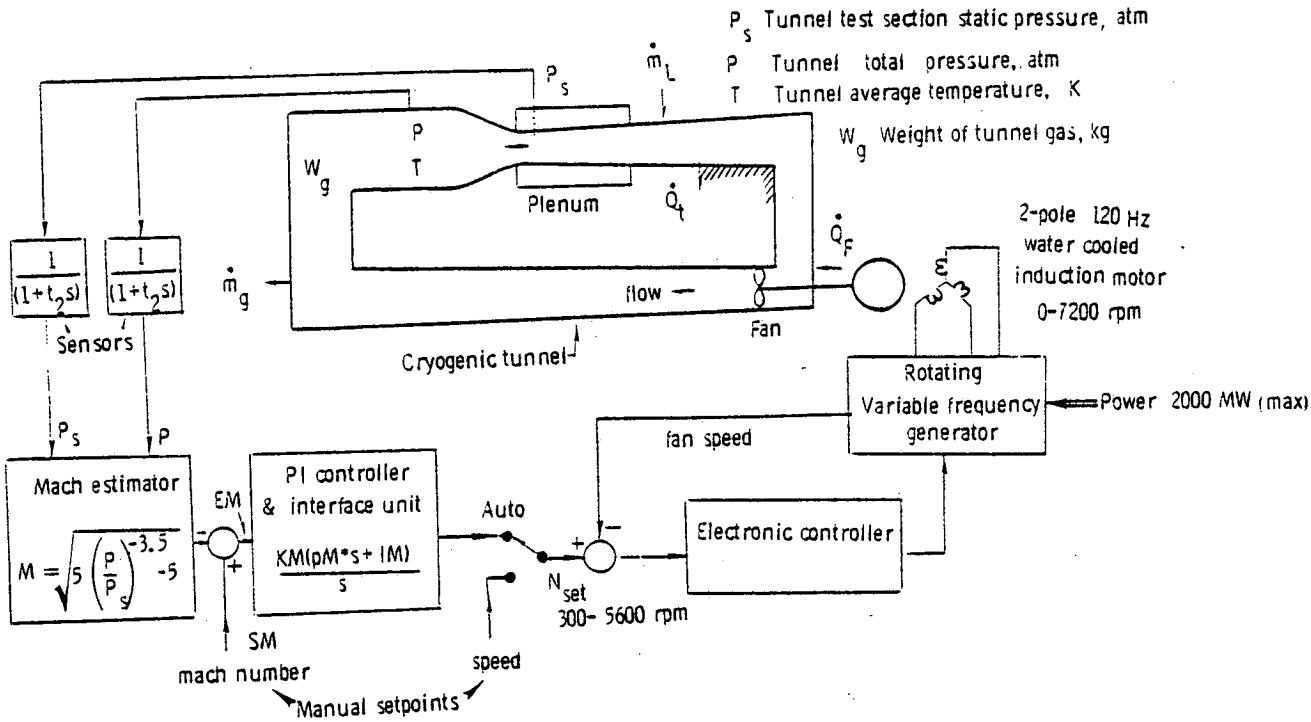

Figure 38. Cryogenic wind tunnel Mach number control analysis.